Cavity quantum electrodynamics and intersubband polaritonics of a two dimensional electron gas

Simone de Liberato

UNIVERSITÉ PARIS DIDEROT (Paris 7)

ECOLE DOCTORALE: ED107

DOCTORAT

Physique

SIMONE DE LIBERATO

CAVITY QUANTUM ELECTRODYNAMICS AND INTERSUBBAND POLARITONICS OF A TWO DIMENSIONAL ELECTRON GAS

Thèse dirigée par Cristiano Ciuti

Soutenue le 24 juin 2009

JURY

M.	David S. CITRIN	Rapporteur
M.	Michel DEVORET	Rapporteur
M.	Cristiano CIUTI	Directeur
M.	Carlo SIRTORI	Président
M.	Iacopo CARUSOTTO	Membre
M.	Benoît DOUÇOT	Membre

Contents

Acknowledgments

There is a quite long list of people who have helped me in different ways during the three years of my Ph.D. and to whom I am greatly indebted.

The first person I have to thank is my advisor Cristiano Ciuti, not only for having always been kind and available, and for having taught me so much, but also for having trusted me enough to grant me complete scientific freedom in these years. He always encouraged me to pursue my ideas, even when completely unrelated to his research and the main body of my thesis. Without his guidance and foresight, a good deal of the work I accomplished during these years would not have been possible.

I also have to thank three colleagues I had the pleasure to work with in multiple occasions during my Ph.D.: Iacopo Carusotto, my *unofficial* co-advisor; Aji A. Anappara, who had the uneasy task of being the interface between myself and a working experiment; and Luca De Feo, who introduced me to the domain of algorithmic complexity and often accompanied me during my trips through its lands. Then I acknowledge all the other colleagues I had fruitful an pleasant interactions with. Without pretensions of completeness, I want to thank: Jérôme Faist, Dario Gerace, Rupert Huber, Juan Pablo Paz, Sandu Popescu, Luca Sapienza, Carlo Sirtori, Yanko Todorov and Alessandro Tredicucci.

I would like to thank researchers and administrative staff at Laboratoire Matériaux et Phénomènes Quantiques and Laboratoire Pierre Aigrain (where I performed my undergraduate diploma work) for discussions, assistance and logistical support during my Ph.D. I would like to thank the project ANR INTERPOL and CNRS, who have financed many missions during my Ph.D. years.

Then, in no special order, I want to thank: my father, Luciano De Liberato; my colleagues at Laboratoire Matériaux et Phénomènes Quantiques: Xavier Caillet, Simon Pigeon, Erwan Guillotel, Marco Ravaro and all the others;

Oussama Ammar and all the friends of Hypios; Florian Praden and all my friends at École Normale Supérieure. It is also a pleasure to thank Alessandro Colombo, Stefano Bertani, Domenico Bianculli and all the other friends I met during my years at the Politecnico di Milano. They made life enjoyable and travel cheap.

A special thanks goes to Alberto Santagostino, because nothing says *old school scientist* more than having a Mecenate; to Steve Jobs, because without him this thesis would not have been 100% Microsoft-free; to Hugh Everett III, for having taken quantum mechanics seriously enough; and to all the people who do not consider *shut up and calculate* a valid interpretation of quantum mechanics.

Curriculum vitae

Personal data

Name:	Simone
Surname:	De Liberato
Date of birth:	26 September 1981
Nationality:	Italian

Education

2006-2009:	Ph.D. student at Université Paris Diderot-Paris 7
2005-2006:	Master in Quantum Physics at École Normale Supérieure
2003-2005:	Graduation in Physics at École Normale Supérieure
2000-2003:	Student at Politecnico di Milano

Conferences, Schools

September 2008:	Workshop on Quantum Coherence and Decoherence (Benasque, Spain)
September 2008:	ICSCE4 conference (Cambridge, England)
July 2008:	ICPS08 conference (Rio De Janeiro, Brazil)
June 2008:	Fermi Summer School (Varenna, Italy)
December 2007:	25th Winter School in Theoretical Physics at the IAS (Jerusalem, Israel)
July 2007:	EP2SD 17 + 13 MSS conference (Genova, Italy)
June 2007:	Vienna Symposium on the Foundations of Modern Physics (Wien, Austria)
September 2006:	XXIV Convegno di Fisica Teorica e Struttura della Materia (Levico Terme, Italy)
June 2006:	Poise Summer School (Cortona, Italy)
July 2004:	Diffiety Summer School (Santo Stefano del Sole, Italy)

Internships

July-September 2008:	Visiting scholar at the University of Buenos Aires, in the group of Prof. Juan Pablo Paz
January-July 2006:	Internship at Laboratoire Pierre Aigrain (ENS Paris) under the direction of Prof. C. Ciuti
February-August 2005:	Internship at Clarendon Laboratory (Oxford, England) under the direction of Prof. C. J. Foot
June-August 2004:	Internship at University Tor Vergata (Rome, Italy) under the direction of Prof. M. Cirillo

Teaching Experience

2006-2009: Teaching assistant at Université Pierre et Marie Curie, for the class LP104, Introduction to physics

Spoken Languages

Italian: fluent

Engish: fluent

French: fluent

Spanish: basic

Publication list

Publications treated in this manuscript

7. *Signatures of the ultra-strong light-matter coupling regime*
   A. A. Anappara, S. De Liberato, A. Tredicucci, C. Ciuti, G. Biasiol, L. Sorba and F. Beltram
   Physical Review B **79**, 201303(R) (2009)

6. *Stimulated scattering and lasing of intersubband cavity polaritons*
   S. De Liberato and C. Ciuti
   Physical Review Letters **102**, 136403 (2009)

5. *Sub-cycle switch-on of ultrastrong light-matter interaction*
   G. Guenter, A. A. Anappara, J. Hees, G. Biasiol, L. Sorba, S. De Liberato, C. Ciuti, A. Tredicucci, A. Leitenstorfer, and R. Huber
   Nature **458**, 178 (2009)

4. *Quantum theory of electron tunneling into intersubband cavity polariton states*
   S. De Liberato and C. Ciuti
   Physical Review B **79**, 075317 (2009)

3. *Quantum model of microcavity intersubband electroluminescent devices*
   S. De Liberato and C. Ciuti
   Physical Review B **77**, 155321 (2008)

2. *Cavity polaritons from excited-subband transitions*
   A. Anappara, A. Tredicucci, F. Beltram, G. Biasiol, L. Sorba, S. De Liberato and C. Ciuti
   Applied Physics Letters **91**, 231118 (2007)

1. *Quantum vacuum radiation spectra from a semiconductor microcavity with a time-modulated vacuum Rabi frequency*
   S. De Liberato, C. Ciuti and I. Carusotto
   Physical Review Letters **98**, 103602 (2007)

Other publications

4. *Fermionized photons in an array of driven dissipative nonlinear cavities*
   I. Carusotto, D. Gerace, H. Tureci, S. De Liberato, C. Ciuti and A. Imamoğlu
   Physical Review Letters **103**, 033601 (2009)

   In this paper we theoretically investigated the optical response of a one-dimensional array of strongly nonlinear optical microcavities. We discovered than when the optical nonlinearity is the dominant energy scale, the non-equilibrium steady state of the system is reminiscent of a strongly correlated Tonks-Girardeau gas of impenetrable bosons.

3. *Optical properties of atomic Mott insulators: from slow light to the dynamical Casimir effects*
   I. Carusotto, M. Antezza, F. Bariani, S. De Liberato and C. Ciuti
   Physical Review A **77**, 063621 (2008)

   In this paper we theoretically studied the optical properties of a gas of ultracold, coherently dressed three-level atoms in a Mott insulator phase of an optical lattice. In the weak dressing regime, the system shows unique ultra-slow light propagation properties without absorption. In the presence of a fast time modulation of the dressing amplitude, we predicted a significant emission of photon pairs due to the dynamical Casimir effect.

2. *Observing the evolution of a quantum system that does not evolve*
   S. De Liberato
   Physical Review A **76**, 042107 (2007)

   In this paper I studied the problem of gathering information on the time evolution of a quantum system whose evolution is impeded by the quantum Zeno effect. I found it is in principle possible to obtain some information on the time evolution and, depending on the specific system, even to measure its average decay rate, even if the system does not undergo any evolution at all. This paper has been reviewed by L. Vaidman in a *News & Views* on Nature [1].

1. *Tunnelling dynamics of Bose-Einstein condensate in a four wells loop shaped system*
   S. De Liberato and C. J. Foot
   Physical Review A **73**, 035602 (2006)

   In this brief report, whose research was performed during an undergraduate internship in the group of C. J. Foot, I studied some properties of Bose-Einstein condensates in loop geometries, with particular attention to the creation and detection of currents around the loop.

Introduction

The history of cavity quantum electrodynamics, the study of light-matter interaction in quantum confined geometries, started when Purcell [2] noted that the spontaneous emission rate of an excited atom can be changed by adjusting the boundary conditions of the electromagnetic field with properly engineered cavities. Since then, experiments showing modifications of spontaneous emission rates were realized with ever-growing atom-cavity couplings and cavity quality factors [3, 4, 5, 6, 7]. This lead eventually to systems in which the photon lifetime inside the cavity was substantially bigger than the spontaneous emission rate, that is systems in which a single photon undergoes multiple absorption and reemission cycles before escaping the cavity [8, 9, 10]. The first experiments that reached this regime, named *strong coupling regime*, were performed with Rydberg atoms in superconducting cavities. Strong coupling regime was then achieved in solid-state systems, using quantum well excitons in microcavities [11] and, more recently, Cooper pair boxes in superconducting circuits [12] (in this case the name circuit quantum electrodynamics is often employed).

But what does strong coupling exactly means? Textbooks normally define two coupled systems to be strongly coupled if it is possible to experimentally resolve the energy shift due to the coupling, that is the coupling constant (quantified by the vacuum Rabi frequency Ω_R) needs to be bigger than the linewidth of the resonances. If two systems are strongly coupled, the composite system eigenstates can not be described as a tensorial product of the eigenstates of the two bare ones. That is the interaction is so strong that entangles the systems and the only meaningful information becomes the eigenstate of the coupled system. In the case of two level systems (e. g. the Rydberg atoms in microwave cavities), people usually calls these eigenstates of *dressed states*, in the case of bosonic ones (e. g. excitons in planar microcavities), the name *polaritons* is used.

In the last ten years, exciton polaritonics has become a remarkably rich field in condensed matter physics, fertile both for fundamental and applied research [13, 14, 15, 16, 17, 18, 19]. In such systems, thanks to the small polaritonic mass (inherited from their photonic part), it is possible to reach the quantum degenerate regime at temperatures orders of magnitude bigger than in atomic systems. Exciton polariton Bose-Einstein condensation was recently achieved at a temperature of few kelvin [20], compared to hundreds of nanokelvin needed for atomic cloud Bose-Einstein condensates. New kinds of electroluminescent [21] and lasing [22, 23] devices have been realized with such quasi-particles, often with unprecedented performances.

In 2003 there was a new entry in the list of solid-state strongly coupled systems with the first experimental observation of the strong coupling between a microcavity photon mode and the intersubband transition of a doped quantum well [24]. *Intersubband* transitions are named in opposition to the usual *interband* transitions, occurring between valence and conduction band in semiconductors. They are instead transitions between the subbands in which the conduction band is split due to the quantum well confinement. While this kind of polaritons, quickly dubbed *intersubband polaritons*, are in various respect profoundly different from exciton polaritons, both for the energy range (mid-infrared to Terahertz) and for the nature of the electronic transition (intersubband transitions, contrary to excitons, are not bound states), the main interest of these new polaritons stays in the strength of the light-matter interaction [25].

We just mentioned that the light-matter coupling in these systems, as for excitons or atoms, can be *strong*. Is it possible to go further? The definition of strong coupling in term of energy shifts and linewidths is clearly relevant in spectroscopic experiments: two systems are strongly coupled if we can resolve the effect of the interaction, which produces an energy anticrossing between light and matter resonances. Anyway it does not permit to make any assessment on the real strength of the interaction. Being in the usual strong coupling regime means to have an energy shift due to coupling bigger than the linewidth of the resonance, that can be achieved even with extremely small couplings, if the losses are small enough. In order to assess the real strength of the interaction, the right figure of merit is the ratio between the interaction energy and the bare system excitation energy $\hbar\omega_{12}$ (transition energy). The ratio $\frac{\Omega_R}{\omega_{12}}$ gives a direct assessment of the relative strength of the interaction, not of our ability to spectroscopically observe it.

In atomic systems $\frac{\Omega_R}{\omega_{12}}$ is typically less then 10^{-6} in the case of a single atom. That is the atomic transition resonance shifts of less than one part per million from its unperturbed position. We can still see the shift simply because superconducting cavity can have an astounding quality factor, of the order of 10^9, that permits us to resolve even such tiny shifts. Is it possible to do better? Not in dilute atomic systems [26], where the smallness of this ratio directly depends upon the small value of the fine structure constant $\alpha \simeq \frac{1}{137}$. In condensed matter cavity quantum electrodynamics it is possible to beat this limit, exploiting collective, coherent excitations. If a large number of electrons gets collectively excited, the ensuing excitation has a *collective* dipole, whose intensity scales as the square root of the electron number, in a phenomenon reminiscent of the Dicke superradiance [27]. In excitons for example, where a large number of valence electron states participates to the excitation, experiments have reached values up to 10^{-2} for the ratio $\frac{\Omega_R}{\omega_{12}}$ [28, 29, 30, 31].

In intersubband excitations, the values obtained until now are bigger than 10^{-1}, and there is still a large marge of improvement [32]. That is, the coupling is intrinsically strong, enough to significatively change the spectrum of the system and the nature of the quantum ground state. Other systems in which such large couplings could be achieved are Cooper pair boxes coupled to superconducting line resonators, where theoretical values up to 20 have been predicted [26]. This regime of intrinsic strong coupling was named *ultra-strong coupling*. Such ultra-strong coupling is interesting for various reasons. In particular the ground state turns out to be a squeezed vacuum, containing pairs of virtual photons [25, 33].

While such virtual excitations are normally unobservable, they can become real if the system is modulated in a non-adiabatic way [34]. This effect, the emission of photons out of the ground state when the system is perturbed, is a manifestation of the dynamical Casimir effect [35], an elusive and never observed quantum electrodynamics effect reminiscent of the Unruh effect [36] (colloquially speaking the dynamical Casimir effect predicts that a mirror, shaken in the vacuum, emits photon pairs, the Unruh effect predicts that a thermometer, shaken in the vacuum, measures a non-zero temperature). Intersubband polaritonic systems, together with Cooper pair boxes, seems to be very promising systems for observing this kind of effects.

On a more applied ground, it is important to point out that the light matter coupling could affect electric transport and electroluminescence, opening new

opportunities that could be exploited to create high-efficiency light sources in the mid-infrared and Terahertz regions.

The manuscript consists of five chapters. Chapter 1 serves as a general introduction and reference, the other four follow quite chronologically my Ph.D. work of the last three years. Chapter 2 presents a comprehensive quantum Langevin theory predicting the quantum vacuum radiation induced by the non-adiabatic modulation of the vacuum Rabi frequency in microcavity embedded quantum wells. The theory accounts both for ultra-strong light-matter excitations and losses due to the coupling with radiative and non-radiative baths. Chapter 2 also reports of two experimental milestones [32, 37] toward the observation of such effect.

Chapters 3 and 4 present a general theory to describe the influence of intersubband polaritons on electron transport and electroluminescence. Chapter 3 presents a numerical method [38] capable to model electrical transport through a microcavity embedded quantum well, taking into account the strong coupling of electrons with the microcavity photons. Not only it gives a theoretical explanation to various features observed in electroluminescence experiments [39], but it also shows that, by increasing the light matter coupling in such devices, it may be possible to drastically increase their quantum efficiency, in a strong coupling extension of the Purcell effect [2]. Chapter 4 shows how the coupling with the quantum vacuum fluctuations of the microcavity electromagnetic field can qualitatively change the spectral function of the electrons inside the structure. The spectral function is characterized by a Fano resonance, due to the coupling of the electrons with the continuum of intersubband polaritons. The theory suggests that these features may be exploited to improve the quantum efficiency by selectively excite superradiant states through resonant electron injection. Finally Chapter 5 shows how it is possible to exploit the peculiar properties of intersubband polaritons in order to obtain a new kind of inversionless laser [40]. A theory of polariton stimulated scattering due to interaction with optical phonons is developed, that fully takes into account saturation effects that make the behavior of intersubband polaritons to depart from the one of pure bosons. With realistic parameters, this theory predicts lasing with a threshold almost two orders of magnitude lower than existing intersubband lasers.

Sometimes the algebra behind the presented results may be heavy. In order to improve readability I reduced to the minimum the quantity of equations in the main body of the text, moving all the technical calculations in the Appen-

dices. Each Chapter has thus its own Appendix, in which the reader interested in technical details will find all the calculations that were not included neither in the corresponding Chapter, nor in Letter format publications.

Chapter 1

Introduction intersubband polaritons physics

1.1 Introduction

A number of the following chapters are dedicated to solve various problems linked with the physics of quantum coherent phenomena in microcavity embedded quantum wells. In order to keep the chapters independent, avoiding both boring repetitions and too many inter-chapter references, I decided to collect in this first chapter all the notions necessary for the comprehension of this thesis.

I will start giving an overview of different quantum mechanical concepts. I think that almost all of them are considered as common background for working scientists in condensed matter physics, anyway I prefer to review them, especially because the aspects I am interested in are often not the ones stressed in textbooks. Then I will give a brief review of the physics of quantum wells, microcavities and of their interactions. In the last part I will introduce the main theoretical tools I will need, that is the many body Hamiltonian for the system, in its full form as well as in different simplified forms that will be useful for treating different problems.

1.2 Useful quantum mechanics concepts

1.2.1 Weak and strong coupling

In basic quantum mechanics, when describing the evolution of a system, it is customary to make a strong distinction between the case in which the initial state of such system is coupled only to another discrete state or instead to a *continuum* of final states. In the first case the dynamics exhibits oscillations, called *Rabi oscillations*, while in the second case the dynamics is irreversible and usually described by means of the *Fermi golden rule*.

The apparent dichotomy between these two cases is given by the fact that, due to the coherent nature of quantum mechanics, the initial state couples at the same time to all the possible final states. If the different final states have different energies anyway they will oscillate at different frequencies and thus, even if for long times we expect to still observe Rabi oscillations (or more precisely quantum revival of Rabi oscillations [41, 42, 43]), for short times the phase of the system is randomized on a timescale of the order of the inverse of the continuum frequency width. If this randomization is faster than the Rabi oscillation period, the coherence is lost before even one single oscillation can take place.

It is easy to understand that the real dichotomy is not between a discrete level and a continuum but between a narrow and a broad continuum, where the width of the continuum has to be compared with the frequency of the Rabi oscillations. For this reason the two regimes are called strong and weak coupling respectively, where weak and strong refer to the strength of the coupling, that is proportional to the frequency of the Rabi oscillations. Clearly this definition is equivalent to the more common definition of weak and strong coupling between two coupled systems based on the possibility to resolve the energy anticrossing of the eigenmodes induced, at resonance, by the coupling.

1.2.2 Collective coupling

The phenomenon of superradiance, usually known as Dicke superradiance [27, 44, 45, 46], is basically the drastic enhancement in the spontaneous emission rate of a collection of coherently excited two level systems. This concept has a broad interest, both for fundamental and applied reasons, and it is crucial to almost all the results of this thesis. For this reason I will give here an extremely short introduction on superradiance from a point of view that, while

quite different from the standard textbook definition, is specifically useful for the present work. Superradiance is a consequence of a very basic property of quantum mechanics. If a quantum state $|\psi\rangle$ is identically coupled with N degenerate states $|\phi_j\rangle$ then, applying an unitary transformation on the degenerate subspace $\{|\phi_j\rangle\}$, we can redefine the states in order to have the initial state coupled to a single final state, with a coupling constant $\sqrt{N}$ times bigger than the bare one. The proof of this statement is simple linear algebra. The system Hamiltonian, calling $\hbar\omega$ the energy of the initial state and choosing as zero the energy of the degenerate subspace is

$$H = \hbar\omega|\psi\rangle\langle\psi| + \hbar\Omega\sum_{j=1}^{N}|\psi\rangle\langle\phi_j| + |\phi_j\rangle\langle\psi|. \tag{1.1}$$

Applying to the to the degenerate subspace a linear transformation that maps $\{|\phi_j\rangle\}$ to $\{|\bar{\phi}_j\rangle\}$ such that $|\bar{\phi}_1\rangle = \frac{1}{\sqrt{N}}\sum_j |\phi_j\rangle$ and the other vectors are determined by orthonormality, we obtain

$$\bar{H} = \hbar\omega|\psi\rangle\langle\psi| + \sqrt{N}\hbar\Omega(|\psi\rangle\langle\bar{\phi}_1| + |\bar{\phi}_1\rangle\langle\psi|). \tag{1.2}$$

We see that in the new Hamiltonian there is only one state coupled to the initial one with an enhanced coefficient, while the other $N-1$ are uncoupled and have disappeared from the Hamiltonian.

1.2.3 Bosonic Approximation

The main manifestation of electrons fermionic nature is the existence of Pauli blocking, only one electron can occupy each quantum state at a given time. For an electronic transition between an initial and a final state to be possible we need to have both the initial state full and the final state empty. This means that a collection of N two level systems can only be excited N times before it saturates. For example in a semiconductor, if a significant fraction of valence electrons are pumped into the conduction band, further electrons have a reduced phase space to jump and the light-matter interaction decreases. On the contrary a single bosonic oscillator can absorb an unlimited number of excitations. Given the extreme ease we have in treating bosonic fields, it is tempting, at least as long as we are far from saturation, that is if the number of excitations n is much smaller than N, to approximate the collective excitation of many two level systems with a single bosonic mode.

There is indeed a deeper link between a bosonic field and an ensemble of fermionic transitions. To consider the latter as a boson is substantially the same approximation we make when we say that an atom with an even number of fermions acts as a boson. Formally we can describe a two level system by means of two second-quantized fermionic fields, c_1 and c_2. For example a transition between the first and the second level will be given by the operator $b^\dagger = c_2^\dagger c_1$, that is an electron is annihilated in the first level and is created in the second one. The property of fermionic fields ($c_1^2 = c_2^2 = 0$) assures that such transition is possible only if the first level is full and the second one empty. If we consider a collection of N of such two level systems, indexed by an index j, it is easy to verify that, if $|\psi\rangle$ is a state such that n systems are excited, then on average $\langle\psi|[b_j, b_{j'}^\dagger]|\psi\rangle = \delta_{j,j'} + O(\frac{n}{N})$. That is, the operators b_j, being composed of an even number of fermions have, at low excitation densities, the commutation relations of bosonic fields.

1.2.4 The rotating wave approximation

The rotating wave approximation (RWA) is an approximation scheme consisting of neglecting highly nonresonant (that is quickly oscillating) terms in the Hamiltonian. The RWA is used over almost all the domains of physics, from astronomy to quantum mechanics and permits the exact solution of various otherwise intractable problems.

The breaking of this approximation, or more precisely the physics that emerges if this approximation is not valid, will be an important part of Chapter 2. I will thus take some time here to review the basics of the RWA by analyzing its application to a really simple quantum system.

Let us consider the Hamiltonian of two coupled resonant harmonic oscillators, whose second quantization annihilation operators are a and b, the frequency is ω and the coupling strength Ω. The Hamiltonian is thus

$$H = \hbar\omega(a^\dagger a + b^\dagger b) + \hbar\Omega(a + a^\dagger)(b + b^\dagger). \tag{1.3}$$

Applying the RWA on the system described by Eq. 1.3 means neglecting the terms ab and $a^\dagger b^\dagger$. These terms connect states with a bare energy difference of 2ω and thus their contribution in second order perturbation theory (i.e. to the energy of the ground state) is of the order of

$$\Delta_2 = \frac{\Omega^2}{\omega}. \tag{1.4}$$

If $\omega \gg \Omega$ the effect of *antiresonant* terms is thus suppressed. This is the case in almost all non-driven physical systems. Only in the last few years a number of propositions [47, 48, 26, 25, 33, 34, 32] have been put forward of systems not fulfilling the RWA.

1.3 Physical system

1.3.1 The doped quantum well

A quantum well is a planar heterostructure that quantum confines electrons along the growth axis. This tight confinement strongly influences the density of states of the electrons, that effectively behave as a two dimensional electron gas (2DEG). The confinement in fact splits the electronic Bloch bands into discrete subbands, in Fig. 1.1 it is shown the typical band structure and in-plane dispersion of a quantum well. The electrons are free to move in the plane normal to the growth direction with an effective mass given by the subband dispersion $\hbar\omega_{j,n}(k)$, where $j = v, c$ is the band index, $\mathbf{k}$ is the component of the wavevector in the plane normal to the growth direction and n is an integer giving the subband index. An electronic state in the quantum well will thus be indexed by the two components of the in-plane wavevector k_x and k_y (we will consistently suppose that the growth direction is along the z axis), the band index, the subband index and the spin. The Fermi level of a quantum well, that in an intrinsic semiconductor would be in the gap between the highest energy valence subband and the lowest energy conduction subband, can be easily shifted by doping. This permits to select which of the multiple interband and intersubband transitions is optically active. In the rest of the thesis we will be interested in the coupling of intersubband transitions with light, thus we will consider quantum wells whose Fermi level is between the first and the second conduction subband, even if experimentally other cases are possible [49]. The main interest of considering such transitions is that, due to the parallelness of the conduction subbands and the smallness of the photon wavevector, the 2DEG behave approximately as a collection of two level systems with the same transition frequency. In fact being the photonic wavevector much smaller than the electronic one, photonic induced transitions are almost vertical on the scale of the electronic dispersions of Fig. 1.1. As we have seen in Section 1.2.2 a collection of two level systems coupled to the light can be seen as a single system with a coupling $\sqrt{N}$ times bigger. This is

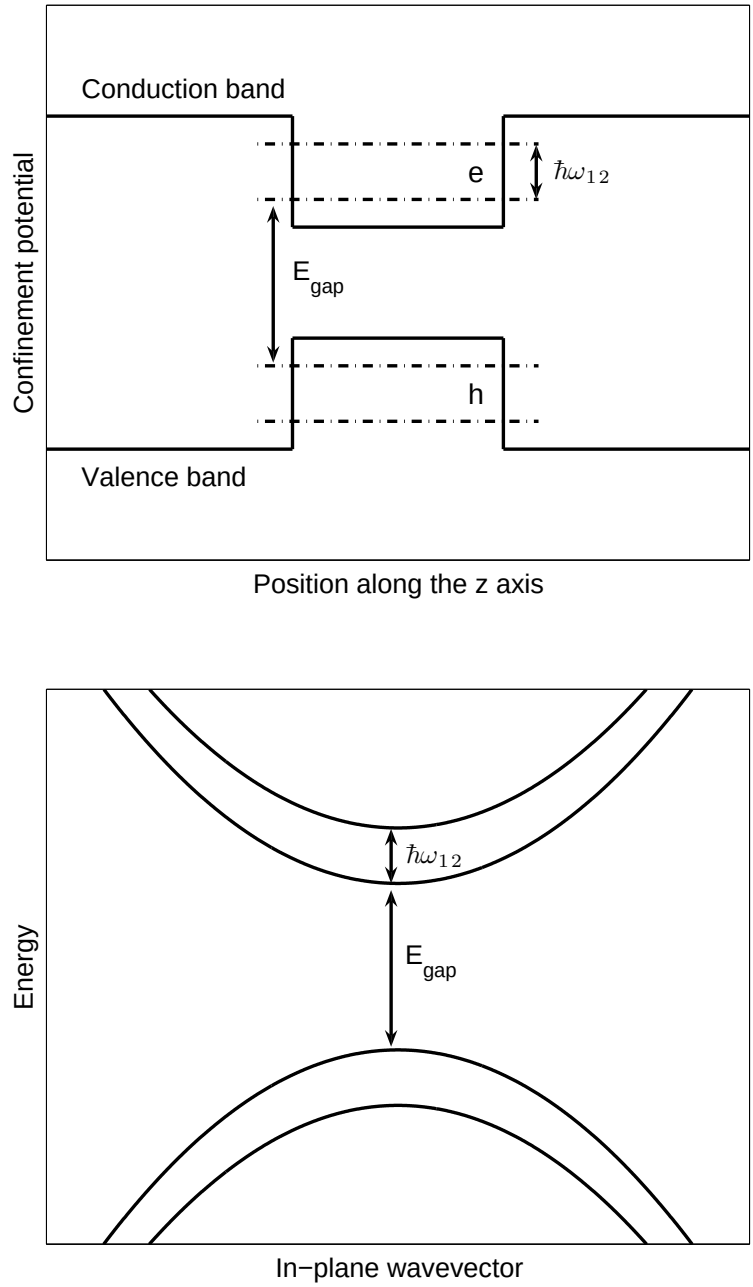

Figure 1.1: Top panel: schema representing the band structure of a semiconductor quantum well. The electronic confinement and the presence of subbands are well visible. Bottom panel: the corresponding band dispersion, as a function of the wavevector in the plane normal to the growth direction.

exactly what happens in the case of intersubband transitions. Only one linear superposition of electronic transitions, called bright intersubband excitation, is coupled to the light field, but with a dipole $\sqrt{N}$ times bigger than the bare one, where N is the number of electrons in the 2DEG. Such dipole is oriented along the z axis, giving a polarization selection rule for intersubband excitations, only Transverse Magnetic (TM) polarized light couple to the quantum well, while Transverse Electric (TE) polarized photons are completely decoupled.

1.3.2 The microcavity

In order to increase the coupling between light and matter, it is favorable to increase the spatial overlap between the photonic modes and the matter excitations. This is at the heart of the so called Purcell effect [2]. In order to increase this overlap it is necessary to confine the photonic mode inside a cavity. A number of different cavity technologies have been devised, spanning different geometries and frequency ranges: from superconducting microwaves [50] to one dimensional transmission lines [51]. In condensed matter systems the interest in increasing the light-matter coupling is not only linked with the possibility to observe interesting new physics [34] but also to the engineering of efficient light emitters [52, 38]. This interest has led to the conception of different kinds of microcavities with planar geometries that can be directly embedded in semiconductor heterostructures. The confinement of the photonic mode can be obtained using dielectric Bragg mirrors, metallic mirrors or even exploiting total internal reflection.

The effect of a planar microcavity is to quantize the photon wavevector along the growth direction. The photonic dispersion is thus given by

$$\omega_{cav,\,j}(q) = \frac{c}{\sqrt{\epsilon_r}}\sqrt{q^2 + q_{z,j}^2}, \tag{1.5}$$

where $q_{z,j}$ is the j-th value of the quantized q_z vector. A typical dispersion is shown in Fig. 1.2.

It is worthwhile to notice the parabolic dispersion around $q = 0$, photons gets an effective mass due to the confinement. In the following we will work in a regime in which the intersubband gap energy $\hbar\omega_{12}$ is resonant with a mode on the first cavity branch. We will thus limit ourselves to consider the first photonic branch, being the others well out of resonance.

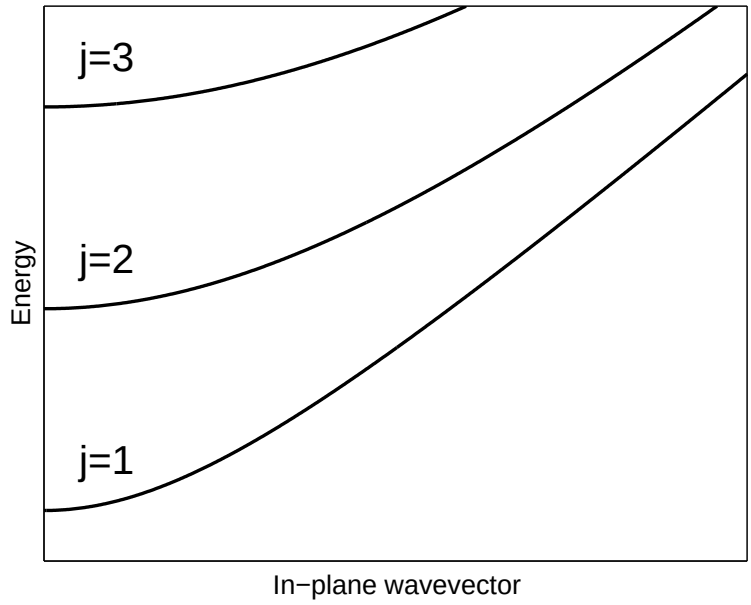

Figure 1.2: Energy dispersion of a planar microcavity as a function of the wavevector in the plane normal to the growth direction. The index j indexes different photonic branches corresponding to different values of the quantized wavevector along the growth direction.

1.3.3 Intersubband polaritons

When the microcavity is resonant with the intersubband transition energy $\hbar\omega_{12}$, due to the strength of the coupling between an intersubband excitation and a microcavity photon, the system can be in the strong coupling regime. In Fig. 1.3 it is shown a typical dispersion of the system resonances as a function of the in-plane wavevector. Dashed lines are the bare resonances of the intersubband transition and of the microcavity photons, while solid lines are the dispersions of normal modes of the coupled system. At resonance, the anticrossing between the dispersions of the two normal modes is clearly visible. In this regime the new eigenmodes of the system are called intersubband polaritons. The experimental observation of their resonances has been reported for the first time in [24]. Their data with the anticrossing of reflectance resonances can be found in Fig. 1.4. Another, more recent observation of polariton reso-

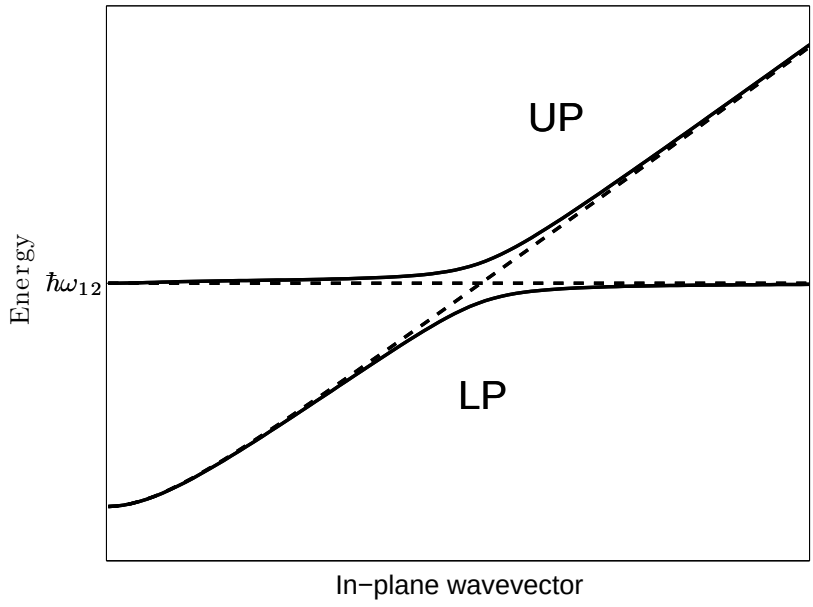

Figure 1.3: Energy dispersions of excitations in a microcavity embedded quantum well as a function of the wavevector in the plane normal to the growth direction. Dashed lines represent the dispersion of the intersubband excitation (dispersionless) and of the bare microcavity photon mode. Solid lines represent the upper (UP) and lower (LP) polariton branches.

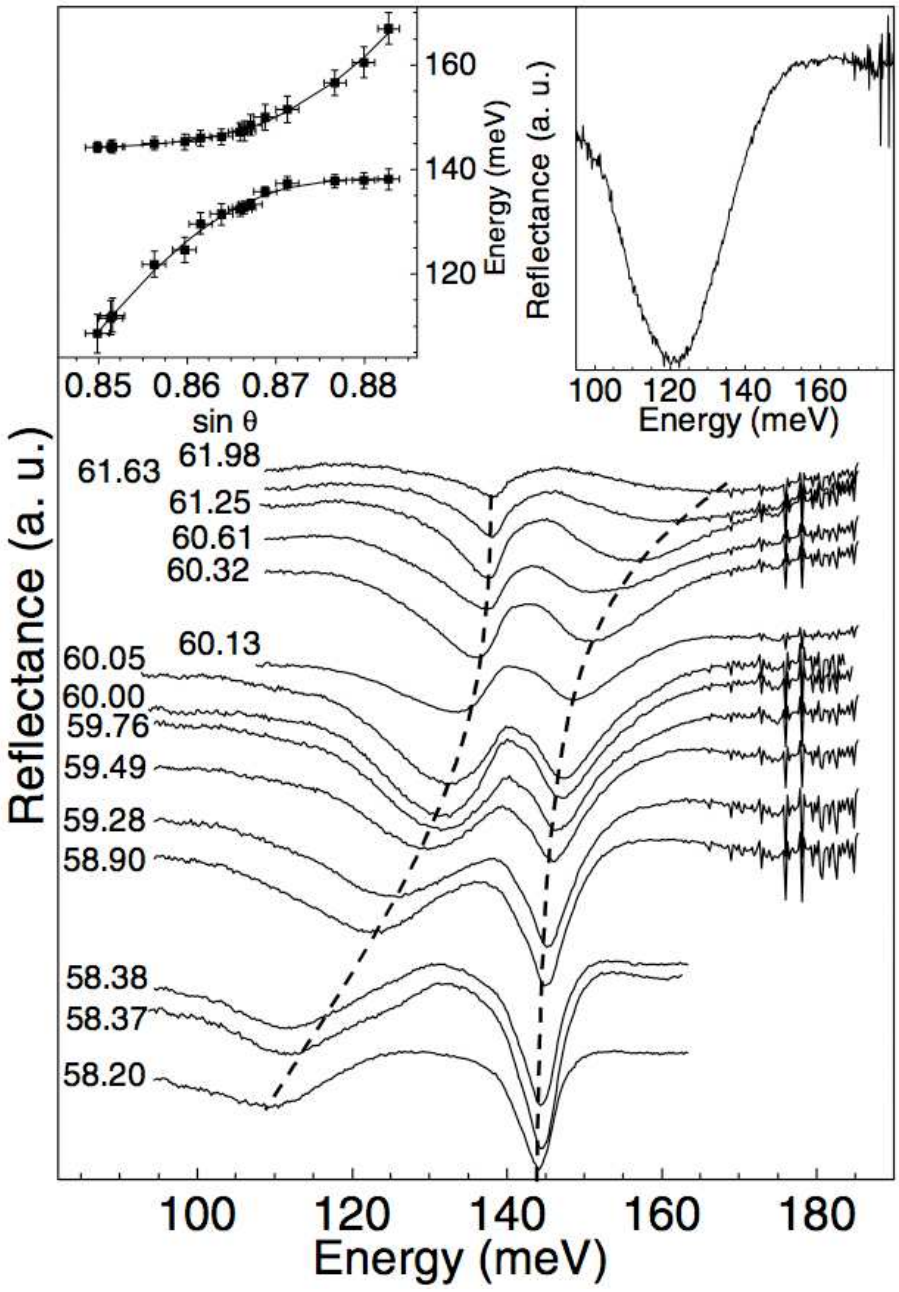

Figure 1.4: Experimental data from Ref. [24]. The reflectance spectra for various angles show clearly the level anticrossing. This is the first experimental observation of intersubband polariton dispersions.

nances in a quantum cascade structure is shown in Fig. 1.5. In Fig. 1.6 there is a sketch of the mesa etched sample and of the corresponding band diagram (Both images are from Refs. [53] and [39]).

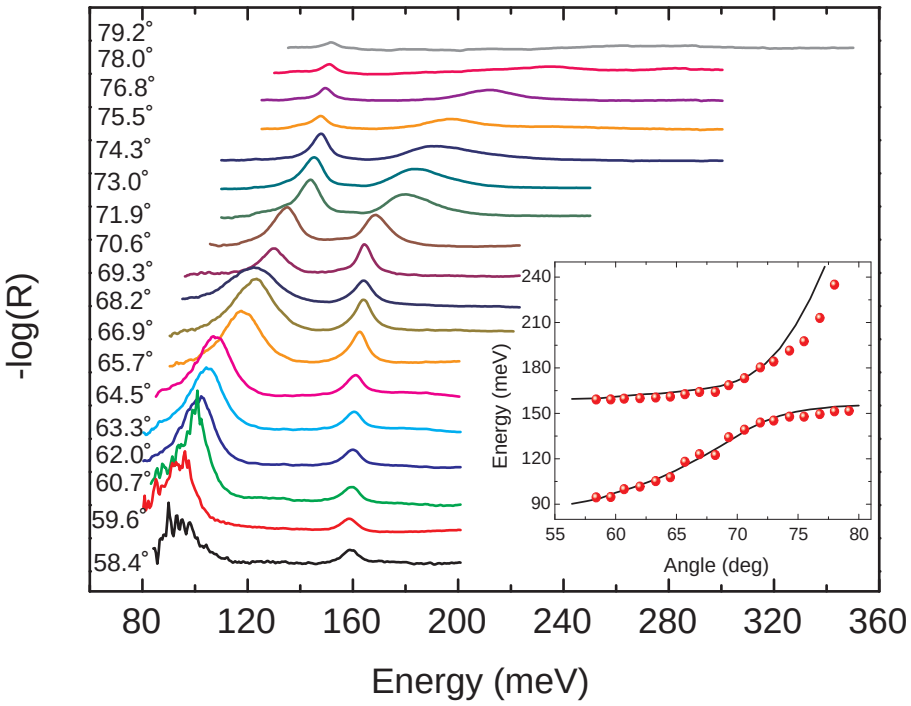

Figure 1.5: Reflectivity spectra as a function of the incident angle. In the inset the position of the peaks (full dots) is compared with the theoretical results of transfer matrix calculations (line). Image taken from Ref. [39].

1.4 Quantum description

1.4.1 The full Hamiltonian

In order to elaborate a theory of a microcavity embedded two dimensional electron gas, we will need to derive the second quantization Hamiltonian for such system. The quantum fields we need to describe are the microcavity photon field and the electron fields in the first and second subbands. We thus introduce the electron creation fermionic operators in the first and second subband ($c^{\dagger}_{1,\sigma,\mathbf{k}}$ and $c^{\dagger}_{2,\sigma,\mathbf{k}}$), and the bosonic creation operator $a^{\dagger}_{\zeta,\mathbf{q}}$, where σ is the electron spin, ζ the photon polarization, while $\mathbf{k}$ and $\mathbf{q}$ are the in-plane

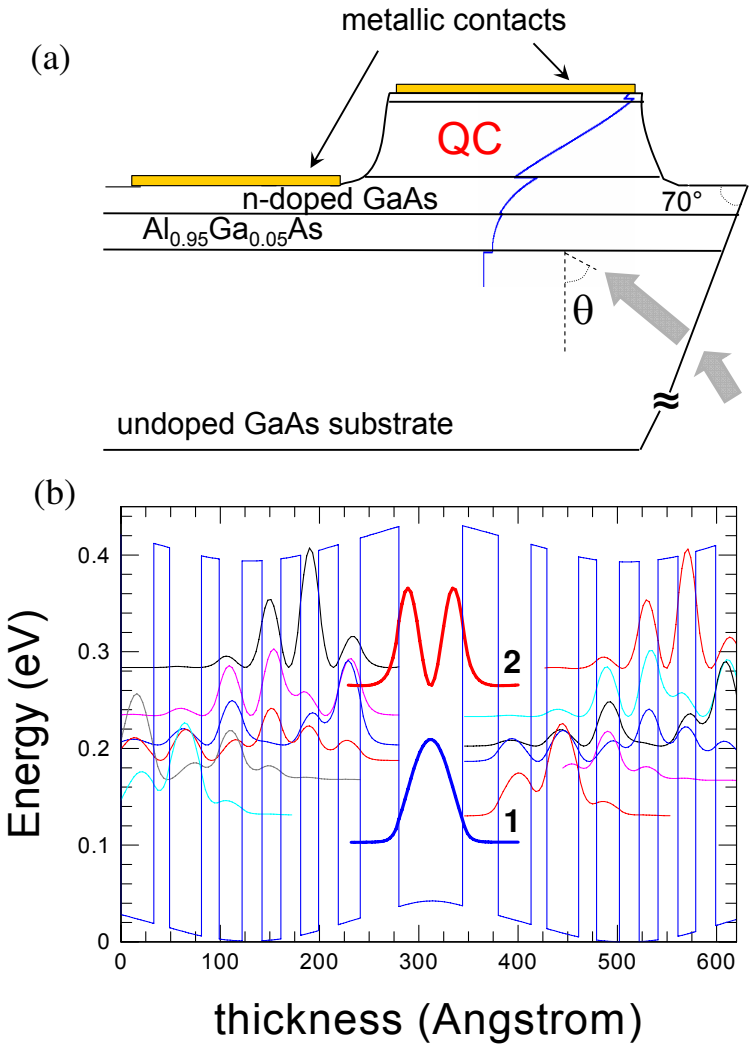

Figure 1.6: Top panel: schema of the mesa etched sample of Ref. [53]. Bottom panel: band diagram of the quantum cascade structure. Images taken from Ref. [53].

wavevectors. Systematically in this thesis, I will use the letters k and q for the electronic and photonic wavevector respectively. This distinction will often be useful due to the smallness of photons wavevectors compared to electronic ones.

The Hamiltonian, whose exact derivation is detailed in Appendix A, is

$$\begin{aligned} H &= \sum_{\mathbf{k}} \hbar\omega_{c,1}(k) c^{\dagger}_{1,\mathbf{k}} c_{1,\mathbf{k}} + \hbar\omega_{c,2}(k) c^{\dagger}_{2,\mathbf{k}} c_{2,\mathbf{k}} \\ &+ \sum_{\mathbf{q}} \hbar\omega_{cav}(q) a^{\dagger}_{\mathbf{q}} a_{\mathbf{q}} + \hbar D(q)(a_{1,-\mathbf{q}} + a^{\dagger}_{1,\mathbf{q}})(a_{1,\mathbf{q}} + a^{\dagger}_{1,-\mathbf{q}}) \\ &+ \sum_{\mathbf{k},\mathbf{q}} \hbar\chi(q)(a_{\mathbf{q}} + a^{\dagger}_{-\mathbf{q}}) c^{\dagger}_{2,\mathbf{k}+\mathbf{q}} c_{1,\mathbf{k}} + \hbar\chi(q)(a_{-\mathbf{q}} + a^{\dagger}_{\mathbf{q}}) c^{\dagger}_{1,\mathbf{k}} c_{2,\mathbf{k}+\mathbf{q}}. \end{aligned} \tag{1.6}$$

The energy dispersions of the two quantum well conduction subbands, shown in Fig. 1.1 as a function of the in-plane wavevector k, are $\hbar\omega_{c,1}(k) = \frac{\hbar^2 k^2}{2m^\star}$ and $\hbar\omega_{c,2}(k) = \hbar\omega_{12} + \frac{\hbar^2 k^2}{2m^\star}$, being $\mathbf{k}$ the electron in-plane wavevector and $m^\star$ the effective mass of the conduction subbands (non-parabolicity is here neglected, see Ref. [54]).

As explained in detail in A, we neglect the electron spin, because all the interactions are spin-conserving. Due to selection rules of intersubband transitions, we omit the photon polarization, which is assumed to be TM. For simplicity, we consider only a photonic branch, which is quasi-resonant with the intersubband transition, while other cavity photon modes are supposed to be off-resonance and can be therefore neglected. Due to the light-matter interaction terms, which are product of three operators, the Hamiltonian in Eq. 1.6 is of formidable complexity, in order to make it tractable, studying different problems we will make various kinds of (controlled) approximations.

1.4.2 The RWA fermionic Hamiltonian

When the light-matter coupling is not too big compared to the intersubband transition frequency, we can safely apply the RWA to the Hamiltonian in Eq. 1.6. This is equivalent to neglect terms in $a^2_{\mathbf{q}}$ that annihilate pairs of photons and terms of the form $a^{\dagger}_{-\mathbf{q}} c^{\dagger}_{2,\mathbf{k}+\mathbf{q}} c_{1,\mathbf{k}}$ that describe an electron jumping from the first to the second subband *emitting* a photon. The resulting Hamiltonian

is thus

$$\begin{aligned} H^{\mathrm{RWA}} &= \sum_{\mathbf{k}} \hbar\omega_{c,1}(k) c^{\dagger}_{1,\mathbf{k}} c_{1,\mathbf{k}} + \hbar\omega_{c,2}(k) c^{\dagger}_{2,\mathbf{k}} c_{2,\mathbf{k}} + \sum_{\mathbf{q}} \hbar[\omega_{cav}(q) + 2D(q)] a^{\dagger}_{\mathbf{q}} a_{\mathbf{q}} \\ &+ \sum_{\mathbf{k},\mathbf{q}} \hbar\chi(q) a_{\mathbf{q}} c^{\dagger}_{2,\mathbf{k}+\mathbf{q}} c_{1,\mathbf{k}} + \hbar\chi(q) a^{\dagger}_{\mathbf{q}} c^{\dagger}_{1,\mathbf{k}} c_{2,\mathbf{k}+\mathbf{q}}. \end{aligned} \tag{1.7}$$

This Hamiltonian, even if it cannot describe regimes of extremely strong couplings, retains all the nonlinearities due to Pauli blocking and can describe both low excited or extremely high excitation regimes. More important for us it retains, contrary to the bosonized Hamiltonian we will see in the next section, the description at the level of the single electron, that is necessary when trying to describe electronic transport.

1.4.3 The bosonic Hamiltonian

The large dopant densities usually used in intersubband polariton experiments (of the order of 10^{12} cm^{-2}) and thus the large number of electrons involved, make the numerical study of Hamiltonian in Eq. 1.6 a formidable task. A way to proceed is to notice that even if a large number of electrons participate in the light-matter interaction, only few degrees of freedom are effectively excited. If we do not bother to lose the possibility to describe the system at the level of single electron, we can thus exploit the techniques developed in Section 1.2.3 and *bosonize* the [55, 56] Hamiltonian in Eq. 1.6. We thus define N bosonic intersubband transition operators as

$$b^{j}_{\mathbf{q}} = \frac{1}{\sqrt{N}} \sum_{\mathbf{k}} \beta^{j}_{\mathbf{k}} c^{\dagger}_{2,\mathbf{k}+\mathbf{q}} c_{1,\mathbf{k}}. \tag{1.8}$$

where $\beta^{1}_{\mathbf{k}} = 1\,\forall\mathbf{k}$ and the other $N-1$ $\beta^{j}_{\mathbf{k}}$ are determined with an orthonormalization procedure.

If we are working in the diluted regime, that is if the number of excitations we wish to treat is much smaller than the number of electrons, it is easy to verify that these operators behave like bosons. If we take the state $|n\rangle$ to be a state with all the electrons in the first subband, except for n that are in the second one, we have

$$\begin{aligned} \langle n|[b^{j}_{\mathbf{q}}, b^{j'\dagger}_{\mathbf{q}'}]|n\rangle &= \delta(\mathbf{q}-\mathbf{q}')\delta_{j,j'} + O(\frac{n}{N}) \\ \langle n|[b^{j}_{\mathbf{q}}, b^{j'}_{\mathbf{q}'}]|n\rangle &= 0. \end{aligned} \tag{1.9}$$

We have thus not only greatly reduced the number of dynamical degrees of freedom, but we have also transformed a cubic Hamiltonian in a quadratic, bosonic one. Again this approximation, as can be seen from Eq. 1.9, is valid only in the diluite regime, where the excitations do not see each other and fermionic saturation effects do not impair intersubband excitations bosonicity. We will see in Chapter 5 how to deal with bosonization at higher excitation densities.

The energy of such intersubband transition excitations can be found by calculating the average value of Hamiltonian over the state $b^{j\,\dagger}_{\mathbf{q}}|F\rangle$, where $|F\rangle = \prod_{k<k_F} c^{\dagger}_{1,\mathbf{k}}|0\rangle$ is the system ground state with all the electrons in the first subband, that we use also as zero of energy and $|0\rangle$ is the vacuum state for the electron and photon modes ($c_{1,\mathbf{k}}|0\rangle = c_{2,\mathbf{k}}|0\rangle = a_{\mathbf{q}}|0\rangle = 0$). We obtain

$$\langle F|b^{j}_{\mathbf{q}} H b^{j\,\dagger}_{\mathbf{q}}|F\rangle = \frac{\hbar}{N}\sum_{\mathbf{k}}[\omega_2(\mathbf{k}+\mathbf{q}) - \omega_1(\mathbf{k})]. \tag{1.10}$$

Given the smallness of the photonic wavevector $\mathbf{q}$ compared to the electronic one $\mathbf{k}$, we can safely consider $\omega_2(\mathbf{k}+\mathbf{q}) - \omega_1(\mathbf{k}) \simeq \omega_{12}$ and thus obtain the bosonic effective Hamiltonian:

$$\begin{aligned} H_{Bos} &= \sum_{\mathbf{q}} \hbar[\omega_{cav}(q) + 2D(q)]a^{\dagger}_{\mathbf{q}}a_{\mathbf{q}} + \sum_{j}\hbar\omega_{12}b^{j\,\dagger}_{\mathbf{q}}b^{j}_{\mathbf{q}} + \hbar\Omega_R(q)(a^{\dagger}_{\mathbf{q}}b^{1}_{\mathbf{q}} + a_{\mathbf{q}}b^{1\,\dagger}_{\mathbf{q}}) \\ &+ \hbar\Omega_R(q)(a_{\mathbf{q}}b^{1}_{-\mathbf{q}} + a^{\dagger}_{\mathbf{q}}b^{1\,\dagger}_{-\mathbf{q}}) + \hbar D(q)(a_{\mathbf{q}}a_{-\mathbf{q}} + a^{\dagger}_{\mathbf{q}}a^{\dagger}_{-\mathbf{q}}). \end{aligned} \tag{1.11}$$

where $\Omega_R(q) = \sqrt{N}\chi(q)$ is the effective vacuum Rabi frequency. It is clear the affinity of transformation in Eq. 1.8 and the superradiant states defined in section 1.2.2. Of the N possible intersubband transitions for a given in-plane wavevector $\mathbf{q}$, only one linear superposition is coupled with the microcavity photon field, with a coupling constant $\sqrt{N}$ times bigger than the coupling constant of a single electron and the other $N-1$ excitations are not coupled at all. We will call the former a *bright intersubband excitation* and the others *dark intersubband excitations*. Being the dark excitations uncoupled, when interested only in optically active excitations, we will drop them out of the Hamiltonian and for simplicity we will call $b_{\mathbf{q}}$ the bright excitation

$$\begin{aligned} H_{Bos} &= \sum_{\mathbf{q}} \hbar[\omega_{cav}(q) + 2D(q)]a^{\dagger}_{\mathbf{q}}a_{\mathbf{q}} + \hbar\omega_{12}b^{\dagger}_{\mathbf{q}}b_{\mathbf{q}} + \hbar\Omega_R(q)(a^{\dagger}_{\mathbf{q}}b_{\mathbf{q}} + a_{\mathbf{q}}b^{\dagger}_{\mathbf{q}}) \\ &+ \hbar\Omega_R(q)(a_{\mathbf{q}}b_{-\mathbf{q}} + a^{\dagger}_{\mathbf{q}}b^{\dagger}_{-\mathbf{q}}) + \hbar D(q)(a_{\mathbf{q}}a_{-\mathbf{q}} + a^{\dagger}_{\mathbf{q}}a^{\dagger}_{-\mathbf{q}}). \end{aligned} \tag{1.12}$$

1.4.4 The RWA bosonic Hamiltonian

If together will all the conditions to be able to use Hamiltonian in Eq. 1.12, we have also a ratio $\frac{\Omega_R}{\omega_{12}}$ small enough for being in the RWA regime, we can apply the RWA to Hamiltonian in Eq. 1.12. This means to neglect terms that creates or annihilates pairs of excitations. The resulting Hamiltonian is thus

$$H_{Bos}^{\mathrm{RWA}} = \sum_{\mathbf{q}} \hbar[\omega_{cav}(q) + 2D(q)]a_{\mathbf{q}}^{\dagger}a_{\mathbf{q}} + \hbar\omega_{12}b_{\mathbf{q}}^{\dagger}b_{\mathbf{q}} + \hbar\Omega_R(q)(a_{\mathbf{q}}^{\dagger}b_{\mathbf{q}} + a_{\mathbf{q}}b_{\mathbf{q}}^{\dagger}). \tag{1.13}$$

Chapter 2

Quantum vacuum radiation phenomena

2.1 Introduction

One of the better known predictions of quantum theory is that the empty space is filled with the vacuum energy of the zero-point fluctuations of the quantum electromagnetic field. This zero-point energy is not measurable in empty space, but if we introduce boundary conditions that make its density inhomogeneous, we can in principle measure the resulting force. In the static case such inhomogeneous zero-point energy gives rise to the so called Casimir force , an usually attractive (but sometime repulsive [57]) force between two conducting bodies in the vacuum. The Casimir effect has been measured with great precision in a number of different experimental setups [58, 59, 60].

If the boundary conditions are time-varying a new class of phenomena arises, in which the zero-point fluctuations of the electromagnetic field are transformed into real photons. This effect is often referred to as dynamical Casimir effect [35]. Theoretical predictions show that a conducting plate, nonuniformly accelerated in the vacuum, can emit (see Fig. 2.1 for a pictorical visualization of the phenomenon). This emission is due to vacuum fluctuations that exert on the plate a sort of viscous friction that slows it down. Mechanical energy is then dissipated in the environment as propagating photon pairs. The radiation generated by a time-modulation of the quantum vacuum is a very general and fascinating phenomenon, bearing various analogies with the Unruh-Hawking radiation [36, 61] in the curved space-time around a black hole. However, contrary to the static case, dynamic effects due to the modulation of

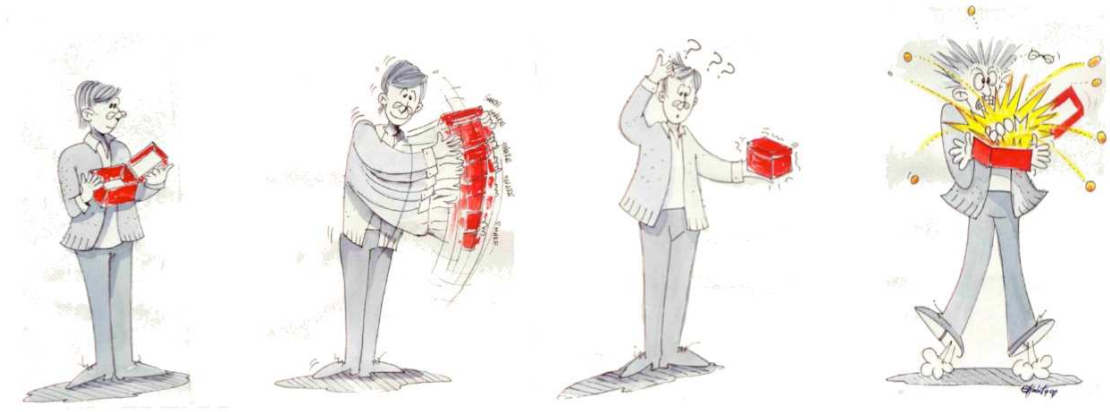

Figure 2.1: An artist view of the dynamical Casimir effect, by G. Ruoso.

the quantum vacuum have not yet been observed due to the extremely small number of photons emitted for realistic mechanical accelerations. Even using as accelerating plates the vibrating mirrors of high-finesse Fabry-Pérot resonators [62, 63], in order to enhance the intensity of the quantum vacuum radiation, the predicted emitted radiation is very challenging to be measured. A big step toward an experimental verification of the dynamical Casimir effect has been the idea to consider, instead of a cavity with moving mirrors, a fixed cavity with a time-varying refractive index [64, 65]. From the point of view of a cavity photon, what is important is the effective optical length of the cavity, given by the bare cavity length times the refractive index of the cavity dielectric spacer. Modulating the refractive index at high frequency anyway is much simpler than modulating the cavity length, as we have to deal only with the inertia of the dielectric properties, not with the mechanical motion of the whole solid. Still, the very weak intensity of the emitted radiation has so far hindered its experimental observation. Working on this line, we discovered that in the case of microcavity embedded quantum wells, the unprecedented strength of the light-matter coupling permits to have a Casimir radiation strong enough to be measured with present day technologies. We were able to estimate both the intensity and the spectral signature of emitted radiation [34]. An experimental realization of our proposal has been built up and has recently given some results, which are very promising towards the observation of quantum vacuum radiation [37]. Other groups are also working on the idea of exploiting ultra-strong light-matter coupled systems for dynamical Casimir experiment.

Especially interesting are experiments exploiting superconducting transmission lines [66] and qubits [47, 26].

2.2 Quantum vacuum radiation as ultra-strong coupling effect

Quantum vacuum radiation, that is the emission of light from a time-dependent vacuum, is often theoretically described (and calculated) as the consequence of field quantization with time-dependent boundaries [65]. In our case we will adopt a different point of view that, while allowing us to calculate all the system observables, will give a much more intuitive understanding of the process and underline the importance of working in a regime of ultra-strong light-matter interaction.

Let us consider a microcavity embedding multiple quantum wells, as described in Section 1.3. The photon emission is due to the light-matter coupling, so that only light-coupled matter excitations play a role. In order to describe the system we will thus use the bosonic Hamiltonian of Section 1.4.3

$$\begin{aligned} H_{bos} &= \sum_{\mathbf{q}} \hbar[\omega_{cav}(q) + 2D(q)] a^{\dagger}_{\mathbf{q}} a_{\mathbf{q}} + \hbar\omega_{12} b^{\dagger}_{\mathbf{q}} b_{\mathbf{q}} + \hbar\Omega_R(q)(a^{\dagger}_{\mathbf{q}} b_{\mathbf{q}} + a_{\mathbf{q}} b^{\dagger}_{\mathbf{q}}) \\ &+ \hbar\Omega_R(q)(a_{\mathbf{q}} b_{-\mathbf{q}} + a^{\dagger}_{\mathbf{q}} b^{\dagger}_{-\mathbf{q}}) + \hbar D(q)(a_{\mathbf{q}} a_{-\mathbf{q}} + a^{\dagger}_{\mathbf{q}} a^{\dagger}_{-\mathbf{q}}). \end{aligned} \tag{2.1}$$

As all the terms in the Hamiltonian are bilinear in the field operators, it can be exactly diagonalized through a Hopfield-Bogoliubov transformation [55]. Introducing the Lower Polariton (LP) and Upper Polariton (UP) annihilation operators

$$p_{j,\mathbf{q}} = w_{j,q}\ a_{\mathbf{q}} + x_{j,q}\ b_{\mathbf{q}} + y_{j,q}\ a^{\dagger}_{-\mathbf{q}} + z_{j,q}\ b^{\dagger}_{-\mathbf{q}}\ , \tag{2.2}$$

where $j \in \{LP, UP\}$ we can thus cast the Hamiltonian in the diagonal form

$$H_{bos} = E_G + \sum_{j\in\{LP,UP\}} \sum_{\mathbf{q}} \hbar\omega_{j,k}\ p^{\dagger}_{j,\mathbf{q}} p_{j,\mathbf{q}}. \tag{2.3}$$

The values of the polariton frequencies, obtained diagonalizing Hamiltonian H_{bos} for different values of $\Omega_R(q)/\omega_{12}$ are shown in Fig. 2.2. From Eq. 2.2 we see that the annihilation operator of a polariton is a linear combination of annihilation and creation operators of intersubband excitations and microcavity photons. The fact of having here both creation *and* annihilation operators is of fundamental importance. It is easy to verify that if $|0\rangle$ is the ground state

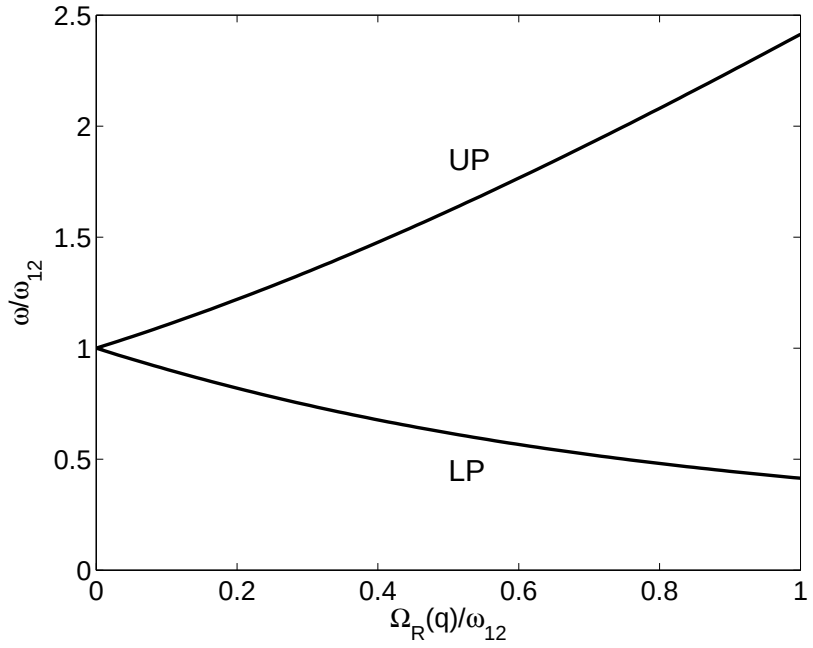

Figure 2.2: Normalized polariton frequencies $\omega_{LP,q}/\omega_{12}$ and $\omega_{UP,q}/\omega_{12}$ as a function of $\Omega_R(q)/\omega_{12}$. The calculation has been performed with $\mathbf{q}$ such that $\omega_{cav}(q) + 2D(q) = \omega_{12}$. See Ref. [25].

for the uncoupled microcavity-quantum wells system, defined by the relation $a_{\mathbf{q}}|0\rangle = b_{\mathbf{q}}|0\rangle = 0$, then $p_{j,\mathbf{q}}|0\rangle \neq 0$. That is the ground state of the coupled system is different from the one of the uncoupled system. If instead of Hamiltonian H_{bos} we would have used the bosonic RWA Hamiltonian of Section 1.4.4 (that is H_{bos} without terms composed of two annihilation or two creation operators), annihilation and creation operators would have been decoupled. In that case we would have $p_{j,\mathbf{q}}|0\rangle = 0$. *Antiresonant terms, which are relevant in the ultra-strong coupling regime, change the quantum ground state.* The squared norm of the coefficients of the Hopfield-Bogoliubov transformation in Eq. 2.2 are shown in Fig. 2.3. Only in the ultra-strong coupling regime, y and z coefficients, that couple annihilation and creation operators, have non-negligible values. We thus introduce the polaritonic vacuum state $|G\rangle$, defined by $p_{j,\mathbf{q}}|G\rangle = 0$. From Eq. 2.2 we can calculate the expectation value of the number of photons in this state

$$\langle G|a^{\dagger}_{\mathbf{q}}a_{\mathbf{q}}|G\rangle \;=\; |y_{LP,q}|^2 + |y_{UP,q}|^2. \tag{2.4}$$

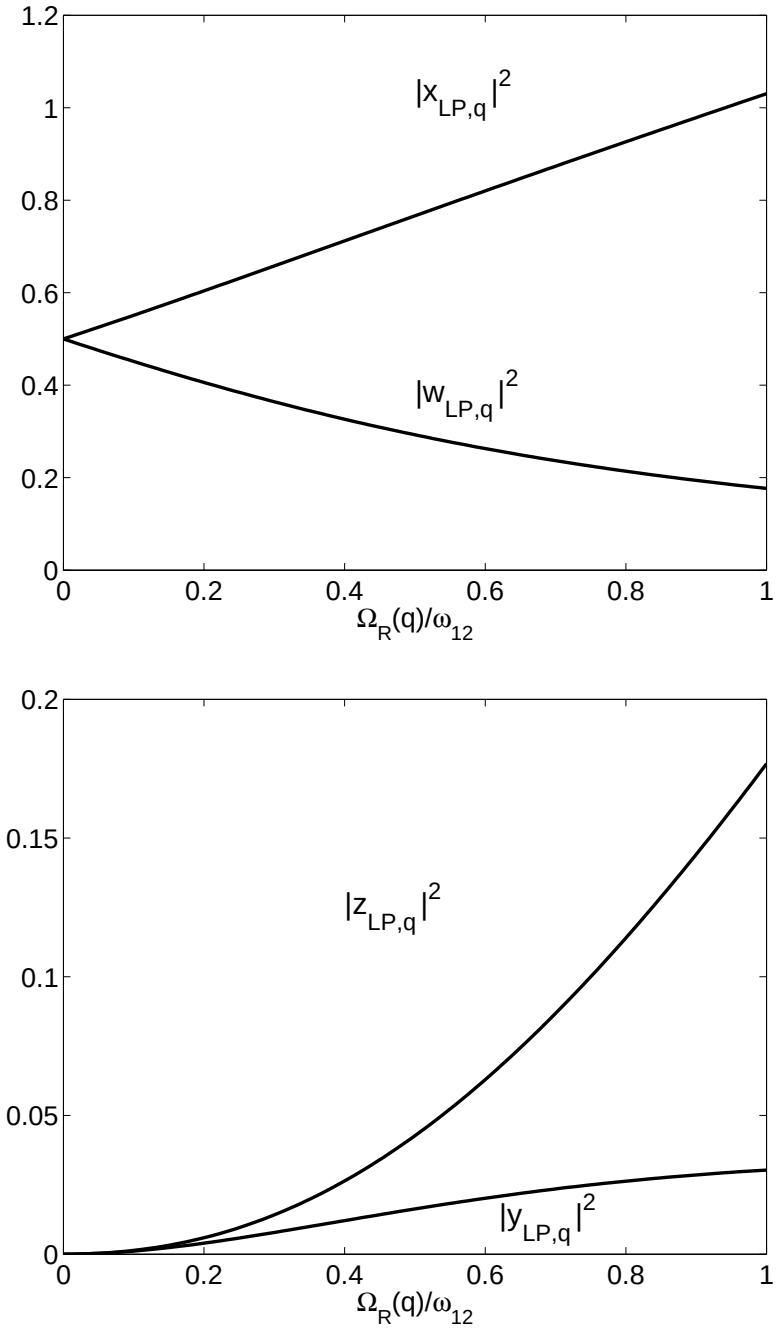

Figure 2.3: Mixing fractions for the Lower Polariton (LP) mode as a function of $\Omega_R(q)/\omega_{12}$. The calculation has been performed with $\mathbf{q}$ such that $\omega_{cav}(q) + 2D(q) = \omega_{12}$. The Upper Polariton (UP) fractions (not shown) are simply $|w_{UP,q}| = |x_{LP,q}|$, $|x_{UP,q}| = |w_{LP,q}|$, $|y_{UP,q}| = |z_{LP,q}|$, $|z_{UP,q}| = |y_{LP,q}|$. See Ref. [25].

This quantity can be quickly estimated from Fig. 2.3. In the ground state of the polaritonic system there is a finite population of *virtual* photons. These photons are *virtual* because, in absence of any time-dependent perturbation, they cannot escape from the cavity.

Now we can imagine a gedanken experiment in which our system is prepared in its ground state $|G\rangle$ and in some way, at the time $t = 0$, we completely and instantly switch off the light-matter interaction (see Fig. 2.4). Being the change non-adiabatic the system will be at the time $t = 0^+$, still in the state $|G\rangle$, that now it is not anymore the ground state. Therefore, it is now an excited state and contains a finite and real photon population. Supposing the system coupled to an external reservoir, it will relax to its real ground state $|0\rangle$, emitting the exceeding energy as quantum vacuum radiation. A non-adiabatic change of the light-matter coupling can thus lead to the emission of photons out of the vacuum. Following Ref. [25] we can give a rough estimate of the number of emitted photons in this gedanken experiment, supposing that all the *virtual* photons are emitted outside the cavity. The number of photon states (per unit area) in the two dimensional momentum volume $d^2\mathbf{q}$ is simply $d^2\mathbf{q}/(2\pi)^2$. Hence the differential density of photons (per unit area) in the two dimensional momentum volume $d^2\mathbf{q}$ is

$$d\rho_{phot} = \frac{d^2\mathbf{q}}{(2\pi)^2}\langle G|a^\dagger_{\mathbf{q}}a_{\mathbf{q}}|G\rangle, \tag{2.5}$$

where the photon number $\langle G|a^\dagger_{\mathbf{q}}a_{\mathbf{q}}|G\rangle$ in the ground state is given by Eq. 2.4. Rewriting Eq. 2.5 as a function of the propagation angle θ ($q(\theta) = q_z \tan(\theta)$) we find that, for the resonance angle such that $\omega_{cav}(q(\theta_{res})) + 2D(q) = \omega_{12}$ we have

$$\frac{d\rho_{phot}}{d\theta} = \frac{\omega_{12}^2\epsilon_r}{2\pi c^2}\tan(\theta_{res})\langle G|a^\dagger_{\mathbf{q}}a_{\mathbf{q}}|G\rangle. \tag{2.6}$$

To give a numerical application of Eq. 2.6, we can consider the following values, taken from Ref. [37]: $\hbar\omega_{12} = 113$ meV, a resonance angle $\theta_{res} = 65°$ and $\hbar\Omega_{R,q(\theta_{res})} = 10$ meV. For these parameters, Eq. 2.6 gives the differential photon density $\frac{d\rho_{phot}}{d\theta} \simeq 2.3 \times 10^9 m^{-2} rad^{-1}$. We will use this reference value later as useful benchmark to test the theory and numerical methods developed in the following sections.

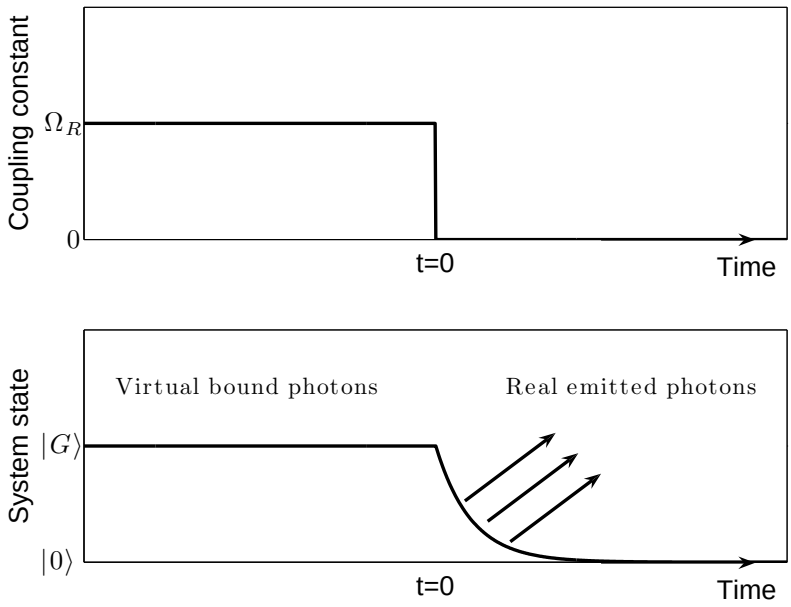

Figure 2.4: Pictorical representation of the gedanken experiment discussed in Section 2.2. The system is initially prepared in its ground state $|G\rangle$, with a vacuum Rabi frequency $\Omega_R(q)$. At the time $t = 0$, the light-matter coupling is completely and abruptly switched off. Being the change non-adiabatic, the system at the time $t = 0^+$ is still in the state $|G\rangle$, that now is not anymore the ground state and has thus (by definition) an energy bigger than the ground state. It will relax to its new ground state $|0\rangle$ (the standard vacuum), emitting the exceeding energy as quantum vacuum radiation.

2.3 Formal theory

The gedanken experiment presented in the previous section showed us that we have to expect the emission of photons when the coupling constant is non-adiabatically modulated in time. In order to fully grasp the problem, we have to build up a quantitative theory capable of calculating the emitted radiation for an arbitrary time modulation of the coupling constant $\Omega_R(q)(t)$, accounting for the coupling with the environment. We need to consider the coupling of the system with an environment for a two-fold reason. On one side the intra-cavity fields, both matter and light, are not observable by themselves. What we can observe are the photons that leak out of the cavity due to the non-perfect reflectivity of the mirrors. On the other side the environment causes fluctuation and dissipation phenomena we have to consider in order to quantitatively model a real experiment.

We will consider a generic time varying vacuum Rabi frequency, composed of a fixed as well as a time dependent part:

$$\Omega_R(q,t) = \bar{\Omega}_R(q) + \Omega_{R,q}^{mod}(t). \tag{2.7}$$

We can take care of the coupling to the environment by using a generalized quantum Langevin formalism. All the details of the derivation can be found in Appendix B. The important point is that we can *trace out* the environment and obtain a self consistent quantum Langevin equation for the intra-cavity fields $a_{\mathbf{q}}$ and $b_{\mathbf{q}}$ only. The effect of the environment will all be contained in a causal memory kernel (making the dynamics non-Markovian) and in a Langevin force term due to the environment-induced fluctuations. The Langevin equations for the system thus read

$$\begin{aligned} \frac{da_{\mathbf{q}}}{dt} &= -\frac{i}{\hbar}[a_{\mathbf{q}}, H_{bos}] - \int dt' \Gamma_{cav,q}(t-t') a_{\mathbf{q}}(t') + F_{cav,\mathbf{q}}(t), \\ \frac{db_{\mathbf{q}}}{dt} &= -\frac{i}{\hbar}[b_{\mathbf{q}}, H_{bos}] - \int dt' \Gamma_{12,q}(t-t') b_{\mathbf{q}}(t') + F_{12,\mathbf{q}}(t), \end{aligned} \tag{2.8}$$

where $\Gamma_{cav,q}(t)$ and $\Gamma_{12,q}(t)$ are the memory kernels associated with the cavity photon and matter fields and $F_{cav,\mathbf{q}}(t)$ and $F_{12,\mathbf{q}}(t)$ are the respective Langevin force operators. Real and imaginary parts of $\Gamma_{cav,q}(t)$ and $\Gamma_{12,q}(t)$ are linked by Kramers-Kroning relations, the real parts give an effective damping while the imaginary parts cause an energy shift due to the interactions. The expression of these quantities as a function of the environment parameters can be found in Appendix B. What is important to know here is that the real part of the

Fourier transform of the memory kernels $\tilde{\Gamma}_{cav,q}(\omega)$ and $\tilde{\Gamma}_{12,q}(\omega)$ are directly linked with the density of states in the environment with energy $\hbar\omega$. Having the excitation modes in the environment all a positive energy we have

$$\Re(\tilde{\Gamma}_{cav,q}(\omega<0)) = \Re(\tilde{\Gamma}_{12,q}(\omega<0)) = 0. \tag{2.9}$$

In other words, the damping occurs only at positive frequencies. In order to solve this system of equations it is useful to pass in Fourier space in order to get rid of the convolution product due to the non-Markovian dynamics. Anyway the resulting equations will not be local in frequency, because of the time dependency of the vacuum Rabi frequency. It is convenient to define the following vectors for the Fourier transformed intra-cavity fields and Langevin forces:

$$\tilde{\mathfrak{a}}^r_{\mathbf{q}}(\omega) \equiv \begin{pmatrix} \tilde{a}_{\mathbf{q}}(\omega) \\ \tilde{b}_{\mathbf{q}}(\omega) \\ \tilde{a}^\dagger_{-\mathbf{q}}(-\omega) \\ \tilde{b}^\dagger_{-\mathbf{q}}(-\omega) \end{pmatrix}, \quad \tilde{\mathfrak{F}}^r_{\mathbf{q}}(\omega) \equiv \begin{pmatrix} \tilde{F}_{cav,\mathbf{q}}(\omega) \\ \tilde{F}_{12,\mathbf{q}}(\omega) \\ \tilde{F}^\dagger_{cav,-\mathbf{q}}(-\omega) \\ \tilde{F}^\dagger_{12,-\mathbf{q}}(-\omega) \end{pmatrix}. \tag{2.10}$$

We will moreover introduce two different Hopfield 4×4 matrices. The first, $\mathfrak{M}_{q,\omega}$, groups all the time independent terms and the second, $\mathfrak{M}^{mod}_{q,\omega}$, all the terms due to the time-modulation of the vacuum Rabi frequency :

$$\mathfrak{M}_{q,\omega} = \begin{pmatrix} \omega_{cav}(q)+2D(q)-\omega-i\tilde{\Gamma}_{cav,q}(\omega) & \Omega_R(q) & 2D(q) & \Omega_R(q) \\ \Omega_R(q) & \omega_{12}-\omega-i\tilde{\Gamma}_{12,q}(\omega) & \Omega_R(q) & 0 \\ -2D(q) & -\Omega_R(q) & -\omega_{cav}(q)-2D(q)-\omega-i\tilde{\Gamma}^*_{cav,q}(-\omega) & -\Omega_R(q) \\ -\Omega_R(q) & 0 & -\Omega_R(q) & -\omega_{12}-\omega-i\tilde{\Gamma}^*_{12,q}(-\omega) \end{pmatrix}, \tag{2.11}$$

$$\mathfrak{M}^{mod}_{q,\omega} = \begin{pmatrix} 2\tilde{D}_q(\omega) & \tilde{\Omega}^{mod}_{R,q}(\omega) & 2\tilde{D}_q(\omega) & \tilde{\Omega}^{mod}_{R,q}(\omega) \\ \tilde{\Omega}^{mod}_{R,q}(\omega) & 0 & \tilde{\Omega}^{mod}_{R,q}(\omega) & 0 \\ -2\tilde{D}_q(\omega) & -\tilde{\Omega}^{mod}_{R,q}(\omega) & -2\tilde{D}_q(\omega) & -\tilde{\Omega}^{mod}_{R,q}(\omega) \\ -\tilde{\Omega}^{mod}_{R,q}(\omega) & 0 & -\tilde{\Omega}^{mod}_{R,q}(\omega) & 0 \end{pmatrix}. \tag{2.12}$$

In this way the Fourier transform of the system in Eq. B.8, can be written in the simple matricial form:

$$\int_{-\infty}^{\infty} d\omega' \sum_s (\mathfrak{M}^{rs}_{q,\omega'}\delta(\omega-\omega') + \mathfrak{M}^{mod\,rs}_{q,\omega-\omega'})\tilde{\mathfrak{a}}^s(\omega')_{\mathbf{q}} = -i\tilde{\mathfrak{F}}^r_{\mathbf{q}}(\omega). \tag{2.13}$$

We can see explicitly from Eq. 2.13 that the $\mathfrak{M}^{mod}_{q,\omega}$ matrix containing the time modulation of the vacuum Rabi frequency couples different frequencies between them, making the system of equations nonlocal in frequency space. If we define

$$\mathfrak{M}^{rs}_q(\omega,\omega') \equiv \mathfrak{M}^{rs}_{q,\omega'}\delta(\omega-\omega') + \mathfrak{M}^{mod\,rs}_{q,\omega-\omega'}, \tag{2.14}$$

we can rewrite Eq. 2.13 in a more compact form:

$$\int_{-\infty}^{\infty} d\omega' \sum_s \mathfrak{M}^{rs}_q(\omega,\omega')\tilde{\mathfrak{a}}^s_{\mathbf{q}}(\omega') = -i\tilde{\mathfrak{F}}^r_{\mathbf{q}}(\omega). \tag{2.15}$$

In the following we will call $\mathfrak{G}^{rs}_q(\omega,\omega')$ the inverse of $\mathfrak{M}^{rs}_q(\omega,\omega')$. By definition

$$\int_{-\infty}^{\infty} d\omega' \sum_s \mathfrak{G}^{rs}_q(\omega,\omega')\mathfrak{M}^{st}_q(\omega',\omega'') \equiv \delta_{rt}\delta(\omega-\omega''). \tag{2.16}$$

We can thus formally solve Eq. 2.15 as:

$$\tilde{\mathfrak{a}}^r_{\mathbf{q}}(\omega) = -i\int_{-\infty}^{\infty} d\omega' \sum_s \mathfrak{G}^{rs}_q(\omega,\omega')\tilde{\mathfrak{F}}^s_{\mathbf{q}}(\omega'). \tag{2.17}$$

Therefore, we have solved, at least formally, the problem of calculating the intra-cavity photon field with an arbitrary time modulation of the vacuum Rabi frequency, fully accounting for the coupling with the environment. Now we would like to calculate the field emitted outside the cavity. As shown in Appendix A, the spectrum of the photonic field emitted outside the cavity can be calculated as a function of the intra-cavity photonic field $\tilde{a}_{\mathbf{q}}(\omega)$ (supposing the extra-cavity field initially in its vacuum state) as

$$S_q(\omega) = \frac{1}{\pi}\Re(\tilde{\Gamma}_{cav,q}(\omega))\langle\tilde{a}^\dagger_{\mathbf{q}}(\omega)\tilde{a}_{\mathbf{q}}(\omega)\rangle. \tag{2.18}$$

Inserting Eq. 2.17 into Eq. 2.18 we obtain:

$$S_q(\omega) = \frac{1}{\pi}\Re(\tilde{\Gamma}_{cav,q}(\omega))\int_{-\infty}^{\infty}\int_{-\infty}^{\infty} d\omega d\omega' \sum_{rs} \mathfrak{G}^{*1r}_q(\omega_{q,\mathbf{q}},\omega)\mathfrak{G}^{1s}_q(\omega_{q,\mathbf{q}},\omega')\langle\tilde{\mathfrak{F}}^\dagger_{\mathbf{q}}(\omega)^r\tilde{\mathfrak{F}}_{\mathbf{q}}(\omega')^s\rangle. \tag{2.19}$$

In Appendix B we calculated the average values for quadratic forms of Langevin forces as

$$\langle \tilde{\mathfrak{F}}^{\dagger}_{\mathbf{q}}(\omega)^r \tilde{\mathfrak{F}}_{\mathbf{q}}(\omega')^s \rangle = 4\pi\delta(\omega-\omega')\delta_{r,s}[\delta_{r,3}\Re(\tilde{\Gamma}_{cav,-\mathbf{q}}(-\omega)) + \delta_{r,4}\Re(\tilde{\Gamma}_{12,-\mathbf{q}}(-\omega))]. \tag{2.20}$$

Exploiting Eqs. 2.19 and 2.20, we can put the result in its final form:

$$\begin{aligned} S_q(\omega) &= 4\Re(\tilde{\Gamma}_{cav,\mathbf{q}}(\omega)) \int_{-\infty}^{\infty} d\omega' |\mathfrak{G}^{13}_{\mathbf{q}}(\omega,\omega')|^2 \Re(\tilde{\Gamma}_{cav,\mathbf{q}}(-\omega')) \\ &+ |\mathfrak{G}^{14}_{\mathbf{q}}(\omega,\omega')|^2 \Re(\tilde{\Gamma}_{12,\mathbf{q}}(-\omega')). \end{aligned} \tag{2.21}$$

It is interesting to notice that if we have no modulation $\mathfrak{M}^{rs}_q(\omega,\omega')$ is proportional to $\delta(\omega-\omega')$ and so is its inverse $\mathfrak{G}_q$. Eq. 2.21 then tells us that $S_q(\omega) \propto \Re(\tilde{\Gamma}_{cav,\mathbf{q}}(\omega))\Re(\tilde{\Gamma}_{cav,\mathbf{q}}(-\omega))$. From Eq. 2.9 we thus conclude that $S_q(\omega) = 0$. *This shows explicitly that, as expected, in absence of any modulation no photon is emitted out of the cavity.*

2.4 Numerical results

In order to obtain the spectrum of emitted radiation, given by Eq. 2.21, we need to numerically calculate $\mathfrak{G}^{rs}_q(\omega,\omega')$. This does not pose any major technical problem as it is easy to verify that Eq. 2.16 defines $\mathfrak{G}^{rs}_q(\omega,\omega')$ as the inverse of the linear operator $\mathfrak{M}^{rs}_{\mathbf{q}}(\omega,\omega')$. It is thus sufficient to discretize the frequency space on a grid of N_ω points, write down $\mathfrak{M}_{\mathbf{q}}$ as a $4N_\omega \times 4N_\omega$ matrix and invert it.

At first, we applied our theory to the case of a periodic sinusoidal modulation, in order to be able to study the emission spectra as a function of only two parameters, the amplitude of the modulation $\Delta\Omega_R(q)$ and its frequency ω_{mod}. We thus consider a vacuum Rabi frequency of the form:

$$\Omega_R(q,t) = \bar{\Omega}_R(q) + \Delta\Omega_R(q)\sin(t). \tag{2.22}$$

Being the modulation periodic (and thus acting for an infinite time) the relevant quantity to consider is not the spectral density of emitted photons per mode $S_q(\omega)$ but the spectral density of emitted photons per mode and per unit time $dS_q(\omega)/dt$. Integrating it over the whole frequency range we can find the total number of emitted photons per mode per unit time

$$dN^{out}_q/dt = \int_{-\infty}^{\infty} \frac{dS_q(\omega)}{dt} d\omega. \tag{2.23}$$

This is the steady quantum vacuum fluorescence rate. Predictions for the rate dN_q^{out}/dt of emitted photons as a function of the modulation frequency ω_{mod} (in units of ω_{12}) are shown in Fig. 2.5 for the resonant case $\omega_{12} = \omega_{cav}(q) + 2D(q)$ for which the emission is the strongest. Thanks to the ultra-strong coupling regime, the emission intensity however has a moderate **q** dependence, remaining important over a wide anticrossing region. For the sake of simplicity, a frequency-independent damping rate has been considered $\Re\{\tilde{\Gamma}_{cav,q}(\omega > 0)\} = \Re\{\tilde{\Gamma}_{12,q}(\omega > 0)\} = \Gamma$, and the imaginary part has been consistently determined via the Kramers-Kronig relations [33]. Values inspired from recent experiments [24, 67, 68] have been used for the cavity parameters. Representative results are shown in Fig. 2.5. The structures in the integrated spectrum shown in Fig. 2.5 can be identified as resonance peaks when the modulation is phase-matched.

We can effectively consider the dynamical Casimir effect as a parametric

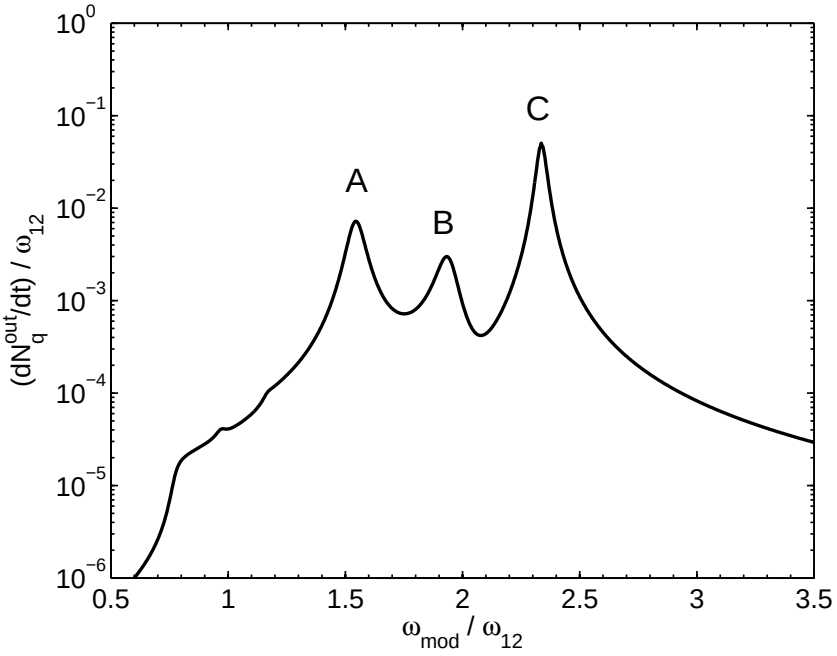

Figure 2.5: Rate of emitted photons dN_q^{out}/dt (in units of ω_{12}) as a function of the normalized modulation frequency ω_{mod}/ω_{12}. Parameters: $(\omega_{cav}(q) + 2D(q))/\omega_{12} = 1$, $\Gamma/\omega_{12} = 0.025$, $\bar{\Omega}_R(q)/\omega_{12} = 0.2$, $\Delta\Omega_R(q)/\omega_{12} = 0.04$. The letters A, B and C indicate three different resonantly enhanced processes.

excitation of the quantum vacuum. As usual for parametric processes [69],

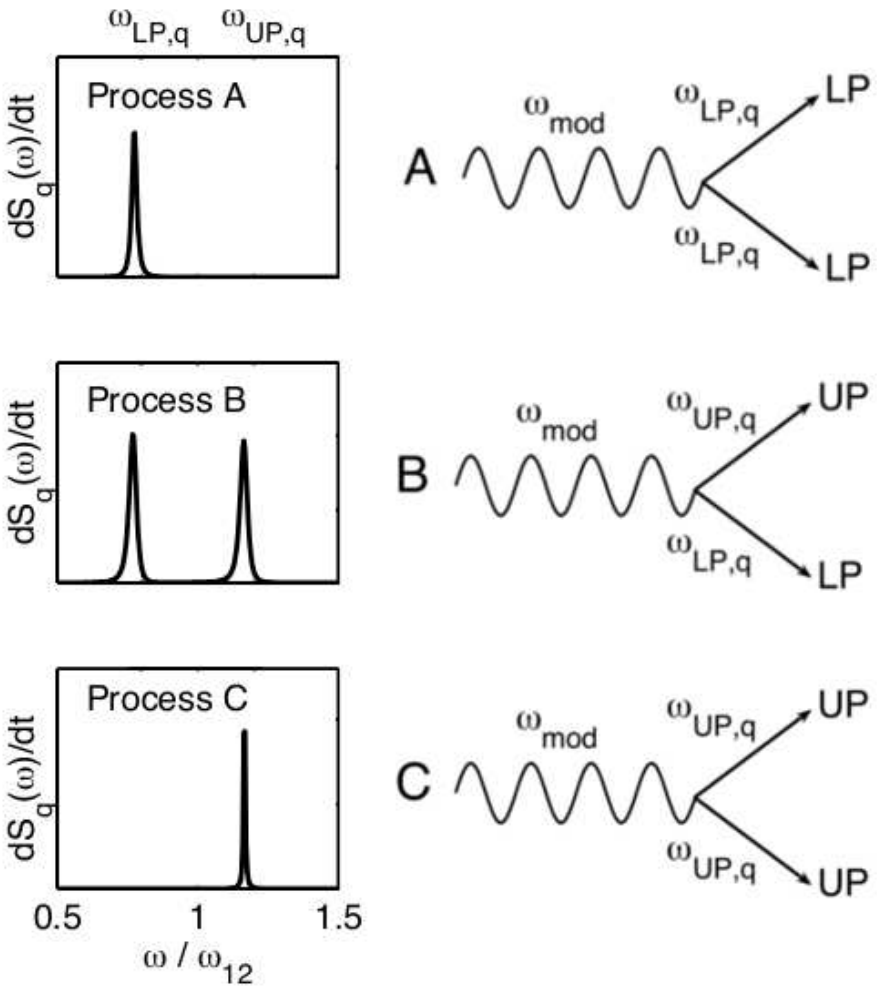

Figure 2.6: On the left are plotted the spectral densities of emitted photons (arb. u.) for the processes A, B and C of Fig. 2.5. On the right there is a schematic representation of the three phase-matched parametric processes involved.

the creation of pairs of real polaritons by the vacuum modulation is indeed resonantly enhanced when the phase-matching condition

$$r\,\omega_{mod} = \omega_j(q) + \omega_{j'}(-q) \tag{2.24}$$

is fulfilled, r being a generic positive integer number, and $j, j' \in \{LP, UP\}$ (see Fig. 2.6). Photons have to be created in pairs in order to conserve in-plane momentum. The dominant features, labeled A, B and C, are the three lowest-order $r = 1$ peaks corresponding to the processes where either two Lower Polaritons (LPs), or one LP and one Upper Polariton (UP), or two UP's are generated. This interpretation is supported by the spectral densities plotted in the three panels of Fig. 2.6 for modulation frequencies corresponding to respectively A, B and C peaks. In each case, the emission is strongly peaked at the frequencies of the final polariton states involved in the process; for the parameter chosen, we have indeed [25, 33] $\omega_{LP}(q) \simeq \omega_{12} - \bar{\Omega}_R(q) = 0.8\,\omega_{12}$ for the lower polariton and $\omega_{UP}(q) \simeq \omega_{12} + \bar{\Omega}_R(q) = 1.2\,\omega_{12}$ for the upper polariton. The shoulder and the smaller peak at $\omega_{mod}/\omega_{12} < 1$ can be attributed to $r = 2$ processes, while higher order processes require a weaker damping to be visible. Note that here we have chosen a low quality factor for the resonances. In other systems (such as Josephson junctions [70, 51]) the quality factors would be much higher. More insight into the properties of the quantum vacuum emission are given in Fig. 2.7. In the top panel, the robustness of the emission has been verified for increasing values of the damping rate Γ: the resonant enhancement is quenched, but the main qualitative features remain unaffected even for rather large damping rates. In the bottom panel, comparison with the black body emission in the absence of any modulation is made: the total rate of emitted black body photons at given $\mathbf{q}$ is shown as a function of ω_{12} (ranging from the Terahertz to the mid-infrared range) for $\mathbf{q}$ corresponding to an intra-cavity photon propagation angle of 60° and different temperatures. Note how the black body emission decreases almost exponentially with ω_{12}, while the quantum vacuum radiation, being a function of $\bar{\Omega}_R(q)/\omega_{12}$ only, linearly increases with ω_{12} at fixed $\bar{\Omega}_R(q)/\omega_{12}$. From this plot, one is quantitatively reassured that for reasonably low temperatures the quantum vacuum radiation can exceed the black-body emission by several orders of magnitude. The increase of the emitted intensity versus the modulation amplitude $\Delta\Omega_R(q)/\omega_{12}$ is shown in the top panel of Fig. 2.8. In particular, it is evident the strongly superlinear increase of the emission intensity around the A and C resonance peaks. In these regions, if the modulation amplitude is

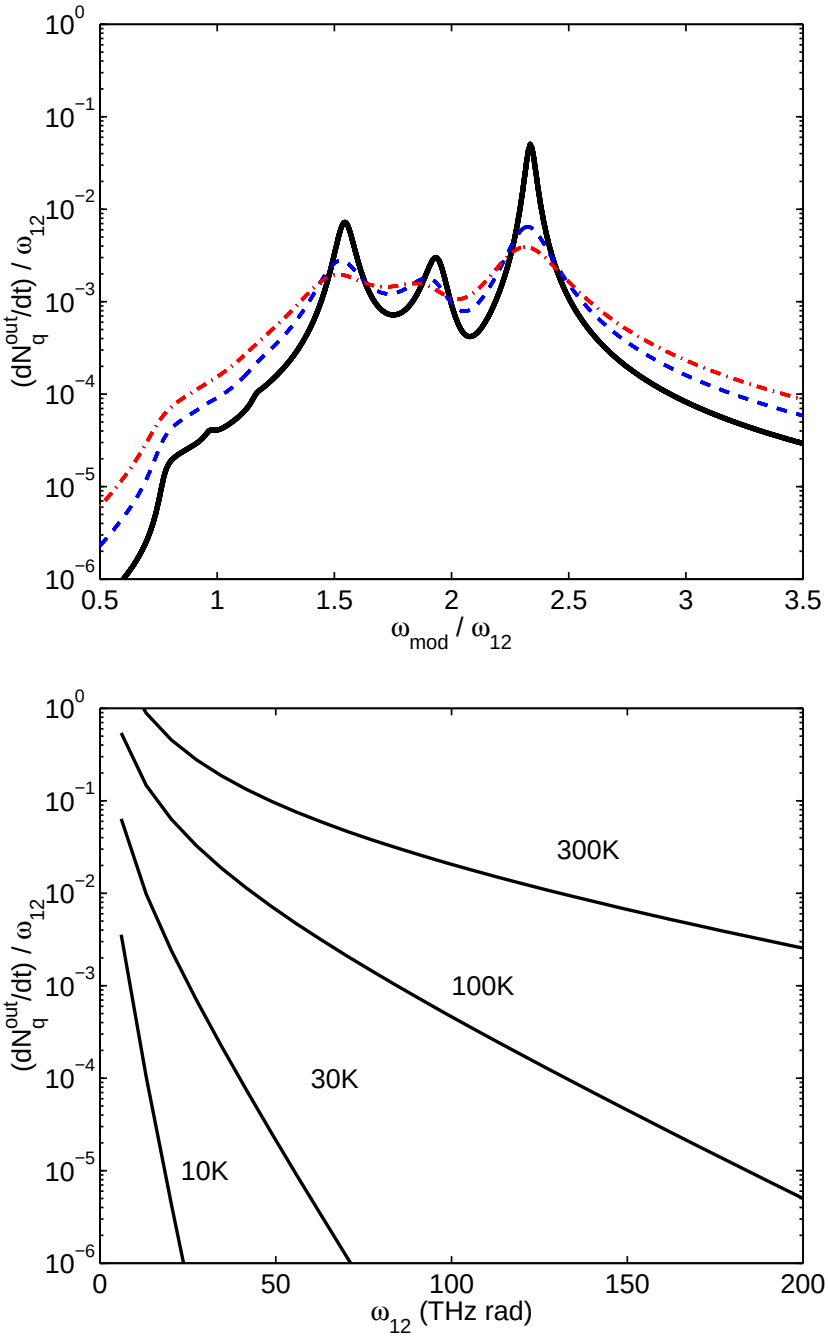

Figure 2.7: Top panel: rate dN_q^{out}/dt (in units of ω_{12}) of emitted photons as a function of ω_{mod}/ω_{12} for different values of the damping $\Gamma/\omega_{12} = 0.025$ (solid black), 0.05 (dashed blue), 0.075 (dot-dashed red). Other parameters as in Fig. 2.5. Bottom panel: normalized rate of emitted photons from a black-body emitter as a function of ω_{12} for different temperatures.

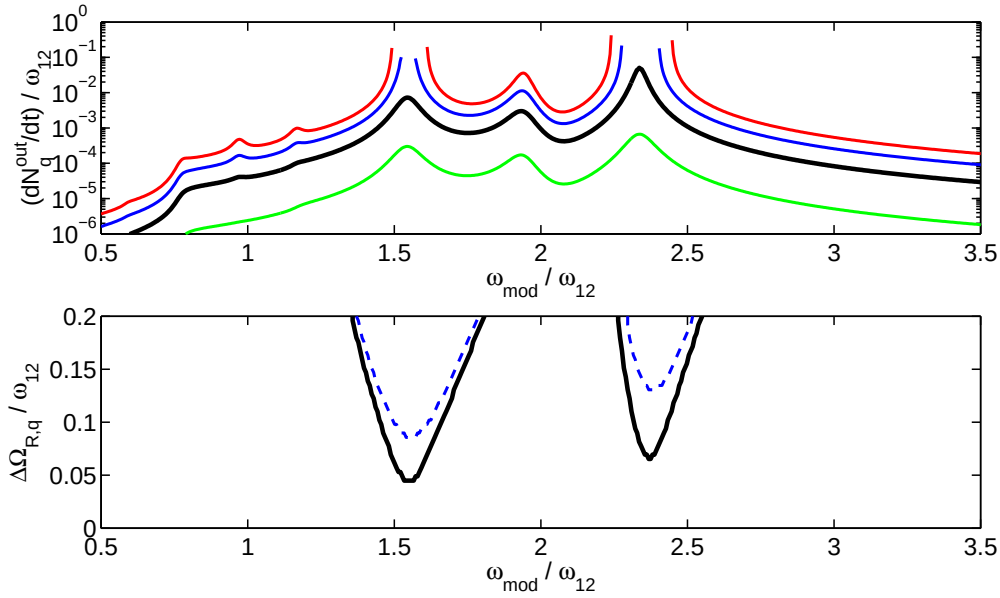

Figure 2.8: Top panel: rate dN_q^{out}/dt (in units of ω_{12}) of quantum vacuum fluorescence as a function of ω_{mod}/ω_{12} for different values of the normalized modulation amplitude $\Delta\Omega_R(q)/\omega_{12} = 0.01, 0.04, 0.07, 0.1$ (from bottom to top) and $\Gamma/\omega_{12} = 0.025$. Other parameters as in Fig. 2.5. Bottom panel: instability boundaries for $\Gamma/\omega_{12} = 0.025$ (solid back) and 0.05 (dashed blue). Above the lines, the system is parametrically unstable.

large enough, the system can develop a parametric instability, the incoherent quantum vacuum radiation being replaced by a coherent parametric oscillation [69]. Above the instability threshold, the results obtained from the solution of Eq. (B.8) in Fourier space are no longer valid, being the field amplitudes exponentially growing with time. Hence they are not shown here. The instability boundaries for parametric oscillation can be calculated applying the Floquet method [71] to the mean-field equations for the intra-cavity fields $\langle a_{\mathbf{q}} \rangle$ and $\langle b_{\mathbf{q}} \rangle$. The result is shown in the bottom panel of Fig. 2.8 as a function of ω_{mod}/ω_{12} and $\Delta\Omega_R(q)/\omega_{12}$: the border of the instability zones agree well with the position of the vertical asymptotes of the spectra in the top panel of Fig. 2.8.

2.5 Experiments: ultra-strong coupling

As we saw in the preceding sections, the quantum vacuum radiation is entirely due to the effect of anti-resonant terms in the Hamiltonian. The relevance of these antiresonant terms increases with the ratio $\frac{\Omega_R}{\omega_{12}}$, explaining why the ultra-strong coupling is important to have large quantum vacuum radiation effects. The first milestone toward an experimental observation of the quantum vacuum radiation has thus been to show, for the first time, that microcavity embedded quantum wells can really be in the ultra-strong coupling regime. - In order to verify that, the idea is to compare the experimental polaritonic dispersions with the theoretical predictions obtained from the full bosonic Hamiltonian in Eq. 2.1 and from the bosonic RWA Hamiltonian of Section 1.4.3.

The experiments were conducted in the laboratory of A. Tredicucci in Pisa. In order to be able to discriminate the role of antiresonant terms, the relevant physical quantities need to be measured. In particular, are essential the experimental dispersion of the bare cavity mode and the intersubband transition frequency ω_{12}. The bare intersubband transition frequency of the active region was measured by collecting transmitted light at an incident angle small enough to exclude any cavity-induced shift of the intersubband absorption (for experimental details see Ref. [32]). Since the bottom mirror of the sample utilizes total internal reflection, one cannot determine precisely the cavity resonance energy through measurements at zero incidence angle, where the intersubband transition does not couple to the radiation. Therefore a second sample, identical in the growth sequence, but without any doping in the active

region was measured in order to determine the energy dispersion of the cavity mode. X-ray diffraction and electron microscopy measurements were performed to check that the control sample had the same layer structure (within experimental errors). The shift of the cavity refractive index induced by the absence of doping in the quantum wells was computed to be at most ~ 1 %. The only remaining free fitting parameter is the vacuum Rabi frequency $\Omega_R(q)$ (defined in Section 1.4.3). We calculated the root mean square deviation from the experimental data for different values of $\Omega_R(q)$ (top panel of Fig. 2.9) using two different theoretical models: the full Hamiltonian of Eq. 2.1 (solid black line) and the bosonic RWA Hamiltonian (dashed blue line). For the full Hamiltonian an excellent agreement is found for a vacuum Rabi energy $\hbar\Omega_R(q) = \hbar\Omega_R(q_{res}) = 16.5$ meV ~ 11 % of the intersubband transition energy, with a fit RMS error of only 0.9 meV. For the bosonic RWA Hamiltonian the agreement is decidedly worse, with a minimum error of 4 meV, well beyond the experimental resolution. The optimal angular dispersions are plotted in the bottom panel and compared with the experimental values (red circles). Note that, as discussed in Ref. [49], the actual value of the vacuum Rabi energy is much smaller than half the splitting observed in the spectra, owing to the fact that the two polariton energies, once measured at the same angle, do not correspond to the same in-plane wavevector q.

We have thus experimentally shown that microcavity embedded quantum wells can be in the ultra-strong coupling regime, and thus the effect of the antiresonant terms makes them optimal candidates for the experimental observation of the dynamical Casimir effect.

2.6 Experiments: ultra-fast modulation

As we have seen (i.e. in Eq. 2.24 and in Fig. 2.5), in order to emit radiation from the vacuum it is necessary to modulate the light-matter coupling at a frequency of the order of $2\omega_{12}$. In the recent years, various propositions on how to change *in-situ* the vacuum Rabi frequency have been put forward. All are based on a modulation of the electronic population inside the quantum wells. In fact, as discussed in Section 1.2.2, the vacuum Rabi frequency is proportional to the square root of the density of the two dimensional electron gas.

The easiest way to modulate the electron density is to shift the Fermi level of the system by means of an electrostatic bias [67]. Unfortunately this option,

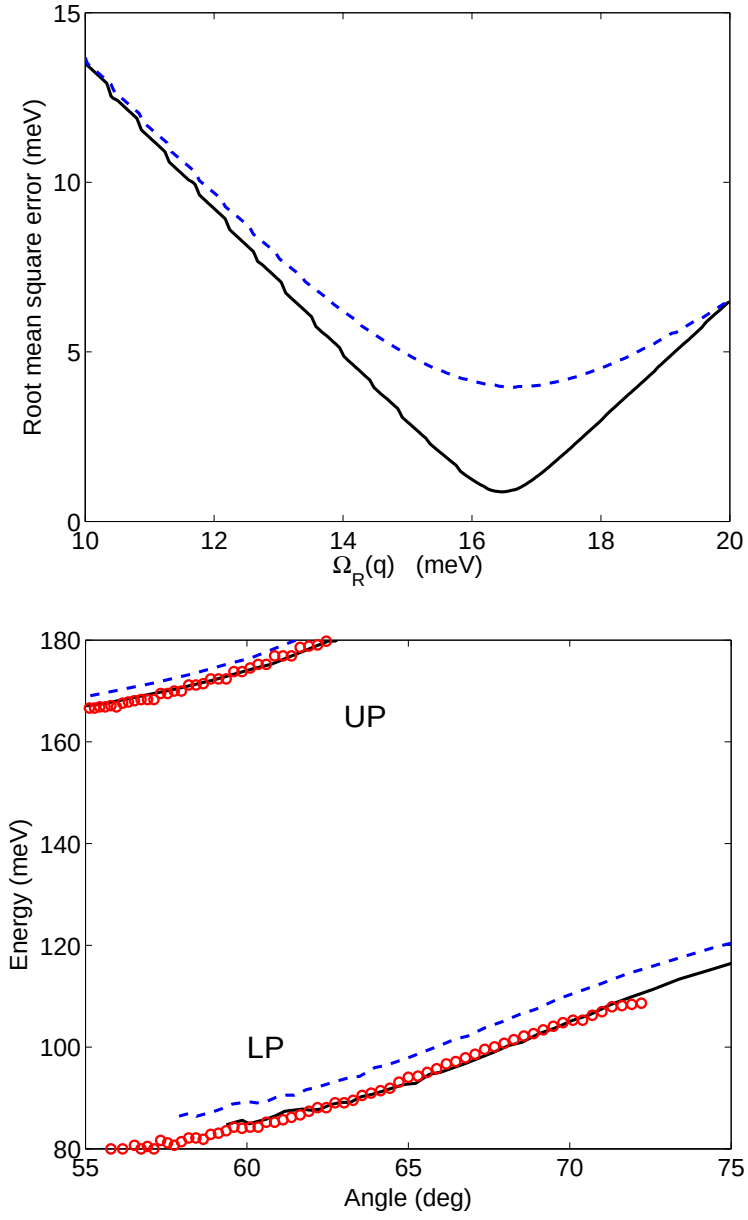

Figure 2.9: Top panel: root mean square deviation from measured dispersion of the calculated polariton energies as a function of the vacuum Rabi energy, the only fitting parameter. The solid black line refers to the $\bar{H}_{bos}$, while the dashed blue one to the bosonic RWA Hamiltonian. Bottom panel: angular dispersions of the lower and upper polaritons in the two cases compared to experimental data (red circles). The $\Omega_R(q)$ used are the ones that minimize the error.

even if technically quite simple, is not well suited for dynamical Casimir experiments due to the intrinsic frequency limit of the electric modulation (ω_{12} varies from few Terahertz to hundreds of Terahertz, while the electronic modulation is limited by the capacitance and cannot typically exceed 100 Gigahertz). An interesting proposition, that could *a priori* give a modulation with the right frequency, has been to exploit coherent tunneling between two energetically aligned quantum wells in order to obtain the desired time modulation of the electronic population [68]. The first realized proposal that accomplishes a modulation fast enough to permit, at least theoretically, the observation of the quantum vacuum radiation, has been recently realized in the group of R. Huber in Konstanz [37]. The idea, schematized in the top panel of Fig. 2.10, is to start with an undoped quantum well and then to use a control femtosecond pulse to pump an electronic population from the valence band into the first conduction subband, effectively switching on the transition on a timescale comparable to the laser pulse duration (12 fs for the actual experimental setup). The cavity dynamics is then probed by a broadband Terahertz beam, whose central frequency is resonant with the intersubband transition. The bottom panel of Fig. 2.10 shows the results of the experiment, that is the probe reflectance spectra as a function of the pump-probe delay. For negative delays (the probe arrives before the control beam) the probe does not see any electron in the conduction subbands, the intersubband transition is thus optically inactive. The only visible resonance is the bare cavity one at 113 meV (blue arrow in Fig. 2.10). For positive delays instead the probe sees the electronic population created by the pump and the relative polaritonic splitting appears non-adiabatically in the reflected spectra. The initial bare photon state is replaced by two coupled polariton branches appearing simultaneously at energy positions of 93 meV and 143 meV (red arrows in Fig. 2.10). Most remarkably, the new resonances do not develop by gradual bifurcation out of the bare cavity mode. In contrast, switching occurs discontinuously once the control pulse promotes electrons into the first conduction subband. With this setup it is thus possible to realize a real non-adiabatic control of the light-matter coupling.

2.7 Conclusions and perspectives

The experiment described in Section 2.6, bears a strong similarity with the gedanken experiment of Section 2.2, with the only difference that here we are

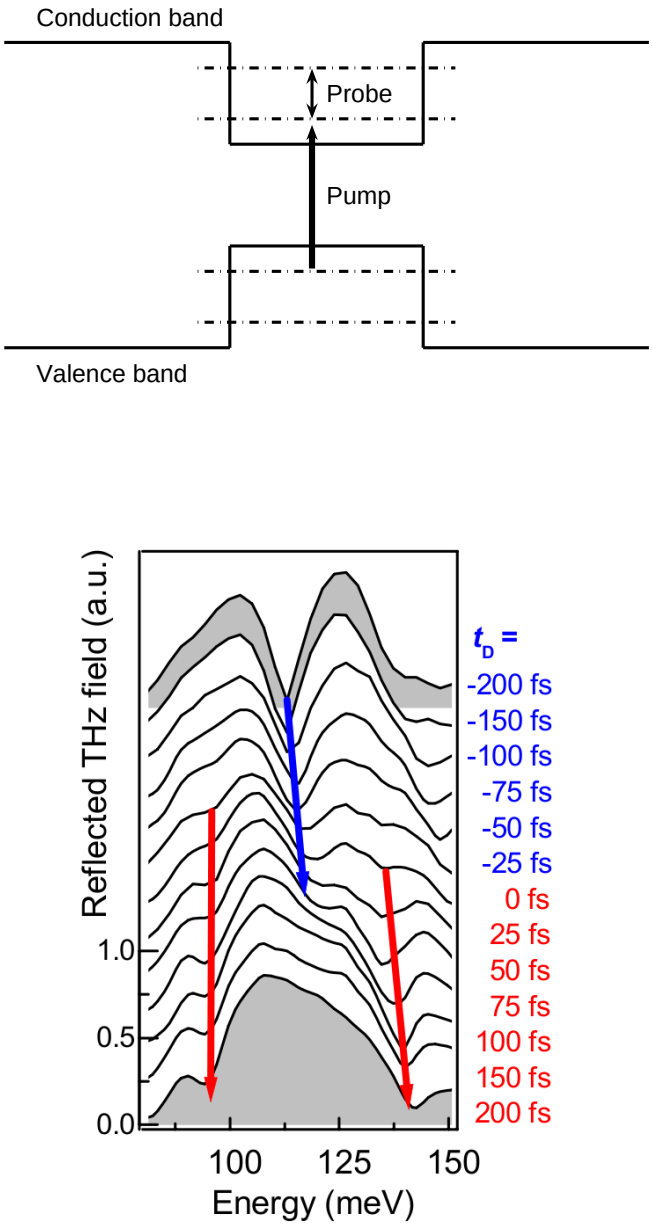

Figure 2.10: On the top there is a schema of the experiment of Ref. [37]. An electronic population is excited in the first conduction subband by a femtosecond control laser and then the intersubband transition is probed by broadband Terahertz beam. On the bottom there are the results of the experiment. Spectra of the reflected probe are given for various pump-probe time delays. The 12 fs pump pulse arrives at $t_D = 0$. Blue arrow: bare cavity resonance, red arrows: ultra-strongly coupled intersubband cavity polariton branches.

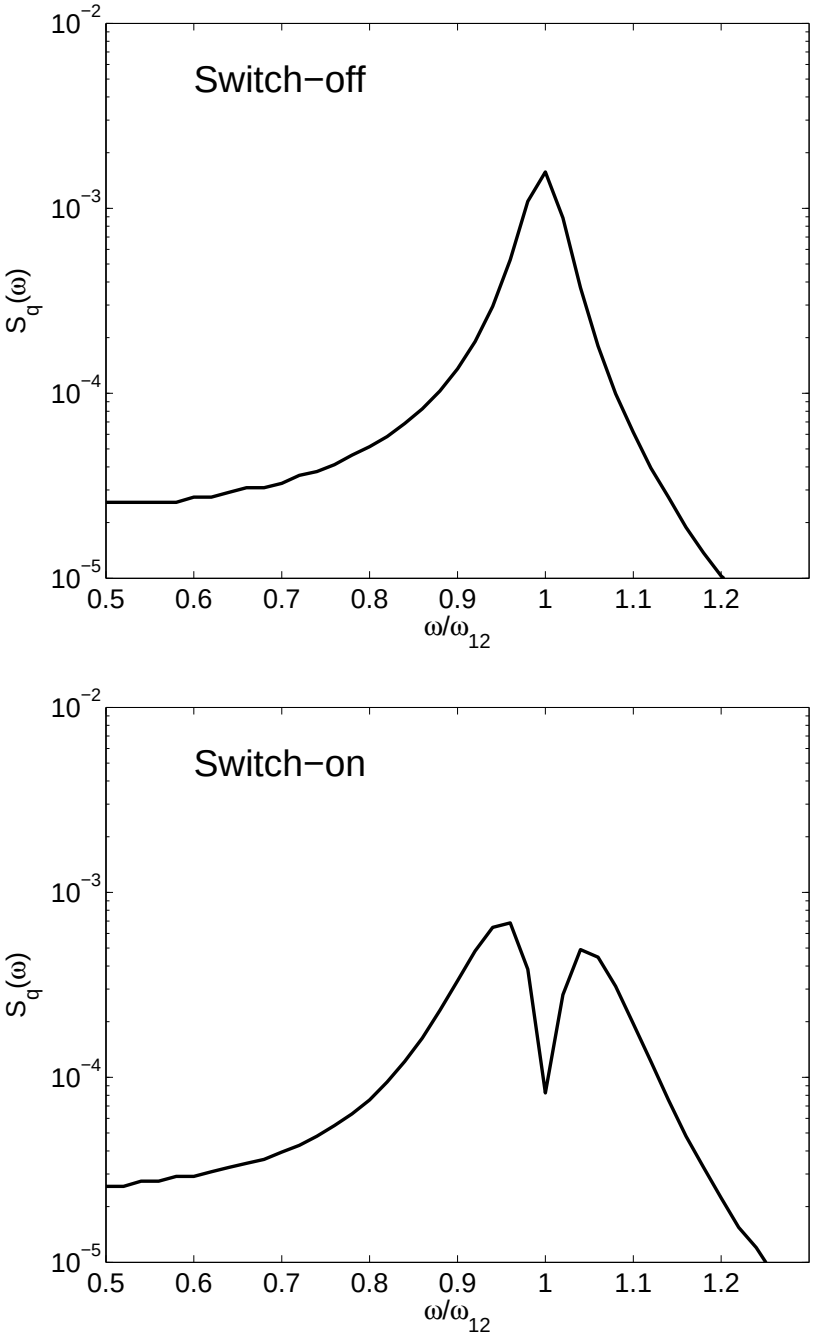

Figure 2.11: Spectra of emitted photons per radiant per unit time in the case of a switch off (top panel) and of a switch on (bottom panel). All the parameters are taken from Ref. [37].

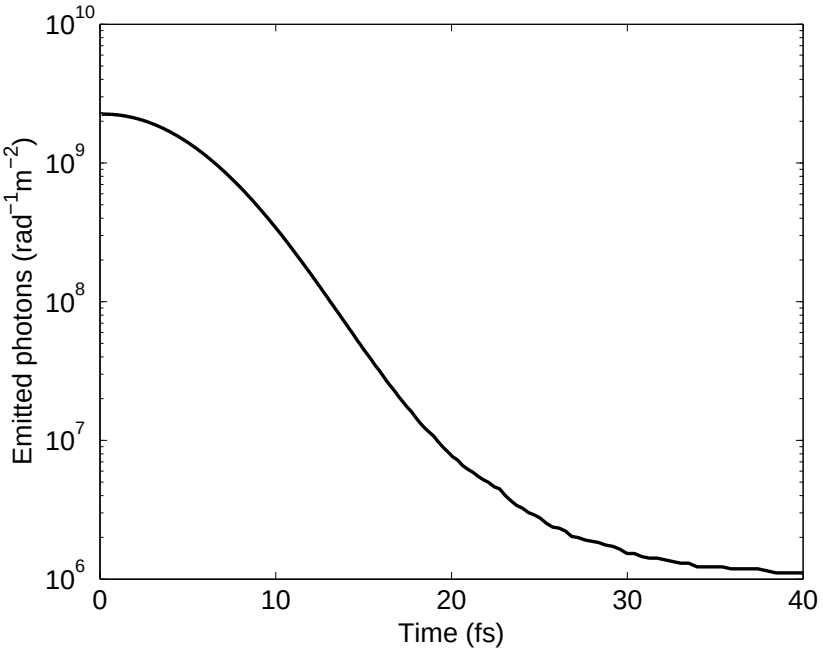

Figure 2.12: Total number of emitted Casimir photons as a function of the full width half maximum length (FWHM) of the pump pulse. All the other parameters are taken from Ref. [37].

considering a sudden switch on instead that a switch off. Given the symmetry of the problem (one case is simply the time-reversal of the other), we expect to have the same number of emitted photons in the two cases. However, if we follow the same reasoning of section 2.2, in the switch-on case we expect to have an emission peaked at the polariton frequencies instead that at the bare cavity one. In the Fig. 2.11 we plotted the calculated spectra of emitted photons with the parameters of the real experiment, in the case of a switch off (top panel) and of a switch on (bottom panel). As we expected the emissions are of the same amplitude, but in the second one we have the appearing of a polaritonic splitting. In Fig. 2.12 it is shown the total calculated number of emitted Casimir photons as a function of the full width half maximum length (FWHM) of the pump impulse. We see that for a 12 fs FWHM pulse we expect to have between 10^8 and 10^9 photons emitted per radiant per squared meter, an emission strength *a priori* high enough for being measured. The measure is anyway challenging because these photons are emitted incoherently and thus a the average emitted field is equal to zero. It will be thus necessary to measure not the field itself but the amplitude noise of the signal, that could give a direct measurement of the number and frequency of emitted photons. Once a solid evidence for quantum vacuum radiation will be obtained, the next important step will be to measure the quantum correlation between the emitted photons. In fact, as we have seen, for example in the right panels of Fig. 2.6, in order to conserve in-plane momentum, photons are emitted in pairs and we expect to have strong quantum correlations between them. Fig. 2.12 is also a good consistency check for the theory and the numerical codes developed. In fact for the pump length that tends toward zero, that is for an instantaneous switch on, we get a value around 2×10^9 photons per radiant per squared meter, that is we recover with good accuracy the result of the estimate in the gedanken experiment of section 2.2.

Chapter 3

Light emitters in the strong coupling regime

3.1 Introduction

In the last two decades, the fundamental research on the physics of intersubband transitions in semiconductor quantum wells led to a number of novel applications in quantum optoelectronics [72]. The interplay between judiciously quantum engineered intersubband transitions and vertical electron transport paved the way to the development of the so-called quantum cascade electroluminescent devices and lasers, which are unipolar optoelectronic sources emitting in the mid- and far-infrared portion of the electromagnetic spectrum [73, 74, 75]. As we have seen in Chapter 1, recent reflectivity experiments [24, 67, 68] have demonstrated that by embedding a doped quantum well structure in a planar microcavity, it is possible to achieve strong coupling regime between an intersubband transition and a cavity photon mode, provided that a dense enough two-dimensional electron gas populates the fundamental quantum well subband. The links between the strong coupling regime and the electron transport have been the object of various theoretical and experimental works. A new kind of microcavity-embedded quantum cascade device in the strong coupling regime was proposed in Ref. [52] and the first experimental demonstrations of a microcavity quantum cascade photovoltaic detector and of an electroluminescent device in the strong coupling regime have been recently reported [53, 39].

One of the central topics of my Ph.D. thesis has been to develop a quantitative theoretical understanding of the effect of strong coupling on electronic

transport and on the efficiency of light emitting devices. This task posed a number of theoretical and numerical problems, because in order to be able to track electron transport and dynamical changes in electronic populations, it is necessary to keep in the Hamiltonian all the degrees of freedom of single electrons, taking care of all the nonlinearities due to Pauli blocking. Thus we can not, as we did in the previous Chapter, rely purely on bosonized Hamiltonians that describe only the few collective degrees of freedom coupled to the microcavity photon mode. In order to make the problem treatable, I will describe two different limits, making in the two cases completely different approximations. In this Chapter, we will treat the case of a macroscopic current flowing through the device. The macroscopic current will modify the electron populations, leading to a highly nonlinear dynamics. Being the dimension of the corresponding Hilbert space too big for a direct diagonalization, I will rely on a sort of higher order mean field theory in order to describe the dynamics of the observable quantities, like the electronic and photonic populations. The mean field approximation will anyway neglect all the effects of the light-matter coupling on the electron spectral function. These subtle quantum mechanical effects will be the object of the next Chapter in which on the contrary, by restraining to the regime of small currents, it will be possible to exactly diagonalize the system Hamiltonian. The approximation used in this Chapter is thus valid only if the spectral width of the electrical contacts are too big to probe the modification in the particles spectral functions induced by the light-matter coupling.

3.2 Hamiltonian and approximations

As explained in Section 3.1, we need to use an Hamiltonian that describes all the degrees of freedom of the single electrons. If we do not consider the ultrastrong coupling limit, we can safely apply the rotating wave approximation, as described in Section 1.4.2. This choice will become still better justified a posteriori because, as we will see, the coupling constant decreases when a voltage difference is applied to the structure. We will thus use the fermionic RWA Hamiltonian of Section 1.4.2

$$\begin{aligned} H &= \sum_{\sigma,\mathbf{k}} \hbar\omega_{c,1}(k) c^{\dagger}_{1,\sigma,\mathbf{k}} c_{1,\sigma,\mathbf{k}} + \hbar\omega_{c,2}(k) c^{\dagger}_{2,\sigma,\mathbf{k}} c_{2,\sigma,\mathbf{k}} + \sum_{\mathbf{q}} \hbar\omega_{cav}(q) a^{\dagger}_{\mathbf{q}} a_{\mathbf{q}} \\ &+ \sum_{\sigma,\mathbf{k},\mathbf{q}} \hbar\chi(q) a_{\mathbf{q}} c^{\dagger}_{2,\sigma,\mathbf{k}+\mathbf{q}} c_{1,\sigma,\mathbf{k}} + \hbar\chi(q) a^{\dagger}_{\mathbf{q}} c^{\dagger}_{1,\sigma,\mathbf{k}} c_{2,\sigma,\mathbf{k}+\mathbf{q}} + H_{other}, \end{aligned} \tag{3.1}$$

where we have explicitly written the electron spin index. The Hamiltonian term H_{other} is meant to include all the interactions other than the light-matter coupling, that is: (i) electron-phonon interaction; (ii) electron-electron interaction; (iii) electron tunneling coupling to the injection and extraction reservoir; (iv) coupling between the cavity photon field and the extracavity field. The Hilbert space relative to Hamiltonian in Eq. 3.1, is too large to permit numerical diagonalization. We will instead try to find an evolution equation for the expectation values of a number of observable quantities, like the electronic and photonic populations in each mode. Unfortunately, due to the cubic light-matter coupling terms in the Hamiltonian (terms like $\hbar\chi(q)a^{\dagger}_{\mathbf{q}}c^{\dagger}_{\sigma,\mathbf{k},1}c_{\sigma,\mathbf{k}+\mathbf{q},2}$ that couple two fermion operators and one boson operator) it is not possible to write down an exact closed set of equations for the evolution of expectation values, being the Heisenberg equation of motion for each product of N operators coupled at least with one product of $N+1$ operators. In other words, the equations of motion of the different observables of the system form an infinite hierarchy. One approximation method that has been used in order to solve this kind of systems is the so-called cluster expansion scheme [76, 77, 78]. Formally, it is based on a systematic development of expectation values of operator products in terms of correlation functions. Practically, it consists to keep as dynamical variables all the expectation values containing up to a certain number of operators and factorizing, like in Wick's theorem, all the others, obtaining a sort of higher order mean field theory. From the Hamiltonian in Eq. 3.1 and from the discussion of bosonized Hamiltonians in Section 1.4.3, it is clear that a bosonic operator $a_{\mathbf{q}}$, couples always to a pair of fermionic operators. In order to obtain a consistent truncation scheme, a pair of fermionic operators has thus to be considered of the same order as a single bosonic operator when deciding what expectation values have to be factorized. In order not to miss, with this type of approximation, important aspects of the physics of polaritons, the hierarchy must be truncated at the level of the product of two bosonic operators (i.e., the product of four fermion operators), that is the level at which polaritonic-induced coherence phenomena become visible. The details of the factorization can be found in Appendix C. The expectation values entering the present cluster factorization, that are our dynamical variables, are the electronic and photonic populations, the correlation between the cavity photon field and the intersubband polarization, as well as polarization-polarization correlations. The electron occupation numbers in the two quantum well conduction subbands are $n_{1,\mathbf{k}} =< c^{\dagger}_{1,\sigma,\mathbf{k}}c_{1,\sigma,\mathbf{k}} >$

and $n_{2,\mathbf{k}} =< c^{\dagger}_{2,\sigma,\mathbf{k}} c_{2,\sigma,\mathbf{k}} >$. Note that, since in the absence of a magnetic field all quantities are spin-independent, we omit the spin-index in the notation of the averaged quantities. The cavity photon number is $n_{a,\mathbf{q}} =< a^{\dagger}_{\mathbf{q}} a_{\mathbf{q}} >$. The correlation between the cavity photon field and the intersubband electronic polarization is represented by the quantity

$$Y(\mathbf{q},\mathbf{k}) =< a^{\dagger}_{\mathbf{q}} c^{\dagger}_{1,\sigma,\mathbf{k}} c_{2,\sigma,\mathbf{k}+\mathbf{q}} > . \tag{3.2}$$

Finally, the polarization-polarization correlation function is given by

$$X(\mathbf{q}+\mathbf{k}',\mathbf{k}',\mathbf{k}) = \sum_{\sigma} < c^{\dagger}_{2,\sigma,\mathbf{q}+\mathbf{k}'} c_{1,\sigma,\mathbf{k}'} c^{\dagger}_{1,\sigma',\mathbf{k}} c_{2,\sigma',\mathbf{k}+\mathbf{q}} > . \tag{3.3}$$

Our aim is thus to obtain a closed set of evolution equations for the variables $n_{1,\mathbf{k}}$, $n_{2,\mathbf{k}}$, $n_{a,\mathbf{q}}$, $Y(\mathbf{q},\mathbf{k})$, $X(\mathbf{q}+\mathbf{k}',\mathbf{k}',\mathbf{k})$. While the light-matter coupling terms in Eq. 3.1 will be treated, as we said, by calculating the Heisenberg evolution for the operators and then factorizing the their expectation values, the terms in H_{other}, namely the phonon scattering, electron-electron interaction, the coupling to the contact reservoirs and the coupling to the external electromagnetic field will be treated in an effective way. The carrier non-radiative relaxation (due to phonon-electron and electron-electron scattering) is modeled in terms of a simple phenomenological relaxation time $\tau_{\mathbf{k}}$ that tends to bring the electronic instantaneous populations $n_{1,\mathbf{k}}$ and $n_{2,\mathbf{k}}$ back to their equilibrium distributions $n^0_{1,\mathbf{k}}$ and $n^0_{2,\mathbf{k}}$. In the same way the dephasing of the light-matter ($Y(\mathbf{q},\mathbf{k},t)$) and matter-matter ($X(\mathbf{q}+\mathbf{k}',\mathbf{k}',\mathbf{k},t)$) coherencies will be quantified by two relaxation constants Γ_Y and Γ_X that tend to bring their values to the factorized values, thus destroying correlations. Note that in the spontaneous photon emission regime, $Y(\mathbf{q},\mathbf{k})$ can not be factorized: in fact, spontaneous emission is incoherent and $< a_{\mathbf{q}} >= 0$, $< c^{\dagger}_{1,\sigma,\mathbf{k}} c_{2,\sigma,\mathbf{k}+\mathbf{q}} >= 0$, meaning that the cavity field and the intersubband polarization have no definite phase. Unlike $Y(\mathbf{q},\mathbf{k})$, $X(\mathbf{k}'+\mathbf{q},\mathbf{k}',\mathbf{k})$ can be factorized in products of non-zero lower-order expectation values of operators. In fact, we have

$$X(\mathbf{k}'+\mathbf{q},\mathbf{k}',\mathbf{k}) = 2n_{2,\mathbf{k}+\mathbf{q}}(1-n_{1,\mathbf{k}})\delta_{\mathbf{k},\mathbf{k}'} + \delta X(\mathbf{k}'+\mathbf{q},\mathbf{k}',\mathbf{k}). \tag{3.4}$$

The first contribution is an uncorrelated plasma term, while $\delta X(\mathbf{k}'+\mathbf{q},\mathbf{k}',\mathbf{k})$ describes the higher-order correlation, which can be destroyed by dephasing processes quantified by the damping rate Γ_X.

Note that the role of Coulomb electron-electron interaction on intersubband transitions has been studied, e.g., in Ref. [79]. In the case of subbands with

parallel parabolic dispersion (e.g., same effective mass), Coulomb interaction produces a moderate renormalization of the intersubband transition frequency ω_{12} and of its oscillator strength, which can be included in the experimentally measured quantities.

The two subbands are coupled to two electronic reservoirs, named respectively left and right contacts (see Fig. 3.1). We will call $\Gamma^{in}_{p,j,\mathbf{k}}$ the electronic tunneling rate into the $\mathbf{k}$-mode of the subband $j = 1, 2$ from the reservoir $p = \text{left}, \text{right}$. Analogously $\Gamma^{out}_{p,j,\mathbf{k}}$ is defined as the electronic tunneling rate from the $\mathbf{k}$-mode of the subband j into the reservoir p. The total in-tunneling and out-tunneling rates are $\Gamma^{in}_{j,\mathbf{k}} = \Gamma^{in}_{\text{left},j,\mathbf{k}} + \Gamma^{in}_{\text{right},j,\mathbf{k}}$ and $\Gamma^{out}_{j,\mathbf{k}} = \Gamma^{out}_{\text{left},j,\mathbf{k}} + \Gamma^{out}_{\text{right},j,\mathbf{k}}$.

The self-consistent local equilibrium occupation numbers $n^0_{1,\mathbf{k}}$ and $n^0_{2,\mathbf{k}}$ are given by quasi-Fermi-Dirac distributions:

$$\begin{aligned} n^0_{1,\mathbf{k}} &= \frac{1}{e^{\beta(\hbar\omega_{c,1}(\mathbf{k})-\epsilon_F)}+1}, \\ n^0_{2,\mathbf{k}} &= \frac{1}{e^{\beta(\hbar\omega_{c,2}(\mathbf{k})-\epsilon_F)}+1}, \end{aligned} \tag{3.5}$$

where $\beta = 1/(KT)$ is the Boltzmann thermal factor, and ϵ_F is the quantum well self-consistent Fermi level, such that:

$$\sum_{\mathbf{k}} n_{1,\mathbf{k}} + n_{2,\mathbf{k}} = \frac{Sm^*}{2\pi\hbar^2}\int_0^\infty d\epsilon \frac{1}{e^{\beta(\epsilon-\epsilon_F)}+1} + \frac{1}{e^{\beta(\epsilon+\hbar\omega_{12}-\epsilon_F)}+1}, \tag{3.6}$$

that is we define the instantaneous equilibrium populations $n^0_{1,\mathbf{k}}$ and $n^0_{2,\mathbf{k}}$ as the thermalized populations containing the same number of electrons as the actual non-equilibrium ones.

Putting all together, the resulting closed system of equations for the one-time expectation values reads:

$$
\begin{aligned}
\frac{d}{dt}n_{a,\mathbf{q}} &= -2\gamma\ n_{a,\mathbf{q}} + 2i\sum_{\mathbf{k}}\chi(q)Y(\mathbf{q},\mathbf{k}) + c.c. \\
\frac{d}{dt}n_{1,\mathbf{k}} &= -\frac{n_{1,\mathbf{k}} - n^0_{1,\mathbf{k}}}{\tau_{\mathbf{k}}} - \Gamma^{out}_{1,\mathbf{k}}n_{1,\mathbf{k}} + \Gamma^{in}_{1,\mathbf{k}}(1-n_{1,\mathbf{k}}) \\
&\quad +i\sum_{\mathbf{q}}\chi(q)Y(\mathbf{q},\mathbf{k}) + c.c. \\
\frac{d}{dt}n_{2,\mathbf{k}} &= -\frac{n_{2,\mathbf{k}} - n^0_{2,\mathbf{k}}}{\tau_{\mathbf{k}}} - \Gamma^{out}_{2,\mathbf{k}}n_{2,\mathbf{k}} + \Gamma^{in}_{2,\mathbf{k}}(1-n_{2,\mathbf{k}}) \\
&\quad -i\sum_{\mathbf{q}}\chi(q)Y(\mathbf{q},\mathbf{k}-\mathbf{q}) + c.c. \\
\frac{d}{dt}Y(\mathbf{q},\mathbf{k}) &= i(\omega_{cav}(\mathbf{q}) + \omega_{c,1}(\mathbf{k}) - \omega_{c,2}(\mathbf{k}+\mathbf{q}) + i\Gamma_Y(\mathbf{q},\mathbf{k}))Y(\mathbf{q},\mathbf{k}) \\
&\quad -i\sum_{\mathbf{q}'}\chi(q)X(\mathbf{q}+\mathbf{q}',\mathbf{q}',\mathbf{k}) + i\chi(q)n_{a,\mathbf{q}}(n_{1,\mathbf{k}} - n_{2,\mathbf{k}+\mathbf{q}}) \\
\frac{d}{dt}X(\mathbf{k}'+\mathbf{q},\mathbf{k}',\mathbf{k}) &= i(-\omega_{c,1}(\mathbf{k}') + \omega_{c,2}(\mathbf{k}'+\mathbf{q}) + \omega_{c,1}(\mathbf{k}) - \omega_{c,2}(\mathbf{k}+\mathbf{q})) \\
&\quad X(\mathbf{k}'+\mathbf{q},\mathbf{k}',\mathbf{k}) - \Gamma_X(\mathbf{k}'+\mathbf{q},\mathbf{k}',\mathbf{k})\,(X(\mathbf{k}'+\mathbf{q},\mathbf{k}',\mathbf{k}) \\
&\quad -2n_{2,\mathbf{k}+\mathbf{q}}(1-n_{1,\mathbf{k}})\delta_{\mathbf{k},\mathbf{k}'}) + i\sum_{\mathbf{q}'}\chi(q'')(Y^*(\mathbf{q}',\mathbf{k})\delta_{\mathbf{k}',\mathbf{k}}n_{2,\mathbf{k}+\mathbf{q}} \\
&\quad +Y^*(\mathbf{q}',\mathbf{q}+\mathbf{k}-\mathbf{q}')\delta_{\mathbf{k}',\mathbf{k}}(1-n_{1,\mathbf{k}})) \\
&\quad +2i\chi(q)Y^*(\mathbf{q},\mathbf{k}')(n_{1,\mathbf{k}} - n_{2,\mathbf{k}+\mathbf{q}}) - 2i\chi(q)Y(\mathbf{q},\mathbf{k})(n_{1,\mathbf{k}'} - n_{2,\mathbf{k}'+\mathbf{q}}).
\end{aligned}
\tag{3.7}
$$

The wavevector dependent injection and extraction rates in Eq. 3.7 can be in principle of different origin. Here we give the formal expression for elastic tunneling processes conserving the in-plane momentum. Additional processes (such as assisted tunneling) can be accounted for by adding their contribution to the expressions for $\Gamma^{in}_{j,\mathbf{k}}$ and $\Gamma^{out}_{j,\mathbf{k}}$. As electronic contact reservoirs, we will consider semiconductor doped superlattices, as it is generally the case in unipolar quantum cascade devices. The chemical potential in each contact is labeled μ_p with $p = \text{left}, \text{right}$. In each reservoir, we will consider miniband states with energy $E^{res}_{p,\mathbf{k},k_z}$. In the elastic tunneling process, electron energy and in-plane momentum are conserved. The tunneling rate from the contact reservoir into the j-th subband can be calculated with the Fermi golden rule

$$
\Gamma^{in}_{p,j,\mathbf{k}} = \frac{2\pi}{\hbar}\sum_{k_z}\frac{|V_{p,j,\mathbf{k},k_z}|^2\delta\left(E^{res}_{p,\mathbf{k},k_z} - \hbar\omega_j(\mathbf{k})\right)}{1+e^{\beta(E^{res}_{p,\mathbf{k},k_z}-\mu_p)}}, \tag{3.8}
$$

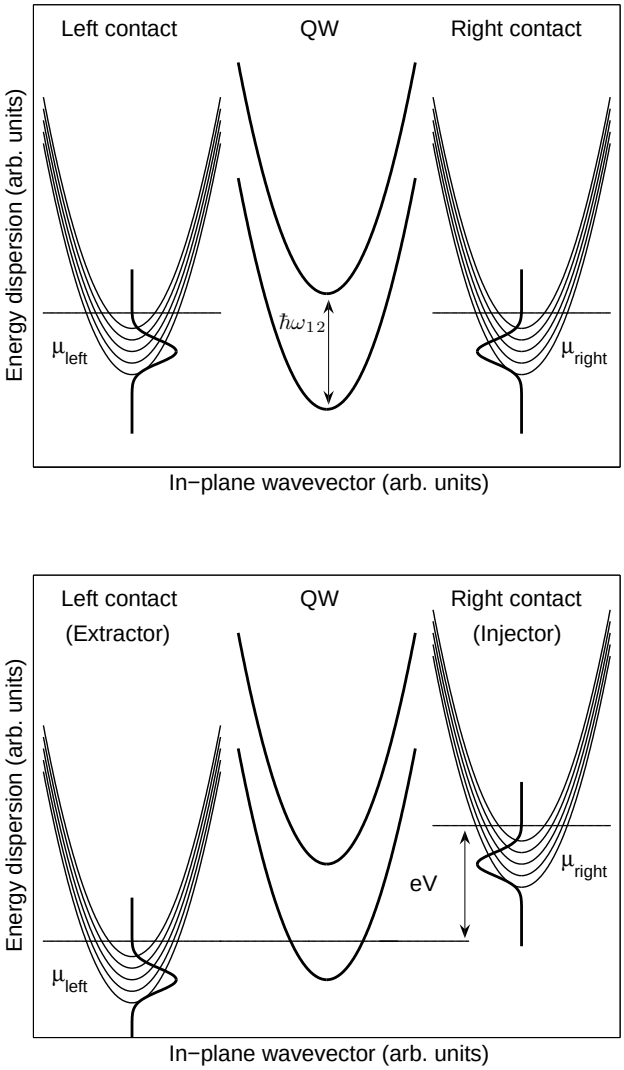

Figure 3.1: Top panel: sketch of the energy dispersion of the two quantum well subbands and of the minibands in the left and right contacts in the zero-bias case. Here the system is in thermal equilibrium and the Fermi level in the quantum well is the same as in the two contacts. The doping level in the contacts determines the equilibrium density in the quantum well. The subband and minibands have an energy dispersion versus the in-plane wavevector, which is a conserved quantity in the planar structure. This electronic structure is embedded in a planar microcavity, with a cavity photon mode quasi-resonant to the intersubband transition. Bottom panel: the same but with an applied voltage bias. Here, the left contact acts as an electronic extractor, while the right one is the injector. In the quantum well, non-equilibrium steady-state populations can be established in the two subbands.

where $V_{p,j,\mathbf{k},k_z}$ is the tunneling matrix element and k_z is in general an index over the electronic states of the miniband with in-plane wavevector $\mathbf{k}$. It can be interpreted as the axial electronic wavevector in the case the two leads are just bulk contacts. $1/(1+e^{\beta(E^{res}_{p,\mathbf{k},k_z}-\mu_p)})$ is the Fermi-Dirac occupation number of the electron states in the contact. Analogously the tunneling rate from the j-th subband of the quantum well into the reservoir p reads

$$\Gamma^{out}_{p,j,\mathbf{k}} = \frac{2\pi}{\hbar}\sum_{k_z}\frac{|V_{p,j,\mathbf{k},k_z}|^2\delta\left(E^{res}_{p,\mathbf{k},k_z}-\hbar\omega_j(\mathbf{k})\right)}{1+e^{-\beta(E^{res}_{p,\mathbf{k},k_z}-\mu_p)}}, \tag{3.9}$$

where

$$\frac{1}{1+e^{-\beta(E^{res}_{p,\mathbf{k},k_z}-\mu_p)}} = 1-\frac{1}{1+e^{\beta(E^{res}_{p,\mathbf{k},k_z}-\mu_p)}} \tag{3.10}$$

is the hole occupation number in the contact. The value of $\Gamma^{in,out}_{p,j,\mathbf{k}}$ can be quantum engineered, depending on the specific structure. In particular, by changing the thickness of the potential barriers, it is possible to tailor considerably the tunneling matrix element. It is straightforward to see that a simple relationship occurs between $\Gamma^{in}_{p,j,\mathbf{k}}$ and $\Gamma^{out}_{p,j,\mathbf{k}}$, namely

$$\frac{\Gamma^{in}_{p,j,\mathbf{k}}}{\Gamma^{out}_{p,j,\mathbf{k}}} = e^{\beta(\mu_p-\hbar\omega_j(\mathbf{k}))}. \tag{3.11}$$

Note that here we have assumed that the bare energy dispersion of the electrons in the two subbands is unaffected. This is valid when the injector miniband energy width is not smaller than the light-matter coupling strength. For large values of the vacuum Rabi frequency, the spectral function of the electrons in the second subband is non-trivially modified as well as the tunneling process using a narrow-band injector, as discussed in Chapter 4.

3.3 Steady-state regime and observable quantities

We are interested in the steady-state solutions for the quantities $n_{a,\mathbf{q}}$, $n_{1,\mathbf{k}}$, $n_{2,\mathbf{k}}$, $Y(\mathbf{q},\mathbf{k})$ and $X(\mathbf{q}+\mathbf{q}',\mathbf{q}',\mathbf{k})$. Hence, we can set the time derivatives equal to zero, transforming the differential system in Eq. 3.7 into an algebraic one. In the steady-state regime, the electronic current (number of electrons per unit

time) through the structure is given by the expression

$$I = 2\sum_{\mathbf{k}} \Gamma^{out}_{left,1,\mathbf{k}} n_{1,\mathbf{k}} + \Gamma^{out}_{left,2,\mathbf{k}} n_{2,\mathbf{k}} - \Gamma^{in}_{left,1,\mathbf{k}}(1-n_{1,\mathbf{k}}) - \Gamma^{in}_{left,2,\mathbf{k}}(1-n_{2,\mathbf{k}}). \tag{3.12}$$

The total rate of photons emitted out of the microcavity reads

$$P = 2\gamma \sum_{\mathbf{q}} n_{a,\mathbf{q}}, \tag{3.13}$$

where $1/(2\gamma)$ is the escape time of a photon out of the microcavity. The *quantum efficiency* η is defined as the ratio between the photonic current out of the cavity and electronic current , i.e., $\eta = \frac{P}{I}$. In the steady-state regime, the momentum-dependent spontaneous photon emission spectra are given by the expression

$$\mathcal{L}_{\mathbf{q}}(\omega) \propto \int_0^\infty dt \Re < a^\dagger_{\mathbf{q}}(0) a_{\mathbf{q}}(t) > e^{(i\omega - 0^+)t}. \tag{3.14}$$

In order to determine $< a^\dagger_{\mathbf{q}}(0) a_{\mathbf{q}}(t) >$, we need to solve the following Heisenberg equations of motion

$$\begin{aligned}
\frac{d}{dt} < a^\dagger_{\mathbf{q}}(0) a_{\mathbf{q}} > &= -i\omega_{cav}(\mathbf{q}) < a^\dagger_{\mathbf{q}}(0) a_{\mathbf{q}} > \\
&\quad + i\chi(q) \sum_{\mathbf{k},\sigma} < a^\dagger_{\mathbf{q}}(0) c^\dagger_{1,\sigma,\mathbf{k}} c_{2,\sigma,\mathbf{k}+\mathbf{q}} > \\
\frac{d}{dt} < a^\dagger_{\mathbf{q}}(0) c^\dagger_{1,\sigma,\mathbf{k}} c_{2,\sigma,\mathbf{k}+\mathbf{q}} > &= -i\omega_{12} < a^\dagger_{\mathbf{q}}(0) c^\dagger_{1,\sigma,\mathbf{k}} c_{2,\sigma,\mathbf{k}+\mathbf{q}} > \\
&\quad - i \sum_{\mathbf{q}'} \chi(q') < a^\dagger_{\mathbf{q}}(0) a_{\mathbf{q}'} c^\dagger_{2,\sigma,\mathbf{k}+\mathbf{q}'} c_{2,\sigma,\mathbf{k}+\mathbf{q}} > \\
&\quad + i \sum_{\mathbf{q}'} \chi(q') < a^\dagger_{\mathbf{q}}(0) a_{\mathbf{q}'} c^\dagger_{1,\sigma,\mathbf{k}} c_{1,\sigma,\mathbf{k}+\mathbf{q}-\mathbf{q}'} > .
\end{aligned} \tag{3.15}$$

Here we have omitted the coupling of the electronic injector and extractor reservoirs to the quantity $< a^\dagger_{\mathbf{q}}(0) c^\dagger_{1,\sigma,\mathbf{k}} c_{2,\sigma,\mathbf{k}+\mathbf{q}} >$. This coupling would involve correlations between the quantum well electronic field and the contact electronic fields. Since we are dealing with incoherent electron transport, we will neglect such correlations with the contact reservoirs, which are also extremely tricky to tackle.

In order to solve the system for two times averages in Eq. 3.15 we exploited the truncation scheme we used for the system of one times averages in Eq.

3.7. Truncating the hierarchy at the level of two bosonic excitations (details in Appendix C) and taking the unilateral Fourier transform ($\int_0^\infty dt e^{i\omega t}$) we obtain:

$$\begin{aligned} S_{\mathbf{q}}(t=0) &= n_{a,\mathbf{q}} = i(\omega - \omega_{cav}(\mathbf{q}) + i\Gamma_S(\mathbf{q}))\tilde{S}_{\mathbf{q}}(\omega) + 2i\chi(q)\tilde{Z}_{\mathbf{q}}(\omega) \quad (3.16) \\ Z_{\mathbf{q}}(t=0) &= \sum_{\mathbf{k}} Y(\mathbf{q},\mathbf{k}) = i(\omega - \omega_{12} + i\Gamma_Z(\mathbf{q}))\tilde{Z}_{\mathbf{q}}(\omega) + i\chi(q)\tilde{S}_{\mathbf{q}}(\omega)D, \end{aligned}$$

where $S_{\mathbf{q}}(t) =< a^\dagger_{\mathbf{q}}(0)a_{\mathbf{q}}(t) >$, $Z_{\mathbf{q}}(t) = \sum_{\mathbf{k}} < a^\dagger_{\mathbf{q}}(0)c^\dagger_{1,\sigma,\mathbf{k}}c_{2,\sigma,\mathbf{k}+\mathbf{q}} >$ and D represents half the difference between the total number of electrons in the fundamental subband and the number in the second one, namely

$$D = \sum_{\mathbf{k}} D_{\mathbf{k}} = \sum_{\mathbf{k}} (n_{1,\mathbf{k}} - n_{2,\mathbf{k}}). \quad (3.17)$$

Note that the total density of electrons is $2\sum_{\mathbf{k}} n_{1,\mathbf{k}} + n_{2,\mathbf{k}}$, where the 2 factor accounts for the two-fold spin degeneracy of the electron states in the conduction subbands. Γ_S and Γ_Z are phenomenological damping rates for $S_{\mathbf{q}}$ and $Z_{\mathbf{q}}$ respectively. The analytical solutions are

$$\tilde{S}_{\mathbf{q}}(\omega) = \frac{in_{a,\mathbf{q}}\left(\gamma(\frac{\omega_{cav}(\mathbf{q})-\omega_{12}}{\Gamma_Y} + i) - (\omega - \omega_{12} + i\Gamma_Z)\right)}{(\omega - \omega_{12} + i\Gamma_Z)(\omega - \omega_{cav}(\mathbf{q}) + i\Gamma_S) - 2\chi(q)^2 D}, \quad (3.18)$$

$$\tilde{Z}_{\mathbf{q}}(\omega) = -\frac{\chi(q)S_{\mathbf{q}}(\omega)D + i\frac{\gamma n_{a,\mathbf{q}}}{2\chi(q)}(\frac{\omega_{cav}(\mathbf{q})-\omega_{12}}{\Gamma_Y} - i)}{\omega - \omega_{12} + i\Gamma_Z}. \quad (3.19)$$

The electroluminescence spectrum is simply $\mathcal{L}_{\mathbf{q}}(\omega) \propto \Re\tilde{S}_{\mathbf{q}}(\omega)$. From the analytical result for $\tilde{S}_{\mathbf{q}}(\omega)$, we see immediately that emission spectrum is resonant at the two polariton frequencies $\omega_\pm(q)$ satisfying the equation

$$(\omega - \omega_{12} + i\Gamma_Z)(\omega - \omega_{cav}(q) + i\Gamma_S) - 2\chi(q)^2 D = 0. \quad (3.20)$$

The quantity $\Omega_R(q) = \chi(q)\sqrt{2D}$ is just the vacuum Rabi frequency of the present system. At resonance (i.e., $\omega_{cav}(q) = \omega_{12}$), the necessary condition for the appearance of a strong coupling polaritonic splitting is $D > D_0 = \frac{(\Gamma_S - \Gamma_Z)^2}{8\chi(q)^2}$, meaning that the total density of electrons in the fundamental subband must be larger enough than the total density in the second. For a vacuum Rabi frequency much larger than Γ_Z and Γ_S, the minimum polariton splitting is given by twice the vacuum Rabi frequency.

Note that here the electroluminescence spectral shape does not depend explicitly on the spectral properties of the injector and extractor reservoirs. The spectrum in Eq. 3.18 has the same shape as the absorption (in presence of the same carrier densities). The dependence on the transport is only implicit, being given by the steady-state carrier and photon populations. The exact diagonalization method described in Chapter 4 indeed shows that the spectral properties of the electronic contact modifies significantly the spectral shape of the electroluminescence in the case of narrow band injectors. Hence, the spectrum predicted by Eq. 3.18 is valid only for broad band injectors. This is not really surprising because, in order to calculate the tunneling rates, we have used bare electronic states in the quantum well and have only considered incoherent population injection and extraction processes.

3.4 Numerical procedure and results

Here, we apply our theory using realistic parameters for a microcavity-embedded quantum cascade electroluminescent source. In order to simplify the algebra, given the huge difference in the typical wavectors of photons and electrons, we have systematically neglected the photon wavevector whenever added to an electronic wavevector, as explained in Section 1.4.3. Applying this approximation, we can obtain a closed set of algebraic equations where the variables are the populations in the two subbands and in the cavity photonic branch, as shown in Appendix C. This system has been solved numerically using a standard Newton method. We achieve numerical convergence in a relatively fast computation time except in the limit of vanishing bias, when the injector and extractor are strongly 'misaligned' with the two subbands. Physically in this case the steady-state situation is reached in times very long compared to the dynamics of the quantum well system, the photon population is extremely small and correspondingly the numerical method fails to converge. Anyway this is not a real limitation, because we are interested in the behavior of the system in presence of a finite voltage bias, producing a significant current flow and photonic output.

In Fig. 3.1, we show a sketch of the energy profile of the injector and extractor with respect to the quantum well subbands respectively without and with an applied bias. Specifically, in the numerical calculations we have used

the following electronic out-tunneling rates:

$$\begin{aligned}\Gamma^{out}_{\text{left},j,\mathbf{k}} &= \frac{\Gamma e^{-\frac{(E_{0,\text{left}}-qV/2)^2}{2\sigma^2}}}{1+e^{\beta(-\hbar\omega_{j,\mathbf{k}}+\mu_{\text{left}}-qV/2)}}, \\ \Gamma^{out}_{\text{right},j,\mathbf{k}} &= \frac{\Gamma e^{-\frac{(E_{0,\text{right}}+qV/2)^2}{2\sigma^2}}}{1+e^{\beta(-\hbar\omega_{j,\mathbf{k}}+\mu_{\text{right}}+qV/2)}},\end{aligned} \tag{3.21}$$

where $\sigma = 0.1\hbar\omega_{12}$, $1/\Gamma = 0.4$ps, $E_{0,\text{left}}$ and $E_{0,\text{right}}$ are the energy offsets of the left and right minibands. The in-tunneling rates are determined by applying the relation in Eq. 3.11. In all the simulations, we have taken $E_{0,\text{left}} = E_{0,\text{right}} = 0.5\hbar\omega_{12}$ and $\mu_{\text{left}} = \mu_{\text{right}} = \frac{1}{3}\hbar\omega_{12}$.

Note that these are just phenomenological injection rates. For the amplitude Γ, we have considered values which are consistent with what realistically obtainable in semiconductor intersubband devices. Importantly, in real structures Γ can be considerably quantum engineered by changing the barrier thickness and/or the miniband structure of the injection superlattices. This is why we have not considered a very specific injector configuration and taken the simplified expression in Eq. 4.17 with realistic parameters.

When a voltage bias is applied, the two reservoirs are shifted symmetrically, as shown in the bottom panel of Fig. 3.1. In all the simulations, except when otherwise stated we used the realistic damping parameters $\Gamma_X = \Gamma_Y = \Gamma_S = \Gamma_Z = 0.1\omega_{12}$, $\gamma = 0.05\omega_{12}$, while the temperature is $T = 77$K. In the simulations we have also considered $\tau_{\mathbf{k}}$ to be independent from $\mathbf{k}$ and such that $\frac{1}{\tau} = 0.005\omega_{12}$, except when otherwise stated. Here we have considered only an active quantum well. For quantum cascade structures with several active quantum wells repeated in a periodic way, the dynamics is similar and the present treatment can be generalized without major difficulties. In the simulations, the intersubband transition energy $\hbar\omega_{12}$ is, except where otherwise stated, equal to 150 meV and the coupling constant $\chi(q)$ is such that the vacuum Rabi frequency is $0.1\omega_{12}$ for an electron density of 5×10^{11} cm^{-2} (all in the fundamental subband). When $\hbar\omega_{12}$ is changed, the coupling constant is adjusted in order to keep the ratio between the vacuum Rabi frequency and transition frequency constant. The effective mass m^* has been taken to be one tenth of the bare electronic mass. In the numerical calculations, the cavity spacer dielectric constant is $\epsilon_r = 10$. For each simulation, the resonance in-plane wavevector q_{res}, given by the condition $\omega_{cav}(q_{res}) = \omega_{12}$, corresponds to an internal cavity photon propagation angle θ_{res} equal to 70 degrees, where $\tan\theta_{res} = q_{res}/q_z$. In the top panel of Fig. 3.2, we show the current density

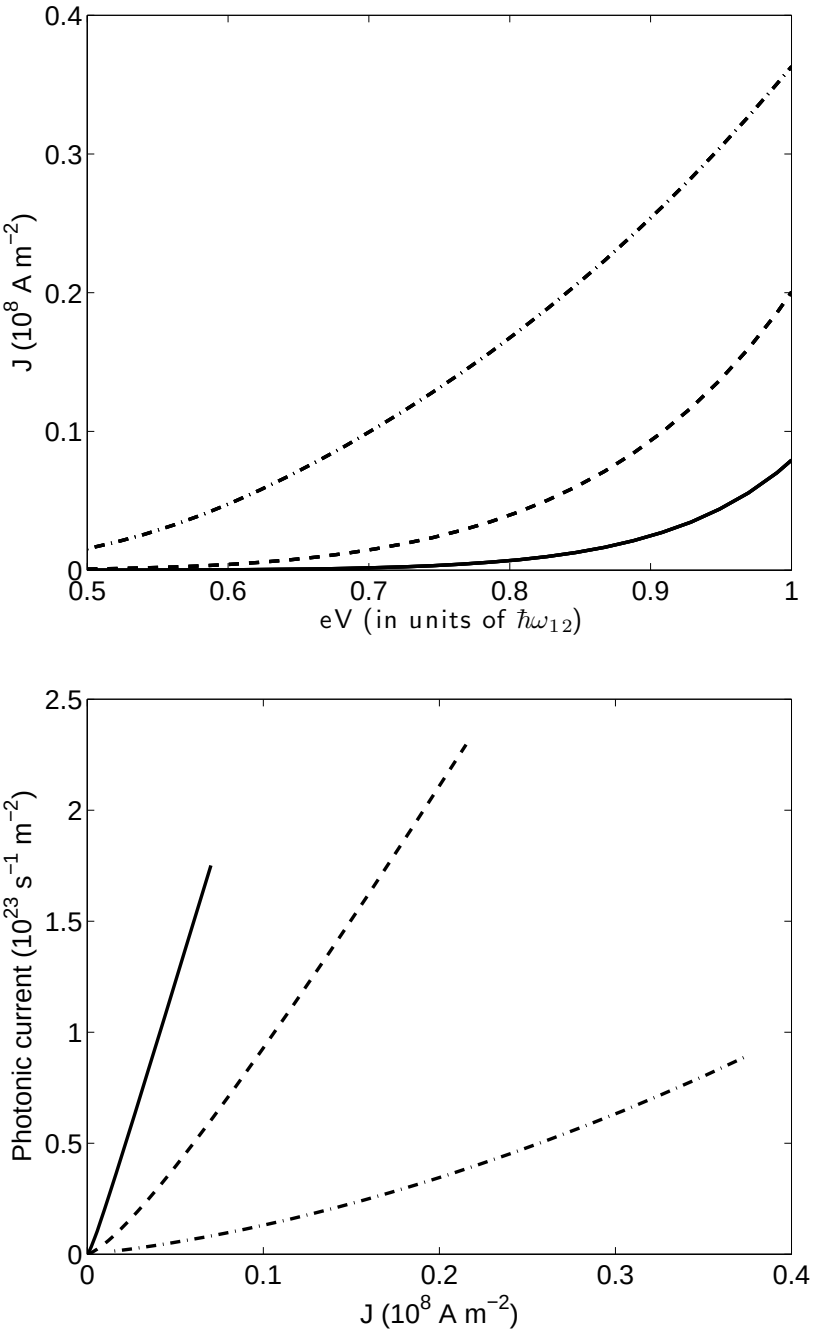

Figure 3.2: Current density versus applied voltage (top panel) and Photonic current density versus electronic current (bottom panel) for different values of the intersubband transition energy: $\hbar\omega_{12} = 50$ meV, (dashed-dotted line), 100 meV (dashed line) and 150 meV (solid line).

versus applied voltage (between the injector and extractor) for different values of $\hbar\omega_{12}$. The current-voltage profile is characteristic of an unipolar quantum cascade light emitting diode. The current grows superlinearly in the voltage region where the injector Fermi level approaches the second subband. The current is bigger for smaller $\hbar\omega_{12}$ because, keeping the injection rate Γ constant (but all the internal rates of the system proportional to $\hbar\omega_{12}$), the injection and extraction processes become the dominant processes. The rates of emitted photons per unit area (integrated all over the in-plane wavevectors) are shown in the bottom panel of Fig. 3.2 as a function of the flowing current, showing an approximately linear behavior. Fig. 3.3 shows contour plots of the electron occupation numbers of the first and second subband respectively as a function of the applied voltage and of the kinetic energy. The insets in Fig. 3.3 show respectively the integrated density of electrons in the first and second subband. It is apparent that with increasing voltage the population in the first subband decreases, while the population in the second subband increases. When the injector Fermi level becomes aligned with the second subband, as expected, the carrier occupation numbers in the two subbands are considerably out of equilibrium. The decrease of the first subband carrier occupation numbers is beneficial for the radiative efficiency of the spontaneous emission, because the influence of Pauli blocking is reduced. Moreover, in the considered conditions, the density of electrons in the first subband is still considerably larger than in the second subband, thus producing a large vacuum Rabi coupling and efficient emission rate. Fig. 3.4 contains a contour plot of the cavity photon occupation number versus the bare photon energy, showing that the maximum of emission is obtained when the bare photon energy is resonant with the intersubband transition, as expected and as observed experimentally [39, 80]. With the considered parameters, the density of electrons in the first subband is high enough to be in the strong coupling regime, as depicted in Fig. 3.5, where the anticrossing of two polariton branches is clearly present. The minimum polariton splitting, given by the expression $2\chi(q)\sqrt{2D}$ is reported in Fig. 3.5 as a function of the applied bias. With increasing voltage, the population difference $D = \sum_{\mathbf{k}} D_{\mathbf{k}} = \sum_{\mathbf{k}}(n_{1,\mathbf{k}} - n_{2,\mathbf{k}})$ diminishes. This results in a decrease of the vacuum Rabi frequency and consequently of the polariton splitting. This high-excitation feature has been already observed in experiments [39, 80].

It is interesting to analyze the quantum efficiency η, defined as the ratio

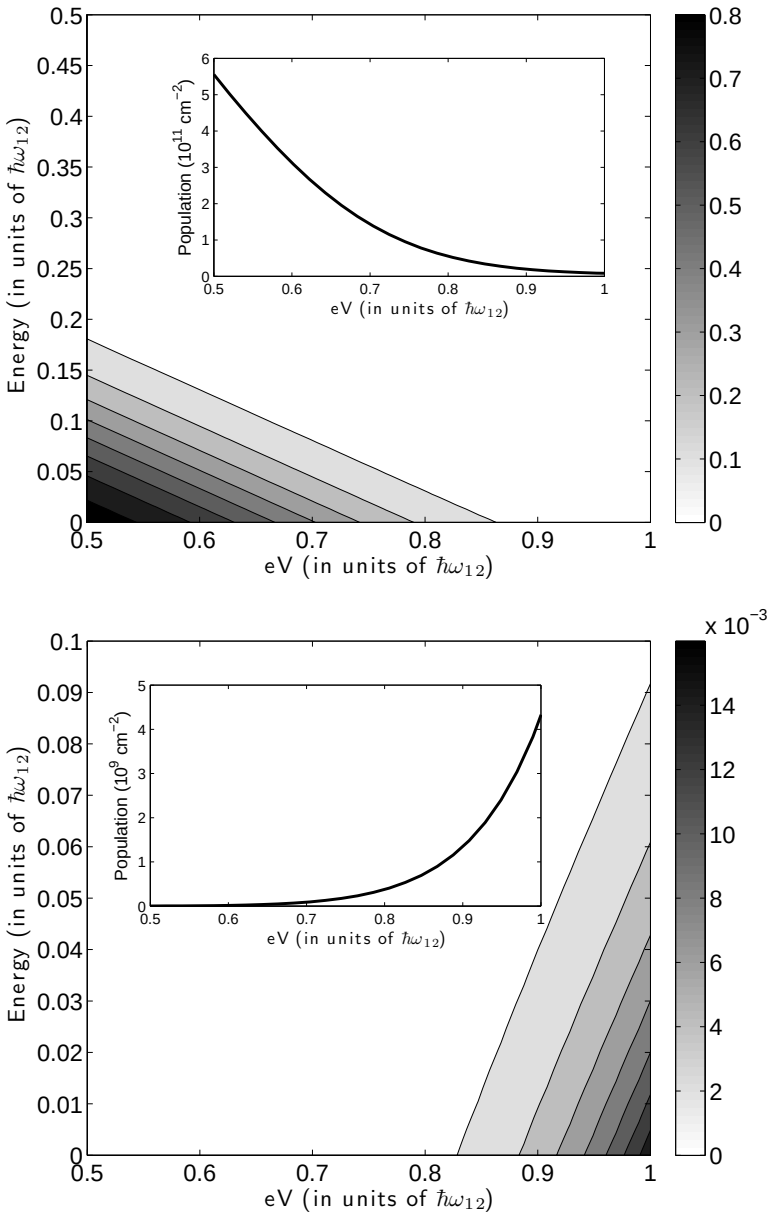

Figure 3.3: Electron occupation number in the first (top panel) and second (bottom panel) conduction subband as a function of kinetic energy and applied voltage. In the insets there are the integrated density of electrons in the two subbands versus voltage. In these simulations $\hbar\omega_{12} = 150$ meV.

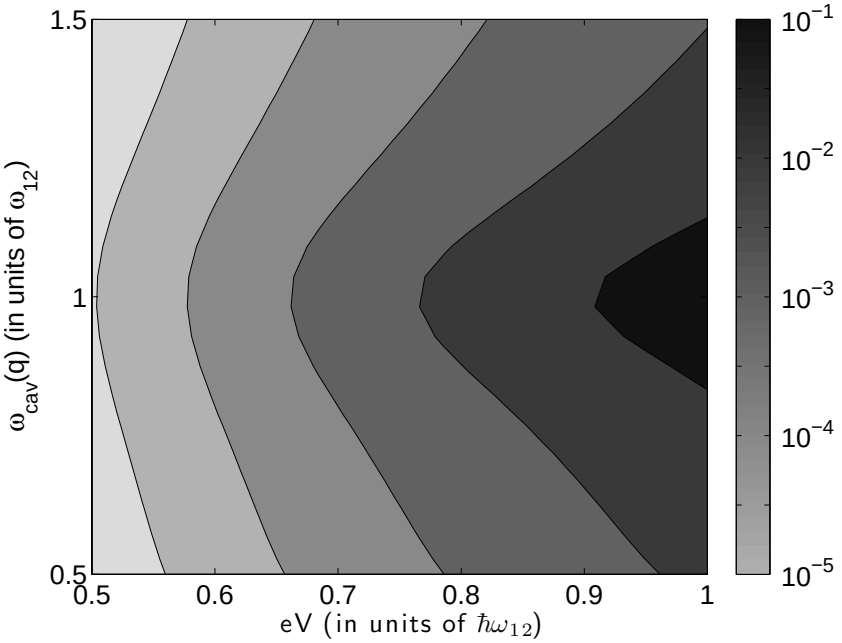

Figure 3.4: Contour plot of the photon occupation (log scale) versus the applied voltage and the frequency of the bare cavity photon mode.

between the photonic emission rate and the electronic current, namely

$$\eta = \frac{2\gamma \sum_{\mathbf{q}} n_{a,\mathbf{q}}}{\sum_{\mathbf{k}} [\Gamma^{out}_{1,\mathbf{k}} n_{1,\mathbf{k}} - \Gamma^{in}_{1,\mathbf{k}}(1 - n_{1,\mathbf{k}})]}. \tag{3.22}$$

In Fig. 3.6, we plot the quantum efficiency η at $eV = \hbar\omega_{12}$ versus the resonant vacuum Rabi frequency $\Omega_R = \Omega_R(q_{res})$ at the same voltage (log-log scale). In the simulations, the vacuum Rabi frequency has been varied by changing the coupling constant $\chi(q)$. In a realistic quantum engineered device, $\chi(q)$ can be tailored in different ways. For example, by growing the active quantum wells in a spatial region where the cavity mode field is very small, it is possible to quench dramatically the value of $\chi(q)$. Moreover, by using different shape of quantum wells, it is also possible to tailor the transition dipole d_{12}. Fig. 3.6 shows that in the weak coupling regime (small values of Ω_R) the efficiency grows like Ω_R^2. In the strong coupling regime, the efficiency becomes impressive and then tends to saturate. It is apparent that the radiative efficiency smoothly increases passing from the weak to the strong coupling regime. This crossover occurs because the radiative efficiency depends on the spectrally integrated emission and it is therefore insensitive to the sudden appearing of the polariton doublet in the strong coupling emission spectra. In Fig. 3.6, the efficiency is plotted for different values of the damping coefficients (top panel) and of the nonradiative population relaxation rate $1/\tau$ (bottom panel). The nonradiative population relaxation rate has clearly the most significant effect, in the considered regime of parameters, the efficiency is proportional to τ. It is interesting to compare our results for this microcavity system with the standard free space case. In the free-space case, the photon current, obtained by applying the Fermi golden rule, is given by the formula

$$P = \frac{2d_{12}^2\omega_{12}^3\sqrt{\epsilon_r}}{3\pi c^3\hbar\epsilon_0} \sum_{\mathbf{k}} n_{2,\mathbf{k}}(1 - n_{1,\mathbf{k}}). \tag{3.23}$$

As it is well known, the free-space radiative efficiency dramatically decreases with the intersubband emission wavelength due to the $\omega_{12}^3 d_{12}^2$ dependence of the spontaneous emission rate ($d_{12}^2 \propto 1/\omega_{12}$, so the spontaneous emission rate scales effectively as ω_{12}^2). In the mid-infrared, by using the same parameters, for a transition of 150 meV, the quantum efficiency is of the order of $10^{-4}-10^{-5}$ (see the red line in the top panel of Fig. 3.6). Hence, it is clear from our results that a strong coupling light-emitting diode based on a planar microcavity system can provide a dramatic enhancement with respect to the free space

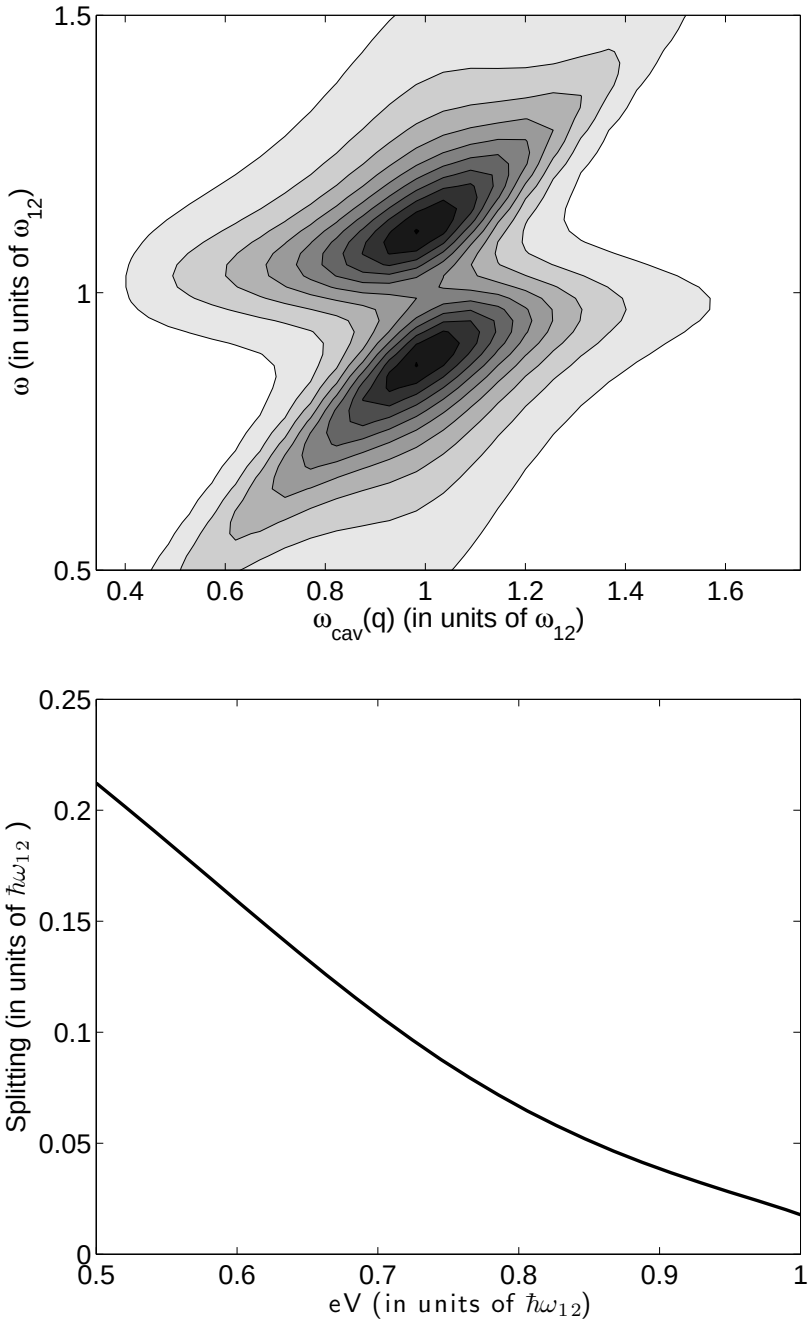

Figure 3.5: Top panel: contour plot of the electroluminescence (arb. units) as a function of the bare cavity photon energy $\omega_{cav}(q)$ and of the emission frequency ω for an applied voltage $eV = 0.5\hbar\omega_{12}$. Bottom panel: minimum polariton splitting as a function of the applied voltage for $\hbar\omega_{12} = 150$ meV.

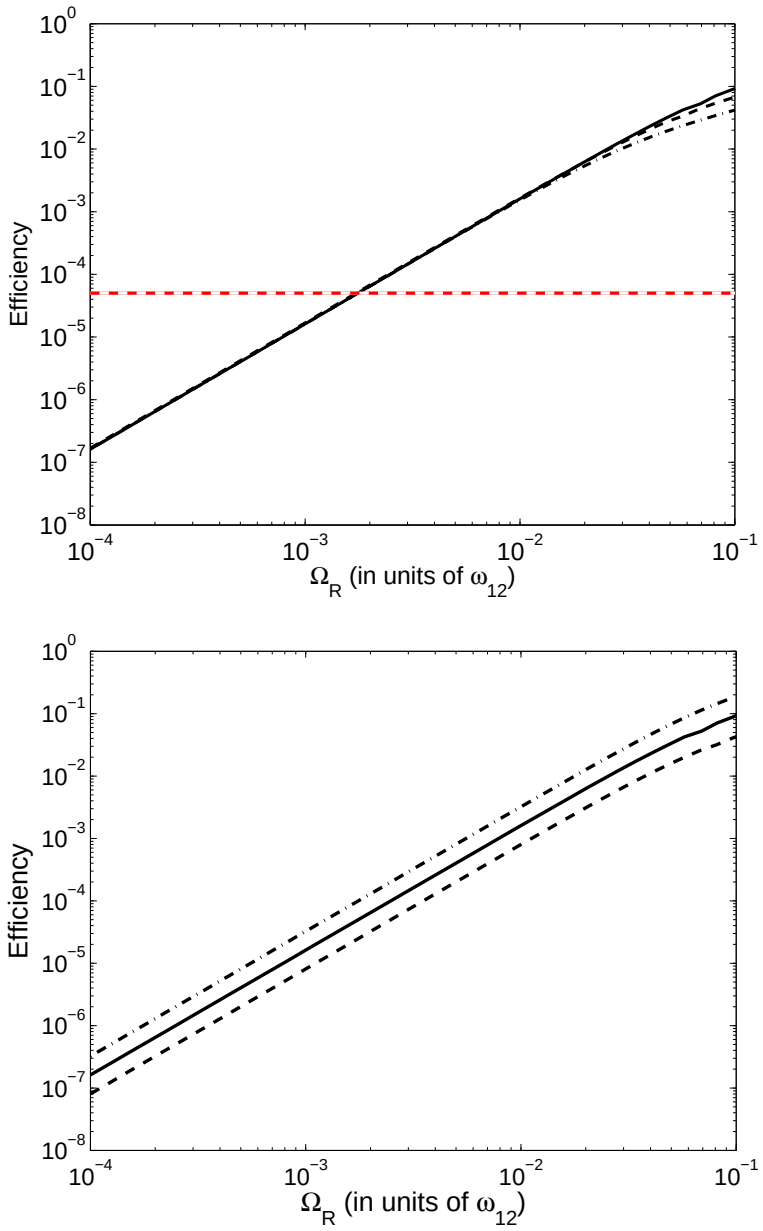

Figure 3.6: Quantum efficiency versus the corresponding resonant vacuum Rabi frequency at the voltage $eV = \hbar\omega_{12}$ for $\hbar\omega_{12} = 150$ meV. The three lines in the top panel are obtained with different values of the coherence damping coefficients: $\Gamma_X = \Gamma_Y = 0.1\omega_{12}$ (solid line), $0.05\omega_{12}$ (dashed line) and $0.025\omega_{12}$ (dashed-dotted line). The three lines in the bottom panel are obtained with different values of the non-radiative relaxation rate: $\frac{1}{\tau} = 0.01\omega_{12}$ (dashed line), $0.005\omega_{12}$ (solid line) and $0.0025\omega_{12}$ (dashed-dotted line). In red is marked a typical efficiency value in the free space (no cavity) case.

case (even three orders of magnitude for the larger vacuum Rabi frequency case).

3.5 Conclusions and perspectives

We developed a numerical method to study the effect of strong coupling on electron transport and electroluminescence. Our results agree with the data from the first transport experiments in the strong coupling regime [53, 39, 80]. In particular our theory predicts correctly that, being the vacuum Rabi frequency proportional to the population imbalance between the first and the second conduction subband, it decreases when a large current flows through the structure. Moreover we showed that even in presence of non-radiative relaxation and Pauli blocking, the quantum efficiency of the microcavity intersubband electroluminescence can be considerably enhanced by increasing the vacuum Rabi frequency, giving the first evidence of Purcell effect in the strong coupling regime. We expect that, given the actual trend in the increase of the vacuum Rabi frequency, it will soon be possible to experimentally measure this effect. On this topic it is important to stress that the Ω_R in the abscissa of Fig. 3.6 is the vacuum Rabi frequency at the corresponding working point. From the bottom panel of Fig. 3.5 we see that the splitting (and thus the vacuum Rabi frequency) at the working point can easily be one order of magnitude smaller than the zero-bias one. This means that present-day state-of-the-art experiments, that have vacuum Rabi frequencies of the order of few percents of ω_{12}, have an efficiency comparable with the free space case. In order to experimentally measure the strong coupling Purcell effect it will thus be necessary to work in order to obtain samples with bigger vacuum Rabi frequencies, of the order at least of a tenth of ω_{12}. Samples with such large couplings have been recently reported [32]. We thus not only expect a rapid experimental verification of our predictions, but we also hope to see it applied in real word devices, to considerably increase the efficiency of mid-infrared and Terahertz light emitting devices.

Our method is well suited to model a large spectrum of possible devices, giving quantitative results with very limited computational resources and we expect it will be thoroughly exploited to design the next generation of optoelectronics polaritonic devices.

Chapter 4

Electron tunneling into polariton states

4.1 Introduction

In the previous Chapter we developed a theory able to describe light emitting devices in the strong coupling regime, under the assumption of incoherent, broadband injection. In this Chapter we will instead try to understand what happens when the injector is spectrally narrow.

If we consider the bare quantum well, neglecting light-matter coupling, electrons can occupy a certain number of eigenstates $|\eta\rangle$, each one identified by its own set of quantum numbers (that here we will collectively identify as η) and to each one corresponds a well defined energy E_η. In the case of resonant electron tunneling, conservation of energy implies that in order to excite an electron in the state $|\eta\rangle$, we need to inject an electron with an energy equal to E_η.

This is not anymore the case when we consider the quantum well coupled with the microcavity photon field. The eigenstates of the light-matter coupled system, with a well defined energy, will be instead linear superpositions of different electronic and photonic states. If we are able to accurately select the energy of the injected electrons, we can thus choose which particular linear superposition of electronic states to excite. The interest being that, as we have seen in Section 1.2.2, only one linear superposition of electronic excitations (the *bright* state) is coupled, in a superradiant way, to the electromagnetic field. We could thus, by injecting an electron with exactly the right energy, put it in the state maximally coupled to the microcavity photonic field. The extremely

short radiative lifetime of such states would thus permit us to dramatically increase the efficiency of these systems as light emitting devices.

The energy shift between unperturbed electronic states and light-matter coupled states is of the order of the vacuum Rabi frequency. In order to exploit this effect we thus need to have an injector narrow enough to excite selectively superradiant states, that is we need an injector whose spectral width is smaller than the vacuum Rabi frequency itself.

In this Chapter we will lay out the theory for such resonant electron injection into superradiant states. We will show that the electronic eigenstates originate from a Fano-like coupling between the bare injected electron and the continuum of cavity polariton modes. Our theory will demonstrate that resonant electron tunnelling from a narrow-band injector contact can effectively lead to ultraefficient polariton electroluminescence.

4.2 General formalism

As in the previous Chapter, we will use here the RWA fermionic Hamiltonian of Section 1.4.2. The system will thus be described by the Hamiltonian

$$\begin{aligned} H &= \sum_{\mathbf{k}} \hbar\omega_{c,1}(k) c^{\dagger}_{1,\mathbf{k}} c_{1,\mathbf{k}} + \hbar\omega_{c,2}(k) c^{\dagger}_{2,\mathbf{k}} c_{2,\mathbf{k}} + \sum_{\mathbf{q}} \hbar\omega_{cav}(q) a^{\dagger}_{\mathbf{q}} a_{\mathbf{q}} \\ &+ \sum_{\mathbf{k},\mathbf{q}} \hbar\chi(q) a_{\mathbf{q}} c^{\dagger}_{2,\mathbf{k}+\mathbf{q}} c_{1,\mathbf{k}} + \hbar\chi(q) a^{\dagger}_{\mathbf{q}} c^{\dagger}_{1,\mathbf{k}} c_{2,\mathbf{k}+\mathbf{q}}, \end{aligned} \tag{4.1}$$

where for simplicity we neglected the electron spin. In this Chapter we will thus consider that each sum over the electronic in-plane wavevector $\mathbf{k}$ is implicitly also a sum over the electron spin.

It is well known in the theory of quantum transport [81] that, if we wish to study the tunneling injection of one electron at low temperature, we have to determine the electron spectral function, defined as:

$$A^{+}_{j}(\mathbf{k},\omega) = \sum_{\zeta} |\langle \zeta | c^{\dagger}_{j,\mathbf{k}} | F_N \rangle|^2 \delta(\omega - \omega_{\zeta}) \ , \tag{4.2}$$

where $|F_N\rangle$ is the N-electron Fermi sea ground state times the vacuum state for the cavity photon field and $j = 1, 2$ is the conduction subband index. The index ζ labels the excited (N+1)-electron eigenstates and $\hbar\omega_{\zeta}$ are the corresponding eigenenergies. Note that here we will develop our theory at zero temperature, but it will remain valid as long as KT is much smaller than the

Fermi energy of the two-dimensional electron gas ($\simeq 600$K). As apparent from Eq. 4.2, the electron spectral function is the density of quasi-electron states, weighted by the overlap with the bare electron state $c^\dagger_{j,\mathbf{k}}|F_N\rangle$. In other words, it is the many-body equivalent of the single-electron density of states. This is the key quantity affecting the electron tunneling and can be non-trivially modified by interactions like in the case of superconductors. It is important to understand that the spectral function describes the density of electronic states *for a given initial state*. That is, in our case, it describes the available states in presence of an unperturbed Fermi sea. Within this framework, we will thus be unable to account for the nonlinear effects induced by the fact that the current can modify the equilibrium electronic population. This means that the theory we will develop in this Chapter is valid only in a regime of currents small enough not to perturb the electronic population. As we explained in the previous Chapter, this is the price to pay in order to be able to look for an exact solution of the many body problem, instead that adopting truncated mean field theories (as we did in Chapter 3).

For a non-interacting electron gas, $c^\dagger_{1,\mathbf{k}}|F_N\rangle$ and $c^\dagger_{2,\mathbf{k}}|F_N\rangle$ are eigenstates of the Hamiltonian and thus all the other eigenstates are orthogonal to them. Therefore the non-interacting spectral functions are

$$A_1^+(\mathbf{k},\omega) = \delta(\omega-\omega_{c,1}(k))\theta(k-k_F), \tag{4.3}$$

$$A_2^+(\mathbf{k},\omega) = \delta(\omega-\omega_{c,2}(k)), \tag{4.4}$$

where k_F is the Fermi wavevector. $\theta(x)$ is the Heaviside function and its presence is due to Pauli blocking: $c^\dagger_{1,\mathbf{k}}|F_N\rangle = 0$ for $k < k_F$. Eq. 4.3 just says that there are unoccupied electron states in the first subband with energy lower than the Fermi level.

4.3 Spectral function with light-matter interactions

As seen in the previous Section, in the non-interacting case, the electron spectral function is just a Dirac delta. Physically, this means that an electron with wavevector $\mathbf{k}$ can be injected in the subband $j = 1, 2$ only with an energy equal to the bare electron energy $\hbar\omega_{c,j}(k)$ and that such excitation has an infinite lifetime. By contrast, interactions can profoundly modify the nature of electron excitations and therefore produce qualitative and quantitative

changes of the electron spectral functions. In the case of a weakly interacting electron gas, the spectral function has a broadened *quasi-electron* peak: the spectral broadening is due to the finite lifetime of the electronic excitation. In the case of a strongly interacting electron gas (like in the case of superconductors) the electron spectral function can be qualitatively different from the non-interacting gas. Here, we are interested in how the nature of the quasi-electron excitations is modified by the strong coupling to the vacuum field of a microcavity. In particular, we assume that the light-matter interaction is the strongest one. We will provide here a nonperturbative theory to determine the dressed electronic excitations in such a strong coupling limit and their corresponding spectral function. All other residual interactions, i.e. the coupling with an injector contact and the coupling with the extra-cavity photonic modes, will be treated as perturbations. The consistency and limit of validity of such a scheme will be discussed in the next Section, where the theoretical results are applied. In the interacting case, it is easy to verify that $c^{\dagger}_{1,\mathbf{k}}|F_N\rangle$ is still an eigenvector of the Hamiltonian in Eq. 4.1 and thus the first subband spectral function $A^{+}_{1}(\mathbf{k},\omega)$ is still given by Eq. 4.3. Instead for the electrons in the second subband we have to distinguish between two cases: $\mathbf{k}$ well inside or outside the Fermi sea. In the first case, an electron in the second subband can not emit a photon because all the final states in the first subband are occupied (Pauli blocking), hence the spectral function will be given by the unperturbed one (Eq. 4.4). Well outside the Fermi sea, an injected electron can emit and the spectral function will be modified by the light-matter interaction. A smooth transition between the two cases will take place for $|k-k_F|$ of the order of the resonant cavity photon wave-vector q_{res}, where $\omega_{cav}(q_{res})=\omega_{12}$. Being the ratio q_{res}/k_F typically very small, of the order of 10^{-2} (see Ref. [49]), we can safely consider an abrupt transition at the Fermi edge.

In order to evaluate $A^{+}_{2}(\mathbf{k},\omega)$ for $k>k_F$ we need to find all the (N+1)-electron eigenstates that have a nonzero overlap with $c^{\dagger}_{2,\mathbf{k}}|F_N\rangle$. In order to do this we notice that the Hamiltonian in Eq. 4.1 commutes with the number of total fermions

$$\hat{N}_F=\sum_{j=1,2}\sum_{\mathbf{k}} c^{\dagger}_{j,\mathbf{k}}c_{j,\mathbf{k}}, \tag{4.5}$$

the total in plane wave-vector operator

$$\hat{\mathbf{K}}=\sum_{j=1,2}\sum_{\mathbf{k}} \mathbf{k}\; c^{\dagger}_{j,\mathbf{k}}c_{j,\mathbf{k}}+\sum_{\mathbf{q}}\mathbf{q}\; a^{\dagger}_{\mathbf{q}}a_{\mathbf{q}}, \tag{4.6}$$

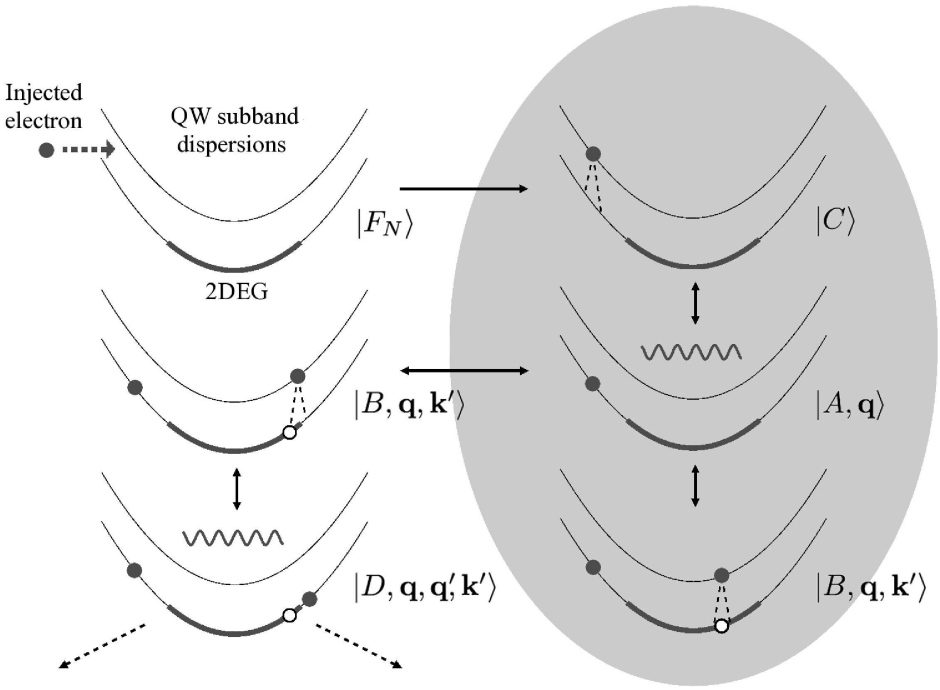

Figure 4.1: Sketch of the dynamical coupling between quantum states in a microcavity-embedded doped quantum well In the ground state, the first subband is doped with a dense two-dimensional electron gas (bold lines at the bottom of the dispersions). Black dots represent bare electrons, while white dots denote holes in the electron gas. The dashed cones depicts the possible final states for an electron radiatively relaxing from the second to the first subband by emission of a cavity photon. The ground state with N electrons is the standard Fermi sea $|F_N\rangle$. The injection (e.g., through electron tunneling) of an additional electron in the second subband creates the state $|C\rangle = c^\dagger_{2,\mathbf{k}}|F_N\rangle$, which, in presence of light-matter interaction, is not an eigenstate. Spontaneous emission of a cavity photon couples the $|C\rangle$ state to the states $|A, \mathbf{q}\rangle = a^\dagger_{\mathbf{q}} c^\dagger_{1,\mathbf{k}-\mathbf{q}}|F_N\rangle$. Reabsorption of the emitted cavity photon can couple back to the $|C\rangle$ state or to the states $|B, \mathbf{q}, \mathbf{k}'\rangle = c^\dagger_{2,\mathbf{k}'+\mathbf{q}} c_{1,\mathbf{k}'} c^\dagger_{1,\mathbf{k}-\mathbf{q}}|F_N\rangle$. Spontaneous emission couples the $|B\rangle$ states back to $|A\rangle$ states or to states of the form $|D, \mathbf{q}, \mathbf{q}', \mathbf{k}'\rangle = a^\dagger_{\mathbf{q}'} c^\dagger_{1,\mathbf{k}'+\mathbf{q}-\mathbf{q}'} c_{1,\mathbf{k}'} c^\dagger_{1,\mathbf{k}-\mathbf{q}}|F_N\rangle$. Being the relevant cavity photon wavevectors very small compared to the Fermi wavevector, spontaneous emission can occur only on narrow emission cone in momentum space. Due to the small probability of photon absorption by electrons on the border the Fermi sea, we can neglect $|D\rangle$ states and assume that the system always jumps from $|B\rangle$ states to $|A\rangle$ states. Thus the relevant dynamics takes place only between the states in the shaded region. We can thus neglect the other marginal states while diagonalizing the light-matter Hamiltonian.

and the excitation number operator

$$\hat{Q} = \sum_{\mathbf{k}} c^{\dagger}_{2,\mathbf{k}} c_{2,\mathbf{k}} + \sum_{\mathbf{q}} a^{\dagger}_{\mathbf{q}} a_{\mathbf{q}}. \tag{4.7}$$

Hence the eigenstates $|\zeta\rangle$ of H can be also labeled by the corresponding eigenvalues $N_\zeta, \mathbf{K}_\zeta$ and Q_ζ. We will thus identify an eigenstate of H in the subspace $(\hat{N_F} = N, \hat{\mathbf{K}} = \mathbf{K}, \hat{Q} = Q)$ as $|N, \mathbf{K}, Q, \zeta\rangle$, where the index ζ now runs over all the eigenstates of the subspace. The states obtained by applying electron creation or destruction operators on the eigenstates $|N, \mathbf{K}, Q, \zeta\rangle$ are still eigenstates of $\hat{N}_F$, $\hat{\mathbf{K}}$ and $\hat{\mathbf{Q}}$. The state $c^{\dagger}_{1,\mathbf{k}}|N, \mathbf{K}, Q, \zeta\rangle$ is in the subspace labeled by the quantum numbers $(N+1, \mathbf{K}+\mathbf{k}, Q)$; $c_{1,\mathbf{k}}|N, \mathbf{K}, Q, \zeta\rangle$ in $(N-1, \mathbf{K}-\mathbf{k}, Q)$; $c^{\dagger}_{2,\mathbf{k}}|N, \mathbf{K}, Q, \zeta\rangle$ in $(N+1, \mathbf{K}+\mathbf{k}, Q+1)$; $c_{2,\mathbf{k}}|N, \mathbf{K}, Q, \zeta\rangle$ in $(N-1, \mathbf{K}-\mathbf{k}, Q-1)$.

Having $|F_N\rangle$ quantum numbers (N,**0**,0) the state $c^{\dagger}_{2,\mathbf{k}}|F\rangle$ is thus in the subspace labeled by the quantum numbers $(N+1, \mathbf{k}, 1)$. We can limit ourselves to diagonalize H in this subspace, which is spanned by vectors of the form: (i) $c^{\dagger}_{2,\mathbf{k}_0} \prod_{j=1}^{N} c^{\dagger}_{1,\mathbf{k}_j}|0\rangle$, where $|0\rangle$ is the empty conduction band state and $\sum_{j=1}^{N} \mathbf{k}_j = \mathbf{k} - \mathbf{k}_0$; (ii) $a^{\dagger}_{\mathbf{q}_0} \prod_{j=1}^{N+1} c^{\dagger}_{1,\mathbf{k}_j}|0\rangle$ with $\sum_{j=1}^{N+1} \mathbf{k}_j = \mathbf{k} - \mathbf{q}_0$. For a large number of electrons, the exact diagonalization of the Hamiltonian in this subspace is an unmanageable task. Here, we show that by a judicious approximation, we can considerably simplify the diagonalization problem, keeping the relevant nonperturbative physics. Namely, we claim that the elements of the $(N+1, \mathbf{k}, 1)$ subspace can be well approximated by vectors of the form

$$\begin{aligned} |N+1, \mathbf{k}, 1, \zeta\rangle \;=\; & \left\{ \mu_\zeta \; c^{\dagger}_{2,\mathbf{k}} + \sum_{\mathbf{q}} \Big[\alpha_\zeta(\mathbf{q}) \; a^{\dagger}_{\mathbf{q}} c^{\dagger}_{1,\mathbf{k}-\mathbf{q}} \right. \\ & \left. + \sum_{|\mathbf{k}'|<k_F} \beta_\zeta \; (\mathbf{q}, \mathbf{k}') c^{\dagger}_{2,\mathbf{k}'+\mathbf{q}} c_{1,\mathbf{k}'} c^{\dagger}_{1,\mathbf{k}-\mathbf{q}} \Big] \right\} |F_N\rangle \; . \end{aligned} \tag{4.8}$$

To understand the origin of our approximation, let us consider the time evolution picture sketched in Fig. 4.1. Suppose that initially the system is in its ground state $|F_N\rangle$. After injection of one bare electron, the state of the system is

$$|C\rangle = c^{\dagger}_{2,\mathbf{k}}|F_N\rangle. \tag{4.9}$$

If $\mathbf{k}$ is well inside the Fermi sphere, as we said before, it is Pauli blocked and can not radiatively relax into the first subband. Instead, when $k > k_F$, the

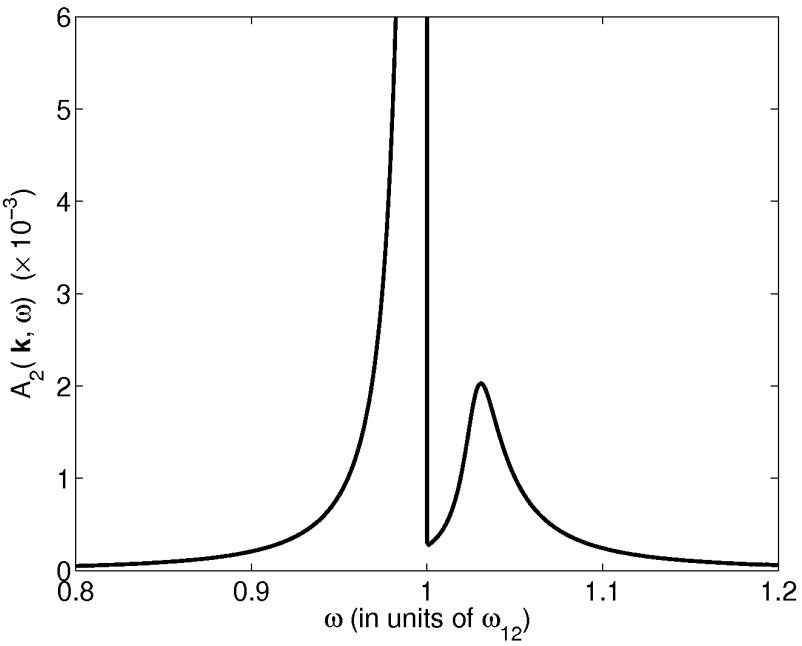

Figure 4.2: Electron spectral function $A_2^+(\mathbf{k},\omega)$ for the second subband , for all $k > k_F$. The spectral function, defined in Eq. (4.2), is the density of quasi-electron states, weighted by the overlap with the bare electron state (the integral of the spectral function is normalized to one). Coupling parameter: $\Omega_R(q_{res}) = \chi(q_{res})\sqrt{N} = 0.1\omega_{12}$.

injected electron can radiatively decay, emitting a photon and falling into the first subband. After the first emission the state will have the form

$$|A, \mathbf{q}\rangle = a^\dagger_{\mathbf{q}} c^\dagger_{1,\mathbf{k}-\mathbf{q}} |F_N\rangle. \tag{4.10}$$

If the cavity system is closed and only the light-matter interaction is considered, the emitted photon will be eventually reabsorbed. The system can evolve back to the state $|C\rangle$ or into one vector of the form

$$|B, \mathbf{q}, \mathbf{k}'\rangle = c^\dagger_{2,\mathbf{k}'+\mathbf{q}} c_{1,\mathbf{k}'} c^\dagger_{1,\mathbf{k}-\mathbf{q}} |F_N\rangle. \tag{4.11}$$

If $\mathbf{k}'$ is well inside the Fermi sea, when the second subband electron decays, the only available final state in the first subband will be the one with wavevector $\mathbf{k}'$, that is the system will go back to state $|A, \mathbf{q}\rangle$. If $\mathbf{k}'$ is on the border of the Fermi sea, on the contrary, the system can evolve into a state of the form $|D, \mathbf{q}, \mathbf{q}', \mathbf{k}'\rangle = a^\dagger_{\mathbf{q}'} c^\dagger_{1,\mathbf{k}'+\mathbf{q}-\mathbf{q}'} c_{1,\mathbf{k}'} c^\dagger_{1,\mathbf{k}-\mathbf{q}} |F_N\rangle$. The probability of ending in any of the $|D, \mathbf{q}, \mathbf{q}', \mathbf{k}'\rangle$ states is negligible. In fact, the probability for $\mathbf{k}'$ to be near enough to the border of the Fermi sea for allowing an emission to electronic states with $k > k_F$ is proportional to the ratio $q_{res}/k_F \ll 1$. Hence, the diagonalization problem can be simplified and we can thus look for vectors of the form shown in Eq. 4.8. Even if the $|A, \mathbf{q}\rangle, |B, \mathbf{q}, \mathbf{k}'\rangle$ and $|C\rangle$ states still form an infinite dimensional space, the Hamiltonian in Eq. 4.1 can be now numerically diagonalized by discretizing the $\mathbf{q}$ and $\mathbf{k}$ in-plane wavevectors. The details of the diagonalization can be found in Appendix D. After the numerical procedure, and some linear algebra, we obtain the following form for vectors in Eq. 4.8

$$|N+1, \mathbf{k}, 1, \zeta\rangle = \mu_\zeta \; c^\dagger_{2,\mathbf{k}} |F_N\rangle + \sum_{q,\sigma=\pm} \lambda_{\zeta,\sigma,q} |\sigma, q\rangle \; . \tag{4.12}$$

The states $|\sigma, q\rangle$, that are linear superpositions of $|A, \mathbf{q}\rangle$ and $|B, \mathbf{q}, \mathbf{k}'\rangle$ states, are given by

$$|\pm, q\rangle = \frac{1}{\sqrt{Lq}} \sum_{|\mathbf{q}|=q} |\pm, \mathbf{q}\rangle \; , \tag{4.13}$$

where

$$|\pm, \mathbf{q}\rangle \;\; = \;\; \frac{(\omega_\pm(q) - \omega_{12})|A, \mathbf{q}\rangle + \chi(q) \sum_{\mathbf{k}} |B, \mathbf{q}, \mathbf{k}\rangle}{\sqrt{(\omega_\pm(q) - \omega_{12})^2 + |\chi(q)|^2 N}} \; , \tag{4.14}$$

are nothing else that the polaritonic states described in Section 1.3.3, $\mathbf{q}$ is the polaritonic in-plane wavevector, σ is the polaritonic branch index and $\omega_\pm(q)$ are the polaritonic energies.

That is $|\sigma, q\rangle$ are superpositions of polaritonic states with in-plane wavevectors $\mathbf{q}$, such that $|\mathbf{q}|= q$, (see Appendix D for details). In conclusion, after having numerically calculated the coefficients in Eq. 4.12, and the relative eigenenergies $\hbar\omega_\zeta$, we can write the spectral function of electrons in the second subband as

$$A_2^+(\mathbf{k},\omega) = \sum_\zeta |\mu_\zeta|^2 \delta(\omega-\omega_\zeta)\theta(k-k_F) + \delta(\omega-\omega_{c,2}(k))\theta(k_F-k). \quad (4.15)$$

In Fig. 4.2, we show numerical results using a vacuum Rabi frequency

$$\Omega_R(q_{res}) = |\chi(q_{res})|\sqrt{N} = 0.1\omega_{12}. \quad (4.16)$$

As it appears from Eq. 4.15, the broadening of the spectral function is intrinsic, being associated to the continuum spectrum of frequencies ω_ζ corresponding to the dressed electronic states. At each frequency ω_ζ, the magnitude of the spectral function is given by the spectral weight $|\mu_\zeta|^2$, depending on the overlap between the dressed state $|N+1,\mathbf{k},1,\zeta\rangle$ and the bare electron state $|C\rangle = c^\dagger_{2,\mathbf{k}}|F_N\rangle$. As shown in Eq. 4.12, the electronic eigenstates of the system are given by the Fano-like coupling between the bare electron state and the continuum of cavity polariton excitations. Indeed, the pronounced dip around $\omega=\omega_{12}$ in the spectral function is a quantum interference feature, typical of a Fano resonance [82].

As we said before the sharp transition in Eq. 4.15 between $k > k_F$ and $k < k_F$ is only a consequence of the approximations we made of neglecting the *border* of the Fermi sea and the effect of the temperature. In a real case both effects will tend to smooth the transition, the first on an energy scale of the order of $\frac{\hbar^2 k_F q_{res}}{m^*}$ and the second on an energy scale of KT.

4.4 Tunneling coupling, losses and electroluminescence

The states $|N+1,\mathbf{k},1,\zeta\rangle$ have been obtained by diagonalizing the Hamiltonian in Eq. 4.1, which takes into account only the coupling between the two-subband electronic system and the microcavity photon quantum field. If, as we have assumed, the light-matter interaction is the strongest one, all other residual couplings can be treated perturbatively. These residual interactions include the coupling to the extracavity fields, the interaction with contacts,

phonon and impurity scattering as well as Coulomb electron-electron interactions [79].

The states $|N+1,\mathbf{k},1,\zeta\rangle$ can be excited for example by resonant electron tunneling from a bulk injector or an injection miniband. If $V_{\mathbf{k}}^{tc}$ is the tunneling coupling matrix element between the state $|F\rangle$ and $c_{2,\mathbf{k}}^{\dagger}|F\rangle$ induced by the coupling with the injector we have, using the Fermi golden rule, the following injection rate

$$\Gamma_{inj}(\mathbf{k},\zeta) = \frac{2\pi}{\hbar}|\mu_{\zeta}|^2|V_{\mathbf{k}}^{tc}|^2\rho_{inj}(\omega_{\zeta})n_F(\omega_{\zeta}), \tag{4.17}$$

where $\rho_{inj}(\omega)$ is the density of electronic states inside the contact and $n_f(\omega)$ its Fermi distribution. $\rho_{inj}(\omega)n_f(\omega)$ determines the spectral shape of the injector. μ_{ζ} comes from Eq. 4.15 and represents the electron spectral weight. It is worthwhile to notice that the formula in Eq. 4.17 is quite independent from the model of injector considered. All the relevant information are contained in the coupling strength $V_{\mathbf{k}}^{tc}$ and the spectral shape $\rho_{inj}(\omega)n_f(\omega)$. Any form of scattering, including in-plane wavevector non-conserving interactions or non-resonant injection, will give a different (and possibly broadened) injector spectral shape. The finite transmission of the cavity mirrors is responsible for a finite lifetime for the cavity photons and consequently for the dressed states $|N+1,\mathbf{k},1,\zeta\rangle$. By using the Fermi golden rule and a quasi-mode coupling to the extracavity field, we find that the radiative lifetime $\tau_{r,\mathbf{k},\zeta}$ reads

$$\frac{1}{\tau_{r,\mathbf{k},\zeta}} = \frac{2\pi}{\hbar}\sum_{\mathbf{q},q_z}|\alpha_{\zeta}(\mathbf{q})|^2|V_{\mathbf{q},q_z}^{qm}|^2\delta(\hbar\omega_{\zeta}-\hbar\omega_{\mathbf{q},q_z})\theta(k-k_F), \tag{4.18}$$

where $V_{\mathbf{q},q_z}^{qm}$ is the quasi-mode coupling matrix element, $\omega_{\mathbf{q},q_z}$ the extracavity photon frequency and $\alpha_{\zeta}(\mathbf{q}) = \langle A,\mathbf{q}|N+1,\mathbf{k},1,\zeta\rangle$ as defined in Eq. 4.8. Having calculated the tunneling injection rate and the radiative lifetime for the different states, we are able to evaluate the electroluminescence spectra. It is convenient to introduce the normalized photon emission distribution corresponding to each eigenstate $|N+1,\mathbf{k},1,\zeta\rangle$, namely

$$L(\mathbf{q},\zeta) = \mathcal{N}\sum_{q_z}|\alpha_{\zeta}(\mathbf{q})|^2|V_{\mathbf{q},q_z}^{qm}|^2\delta(\hbar\omega_{\zeta}-\hbar\omega_{\mathbf{q},q_z}), \tag{4.19}$$

where the normalization $\mathcal{N}$ is fixed by imposing $\sum_{\mathbf{q}}L(\mathbf{q},\zeta)=1$. The number of photons with in-plane wave-vector $\mathbf{q}$ and frequency ω emitted per unit time is

$$N_{ph}(\mathbf{q},\omega) = \frac{1}{\pi}\sum_{\mathbf{k},\zeta}\Gamma_{inj}(\mathbf{k},\zeta)L(\mathbf{q},\zeta)\frac{1/\tau_{r,\mathbf{k},\zeta}}{(\omega-\omega_{\zeta})^2+(1/\tau_{r,\mathbf{k},\zeta}+1/\tau_{nr,\mathbf{k},\zeta})^2}\ , \tag{4.20}$$

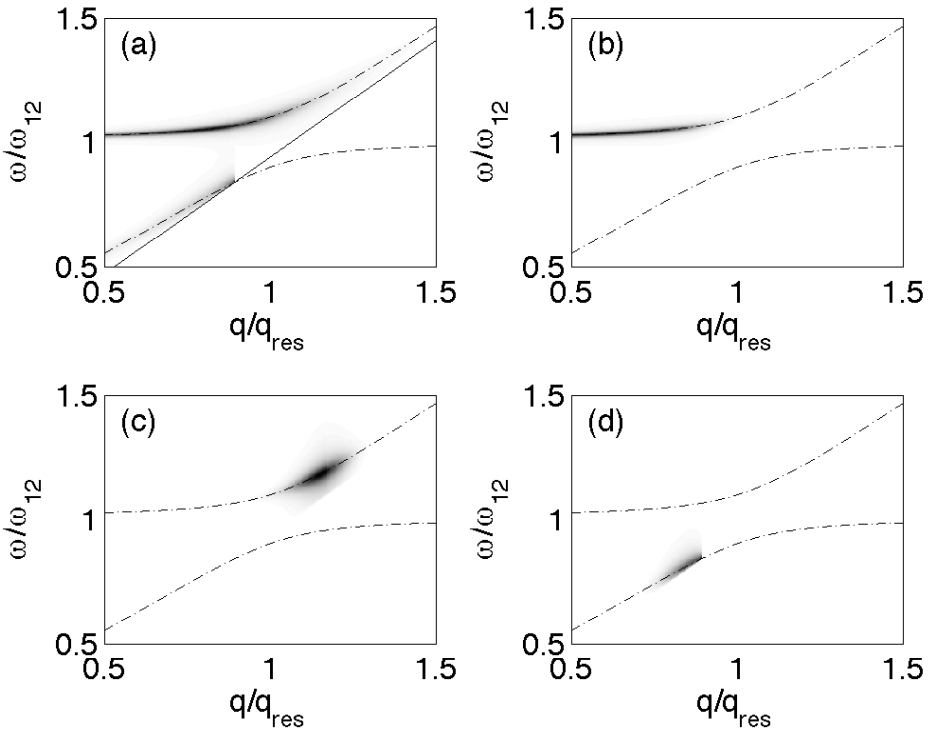

Figure 4.3: Extracavity electroluminescence spectra $N_{ph}(\mathbf{q},\omega)$. Panel (a): the case of a broadband electrical injector (bandwidth equal to ω_{12}, centered at $\omega=\omega_{12}$). The other panels show the results for a narrow-band injector (width $0.05\omega_{12}$) centered respectively at $\omega=\omega_{12}$ (b), $1.2\omega_{12}$ (c) and $0.8\omega_{12}(d)$. The non-radiative relaxation rate $1/\tau_{nr}$ has been taken equal to $0.005\omega_{12}$. In all panels, the dashed-dotted lines are the frequency dispersions of the two intersubband polariton branches. In the first panel the solid line represents the edge of the light cone [49].

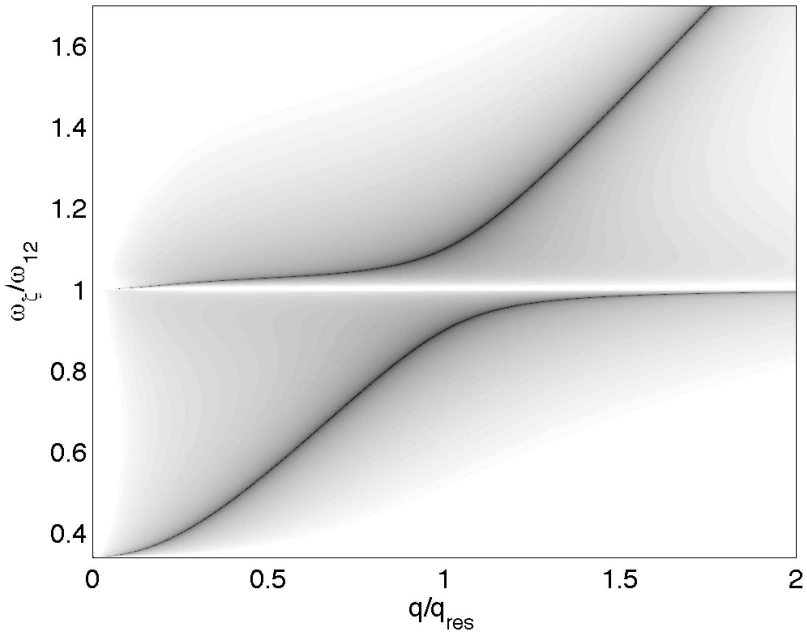

Figure 4.4: Logaritmic plot of the absolute value of the radiative matrix element $\alpha_\zeta(\mathbf{q}) = \langle A, \mathbf{q}|N+1, \mathbf{k}, 1, \zeta\rangle$, responsible for the radiative lifetime of the electronic eigenstates. The image is shown in saturated colors to improve readability. The dispersion of the two cavity polariton branches is apparent.

where the last factor accounts for the Lorentzian broadening due to radiative and non-radiative processes. $\tau_{nr,\mathbf{k},\zeta}$ is the non-radiative lifetime of the electronic excitations and $\Gamma_{inj}(\mathbf{k},\zeta)$ is given by Eq. 4.17. Fig. 4.3 reports representative electroluminescence spectra in the case of a broadband (panel a) and narrowband (panel b,c,d) injector. In the broadband case, the emission is resonant at the intersubband cavity polariton frequencies (dashed lines) and it is significant in a wide range of in-plane wavectors (coherently with the theory developed in Chapter 3). In contrast, in the case of narrowband electrical injector, our theory shows that the photon in-plane momentum and the energy of the cavity polariton emission can be selected by the resonant electron tunneling process. This agrees with what suggested by recent experiments, in which it seems that the injector acts as a *filter*, selecting the energy of the polaritonic emission [39].

One important point to notice is that, consistent with the experiments, our

theory correctly predicts the absence of emission at the unperturbed intersubband frequency ω_{12}. This is a purely quantum mechanical effect and indeed it reassures us of the correctness of our analysis. Effectively if we make a *naive* calculation of the emission spectra, neglecting polaritonic coherence, we would obtain, in the case of a broadband injector, an emission peaked at the bare intersubband frequency ω_{12} instead of the two polaritonic resonances. This is because, due to the big peak in the electron spectral function at the energy of the unperturbed electron (Fig. 4.2), the vast majority of electrons are injected at the bare intersubband transition energy and this compensates for the small photonic fraction (and thus the longer radiative lifetime) of these states. The absence of the central peak is indeed due to an interference effect between lower and upper polaritons. Due to the symmetry lower-upper polariton around ω_{12}, and electrons injected at the bare intersubband energy, emit at the same time a lower polariton and an upper polariton, their destructive interference gives a zero net emission. This can be seen in Fig. 4.4, where the absolute value of the matrix element $\alpha_\zeta(\mathbf{q}) = \langle A, \mathbf{q}|N+1, \mathbf{k}, 1, \zeta\rangle$ is plotted in logaritmic scale as a function of the in-plane wavevector q and of the eigenenergies of the states $|N+1, \mathbf{k}, 1, \zeta\rangle$. The white line at the frequency ω_{12} corresponds to a zero value for the matrix element, impeding thus any emission at this frequency, as shown in Eq. 4.19.

In free-space, the quantum efficiency of electroluminescent devices based on intersubband transitions is poor ($\approx 10^{-5}$ in the mid-infrared) due to the slow radiative recombination of long wavelength transitions. In the microcavity case, the efficiency of the emission from an excited state $|N+1, \mathbf{k}, 1, \zeta\rangle$ is given by $(1 + \tau_{r,\mathbf{k},\zeta}/\tau_{nr,\mathbf{k},\zeta})^{-1}$. Because $1/\tau_{nr,\mathbf{k},\zeta}$ is essentially proportional to the matter component of the excitation and $1/\tau_{r,\mathbf{k},\zeta}$ to its photonic fraction, we have found that it is possible to obtain a quantum efficiency approaching unity by selectively injecting electrons into dressed states with a high photonic fraction. In particular, this is achievable by avoiding injection resonant with the central peak of the electron spectral function in Fig. 4.2, which corresponds to states with strong overlap with the bare electron state.

In the present theory, we have not considered the role of electronic disorder, which is known to break the in-plane translational invariance. However, in the limit of large vacuum Rabi energies (i.e., significantly larger than the energy scale of the disorder potential), the inhomogeneous broadening is expected to have a perturbative role.

Let us point out clearly that in order to achieve a high quantum efficiency,

it is necessary to have a considerably narrow spectral width for the injector, on the order of a small fraction (10^{-2}) of the intersubband transition energy $\hbar\omega_{12}$. This is essential in order to be able to inject electrons selectively into the superradiant states, while avoiding both the peak associated to the *dark* excitations at the bare electron energy and the states with $k < k_F$ that can not radiatively decay. In the experiments in Ref. [39], the spectral width of the injector (a heavily doped superlattice) is comparable to the polariton vacuum Rabi frequency and hence such selective excitations of the superradiant states cannot be reached. In order to have an injector with narrower spectral width, several electronic designs could be implemented. For example, one can grow a *filter* quantum well between the superlattice injector and the active quantum well: resonant electron tunneling through the intermediate quantum well can significantly enhance the resonant character of the excitation. Moreover, for a given injector, improved microcavity samples with larger vacuum Rabi frequency would allow the system a more resonant excitation of the superradiant electronic states.

4.5 Conclusions and perspectives

In conclusion, in this Chapter we have determined in a non-perturbative way the quasi-electron states in a microcavity-embedded two-dimensional electron gas. Such states originate from a Fano-like coupling between the bare electron state and the continuum of cavity polariton excitations. We have proven that these states can be selectively excited by resonant electron tunneling and that the use of narrow-band injector may give rise to efficient intersubband polariton electroluminescence. Even if no experiments have been realized up to date, different experimental groups manifested us their interest on these topics. We are thus confident that our theory will soon get an experimental verification and that the first prototypes of light emitting devices exploiting this technology could be only few years afar.

Chapter 5

Intersubband polariton scattering and lasing

5.1 Introduction

In Chapter 1, we introduced intersubband polaritons as the low-energy excitations of a microcavity-embedded two dimensional electron gas. In Section 1.4.3 we claimed that, in the dilute regime, such excitations behave almost as bosons, with a deviation from pure bosonicity depending on the ratio between the number of polaritonic excitations and the number of electrons in the two dimensional electron gas. It is well known that the scattering of bosons from an initial to a final state can be stimulated, i.e., enhanced, by the occupation of the final state. This remarkable property is in stark contrast with the behavior of fermions, such as electrons, whose scattering is Pauli blocked by final state occupation. So the question is: can intersubband cavity polaritons enjoy stimulated scattering?

Even if in low-energy matter there are no elementary bosons, composite particles acting like bosons are quite ubiquitous in physics. In atomic physics, atoms with even number of fermions act as bosons, and can give rise to Bose-Einstein condensates [83]. In condensed matter systems, the attractive interactions between two electrons can give rise to bosonic particles, like Cooper pairs in metallic superconductors [84] or Coulomb bound electron-hole pairs (excitons) in semiconductors. In contrast to atoms, Cooper pairs and excitons, intersubband excitations do not correspond to any bound state of an attractive interaction. The well definite resonance frequency of intersubband excitations is not due to the presence of a discrete bound state, but to the parabolicity

of intersubband dispersions, as explained in Section 1.3.1. Even if intersubband excitations do not correspond to a bound state, they are still composed of an electron in an excited subband and a hole in the Fermi sea. Hence, we can regard them as composite bosons and expect the occurrence of stimulated scattering.

In this Chapter, we present a microscopic theory of the stimulated scattering of intersubband cavity polaritons [40]. In particular, we will consider the polariton scattering induced by the coupling with optical phonons, which is typically the most important scattering channel affecting semiconductor intersubband transitions, while the Coulomb interaction is known to produce only moderate renormalization effects [79]. Starting from the RWA-fermionic Hamiltonian introduced in Section 1.4.2 and extensively used in Chapters 3 and 4 and by using an iterative commutation procedure, we will determine the phonon-induced polariton scattering for an arbitrary number of excitations in the initial and final intersubband cavity polariton modes. Our results indeed will prove the possibility of final-state stimulation of the intersubband cavity polariton scattering. Our theory also provides the deviations from perfect bosonicity, occurring at high excitation densities. We will apply our results to the case of a GaAs system with realistic losses and study the possibility of intersubband cavity polariton lasing under resonant optical pumping.

5.2 General formalism

We consider the Hamiltonian $H = H^{\mathrm{RWA}} + H_{phon}$ where H^{RWA} is the light-matter term for the cavity system introduced in Section 1.4.2, while H_{phon} describes the coupling to bulk longitudinal-optical phonons (LO-phonons) via the Fröhlich interaction [85]

$$\begin{aligned} H^{\mathrm{RWA}} &= \sum_{\mathbf{k}} \hbar\omega_{c,1}(k) c^{\dagger}_{1,\mathbf{k}} c_{1,\mathbf{k}} + \hbar\omega_{c,2}(k) c^{\dagger}_{2,\mathbf{k}} c_{2,\mathbf{k}} + \sum_{\mathbf{q}} \hbar[\omega_{cav}(q) + 2D(q)] a^{\dagger}_{\mathbf{q}} a_{\mathbf{q}} \\ &+ \sum_{\mathbf{k},\mathbf{q}} \hbar\chi(q) a_{\mathbf{q}} c^{\dagger}_{2,\mathbf{k}+\mathbf{q}} c_{1,\mathbf{k}} + \hbar\chi(q) a^{\dagger}_{\mathbf{q}} c^{\dagger}_{1,\mathbf{k}} c_{2,\mathbf{k}+\mathbf{q}}, \\ H_{phon} &= \sum_{\mathbf{q},q_z} \hbar\omega_{LO}(\mathbf{q},q_z) d^{\dagger}_{\mathbf{q},q_z} d_{\mathbf{q},q_z} + \sum_{\substack{\mathbf{k},\mathbf{q},q_z \\ i,j=1,2}} \hbar C_{ij}(\mathbf{q},q_z) d_{\mathbf{q},q_z} c^{\dagger}_{i,\mathbf{k}+\mathbf{q}} c_{j,\mathbf{k}} \\ &+ \hbar C_{ij}(\mathbf{q},q_z) d^{\dagger}_{\mathbf{q},q_z} c^{\dagger}_{j,\mathbf{k}} c_{i,\mathbf{k}+\mathbf{q}}, \end{aligned} \tag{5.1}$$

where $d^{\dagger}_{\mathbf{q},q_z}$ are the creation operators for optical phonons with three-dimensional wavevectors $(\mathbf{q},q_z)$ and energy $\hbar\omega_{LO}(\mathbf{q},q_z) = \hbar\omega_{LO}$ (the wavevector depen-

dence of the optical phonon energy is negligible). Their phases are chosen in order to make the coupling coefficients $C_{ij}(\mathbf{q}, q_z)$ real. Being that all the interactions with optical phonon conserve spin, we can still omit the spin degree of freedom for the electrons.

In the dilute regime we know that the low energy excitations of H^{RWA} are the two intersubband polaritonic branches. By applying a Hopfield transformation to the bosonized version of H^{RWA} (that is the Hamiltonian H^{RWA}_{bos} introduced in Section 1.4.4), exactly as we did in Chapter 2, we can write the creation operators of such excitations as

$$p^{\dagger}_{\eta,\mathbf{q}} = \alpha_{\eta,\mathbf{q}} a^{\dagger}_{\mathbf{q}} + \beta_{\eta,\mathbf{q}} b^{\dagger}_{\mathbf{q}} \tag{5.2}$$

where $\eta = \{LP, UP\}$ denotes the polariton branch index, $\alpha_{\eta,\mathbf{q}}$ and $\beta_{\eta,\mathbf{q}}$ are real Hopfield coefficients describing the light and matter component respectively, while $\hbar\omega_{\eta}(q)$ are their corresponding energies (see Fig. 5.1).

We will take Eq. 5.2 as the definition of an intersubband polariton creation operator, using it to obtain multiple-polariton states, as common in the theory of composite boson scattering [86, 87]. Our procedure will thus be to define initial and final states as multi-polariton / phonon states, obtained acting on the state $|F\rangle$ (that is the ground state of the system, the electronic ground state times the photon and phonon vacuum) with multiple polaritonic and phononic creation operators and then calculate transition rates between such states with the Fermi golden rule, using as interaction Hamiltonian H_{phon}, defined in Eq. 5.1. Specifically, we are interested in calculating the polariton scattering rate induced by the emission of an optical phonon from an initial polariton *pump* mode (branch η' and in-plane wavevector $\mathbf{q}$') to a final *signal* mode (branch η and in-plane wavevector $\mathbf{q}$). This kind of process is pictured in Fig. 5.1 for the case $\eta' = UP$ and $\eta = LP$. In order to calculate such many-body matrix elements involving multiple photonic, intersubband and phononic operators, we will need to deal with their actual commutation relations.

While the cavity photons are elementary bosons obeying the standard commutation rule $[a_{\mathbf{q}}, a^{\dagger}_{\mathbf{q}'}] = \delta_{\mathbf{q},\mathbf{q}'}$ and the phonons, in the harmonic approximation, also obey standard bosonic commutation rules $[d_{\mathbf{q},q_z}, d^{\dagger}_{\mathbf{q}',q'_z}] = \delta_{\mathbf{q},\mathbf{q}'}\delta_{q_z,q'_z}$, intersubband excitations are not elementary bosons and thus their creation an annihilation operators satisfy modified commutation rules. By writing down the expression for intersubband excitation operators in term of electronic operators

$$b_{\mathbf{q}} = \frac{1}{\sqrt{N}} \sum_{\mathbf{k}} c^{\dagger}_{2,\mathbf{k}+\mathbf{q}} c_{1,\mathbf{k}} \tag{5.3}$$

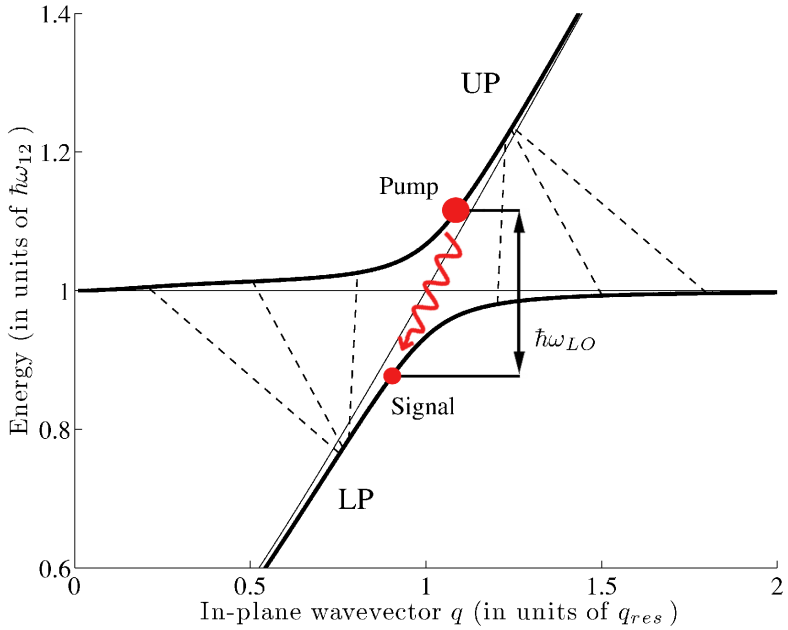

Figure 5.1: A typical energy dispersion (in units of the intersubband transition energy $\hbar\omega_{12}$) of intersubband cavity polaritons versus in-plane wavevector (in units of the resonant wavevector q_{res}). Due to the interaction with bulk optical phonons, a polariton pumped in the upper polariton (UP) branch can scatter into a final state (signal mode) in the lower polariton (LP) branch by emitting an optical phonon with energy $\hbar\omega_{LO}$ (36 meV for GaAs). The considered modes have Hopfield coefficients $\beta_{UP,\mathbf{q}'} = \beta_{LP,\mathbf{q}} = 0.5$. The dashed lines indicate the same kind of scattering process by changing the in-plane momentum of the initial state along the upper polariton branch.

and using anticommutation rules for fermions $\{c_{j,\mathbf{k}}, c^\dagger_{j',\mathbf{k}'}\} = \delta_{\mathbf{k},\mathbf{k}'}\delta_{j,j'}$, we find (the details of the calculation are in Appendix E)

$$\begin{aligned} [b_{\mathbf{q}}, b^\dagger_{\mathbf{q}'}] &= \delta_{\mathbf{q},\mathbf{q}'} - D_{\mathbf{q},\mathbf{q}'}, \\ D_{\mathbf{q},\mathbf{q}'} &= \delta_{\mathbf{q},\mathbf{q}'} - \frac{1}{N}\sum_{|\mathbf{k}|<\mathbf{k_F}} c^\dagger_{1,\mathbf{k}} c_{1,\mathbf{k}+\mathbf{q}-\mathbf{q}'} - c^\dagger_{2,\mathbf{k}+\mathbf{q}'} c_{2,\mathbf{k}+\mathbf{q}}, \end{aligned} \tag{5.4}$$

where $D_{\mathbf{q},\mathbf{q}'}$ is the operator describing the deviation from the behavior of elementary bosons, originally introduced in the context of excitonic composite bosons [86, 87]. By iteration, we find the following commutation relations:

$$\begin{aligned} [D_{\mathbf{q},\mathbf{q}'}, b^{\dagger\, m}_{\mathbf{q}''}] &= \tfrac{2m}{N} b^\dagger_{\mathbf{q}''+\mathbf{q}'-\mathbf{q}} b^{\dagger\, m-1}_{\mathbf{q}''}, \\ [b_{\mathbf{q}}, b^{\dagger\, m}_{\mathbf{q}'}] &= m b^{\dagger\, m-1}_{\mathbf{q}'}(\delta_{\mathbf{q},\mathbf{q}'} - D_{\mathbf{q},\mathbf{q}'}) - \tfrac{m(m-1)}{N} b^\dagger_{\mathbf{2q}'-\mathbf{q}} b^{\dagger\, m-2}_{\mathbf{q}'}, \\ [b^m_{\mathbf{q}}, b^\dagger_{\mathbf{q}'}] &= m(\delta_{\mathbf{q},\mathbf{q}'} - D_{\mathbf{q},\mathbf{q}'}) b^{m-1}_{\mathbf{q}} - \tfrac{m(m-1)}{N} b_{\mathbf{2q}-\mathbf{q}'} b^{m-2}_{\mathbf{q}}. \end{aligned} \tag{5.5}$$

Exploiting Eq. 5.5 we can thus in principle calculate many-body matrix elements by commuting destruction operators multiple times to the right side and applying the annihilation identity $a_{\mathbf{q}}|F>= b_{\mathbf{q}}|F>= 0$. This will leave behind only C-numbers and $D_{\mathbf{q},\mathbf{q}'}$ operators. Due to the fact that typical photonic wavevectors q are much smaller (at least two orders of magnitude) than the electronic Fermi wavevector k_F, we have $D_{\mathbf{q},\mathbf{q}'}|F\rangle \simeq 0$ with corrections of the order of $|\mathbf{q}-\mathbf{q}'|k_F$ due to the electrons occupying the edge of the Fermi sphere. Neglecting these corrections we can thus get rid of all operators and obtain the matrix elements as pure C-numbers.

5.3 Many-body matrix elements calculation

If we wish to investigate the occurrence of stimulated scattering, we need to evaluate the scattering rates for arbitrary occupation numbers m and n of respectively the initial and final polariton modes. The emission of an optical phonon can induce the scattering of one polariton from the pump to the signal mode, leading to a transition from the state

$$p^{\dagger\, m}_{\eta',\mathbf{q}'} p^{\dagger\, n}_{\eta,\mathbf{q}} |F\rangle \tag{5.6}$$

(m polaritons in the pump mode and n polaritons in the signal mode) to the state

$$d^\dagger_{\mathbf{q}'-\mathbf{q},q_z} p^{\dagger\, m-1}_{\eta',\mathbf{q}'} p^{\dagger\, n+1}_{\eta,\mathbf{q}} |F\rangle \tag{5.7}$$

($m-1$ polaritons in the pump mode, $n+1$ polaritons in the signal mode and one optical phonon). Therefore, we need to consider the squared normalized matrix element given by

$$\hbar^2|V_m^n|^2 = \frac{|\langle F|p_{\eta,\mathbf{q}}^{n+1}p_{\eta',\mathbf{q}'}^{m-1}d_{\mathbf{q}'-\mathbf{q},q_z}H_{phon}p_{\eta',\mathbf{q}'}^{\dagger\, m}p_{\eta,\mathbf{q}}^{\dagger\, n}|F\rangle|^2}{\langle F|p_{\eta,\mathbf{q}}^{n}p_{\eta',\mathbf{q}'}^{m}p_{\eta',\mathbf{q}'}^{\dagger\, m}p_{\eta,\mathbf{q}}^{\dagger\, n}|F\rangle\langle F|p_{\eta,\mathbf{q}}^{n+1}p_{\eta',\mathbf{q}'}^{m-1}p_{\eta',\mathbf{q}'}^{\dagger\, m-1}p_{\eta,\mathbf{q}}^{\dagger\, n+1}|F\rangle}. \tag{5.8}$$

The denominator is a normalization factor due to the fact that, by commutation rules in Eq. 5.5, the states defined in Eqs. 5.6 and 5.7 are not normalized. In order to evaluate Eq. 5.8, we have to exploit the expression of the polariton operators in Eq. 5.2 in terms of the cavity photon and intersubband excitation operators. From Eq. 5.5, some algebra (detailed in Appendix E) shows that the unnormalized polaritonic matrix element between initial and final state $\langle F|p_{\eta,\mathbf{q}}^{n+1}p_{\eta',\mathbf{q}'}^{m-1}d_{\mathbf{q}-\mathbf{q}',q_z}H_{phon}p_{\eta',\mathbf{q}'}^{\dagger\, m}p_{\eta,\mathbf{q}}^{\dagger\, n}|F\rangle$ is given by

$$\begin{aligned}(n+1)!m!\beta_{\eta,\mathbf{q}}\bar{\beta}_{\eta',\mathbf{q}'}(C_{22}(\mathbf{q}-\mathbf{q}',q_z)-C_{11}(\mathbf{q}-\mathbf{q}',q_z))\sum_{\substack{l=0,\dots,n\\ h=0,\dots,m-1}}\binom{n}{l} \\ \binom{m-1}{h}|\alpha_{\eta,\mathbf{q}}|^{2l}|\beta_{\eta,\mathbf{q}}|^{2(n-l)}|\alpha_{\eta',\mathbf{q}'}|^{2h}|\beta_{\eta',\mathbf{q}'}|^{2(m-1-h)}f_{m-h}^{n-l},\end{aligned} \tag{5.9}$$

where $f_m^n = \frac{n}{m}\mathcal{K}_{n+1,n-1}^{m-1,m} + \mathcal{K}_{n+1,n}^{m-1,m-1}$and the quantity $\mathcal{K}_{m,r}^{n,s}$ is defined by the relation

$$n!m!\mathcal{K}_{m,r}^{n,s} = \langle F|b_{\mathbf{q}}^n b_{\mathbf{q}'}^m b_{\mathbf{q}}^{\dagger\, s}b_{\mathbf{q}'}^{\dagger\, r}b_{\mathbf{Q}}^{\dagger}|F\rangle \tag{5.10}$$

with $\mathbf{Q} = \mathbf{q}(n-s) + \mathbf{q}'(m-r)$. Analogously, for the normalization factors in Eq. 5.8, we find

$$\begin{aligned}\langle F|p_{\eta,\mathbf{q}}^{n}p_{\eta',\mathbf{q}'}^{m}p_{\eta',\mathbf{q}'}^{\dagger\, m}p_{\eta,\mathbf{q}}^{\dagger\, n}|F\rangle = n!m!\sum_{\substack{l=0,\dots,n\\ h=0,\dots,m}}\binom{n}{l}\binom{m}{h} \\ |\alpha_{\eta,\mathbf{q}}|^{2l}|\beta_{\eta,\mathbf{q}}|^{2(n-l)}|\alpha_{\eta',\mathbf{q}'}|^{2h}|\beta_{\eta',\mathbf{q}'}|^{2(m-h)}\mathcal{K}_{m-h,m-h-1}^{n-l,n-l}.\end{aligned} \tag{5.11}$$

Therefore we have reduced the problem of calculating the many-body matrix elements needed to determine the scattering rates, to the problem of determining the four indexes $\mathcal{K}$ coefficients. Commuting, by means of Eq. 5.5, one destruction operator from the right to the left in Eq. 5.10, it is possible to obtain, as shown in Appendix E, a recurrence relation that allows us to numerically evaluate $\mathcal{K}_{n,r}^{m,s}\ \forall m,n,s,r$. Namely the $\mathcal{K}$ coefficients obey the following

equation

$$\begin{aligned}\mathcal{K}^{n,s}_{m,r} &= \delta_{m,r}\delta_{n,s+1}\mathcal{K}^{n-1,n-1}_{m,m-1} + \delta_{m,r+1}\delta_{n,s}\mathcal{K}^{n,n-1}_{m-1,m-1} \\ &- \frac{s!r!}{n!m!N}[n(n-1)\mathcal{K}^{s,n-2}_{r,m} + m(m-1)\mathcal{K}^{s,n}_{r,m-2} + 2nm\mathcal{K}^{s,n-1}_{r,m-1}].\end{aligned} \tag{5.12}$$

As it can be shown by calculations in Appendix E, the $\mathcal{K}$ coefficients also obey a few algebraic identities that greatly simplify their numerical calculation, namely

$$\begin{aligned}\mathcal{K}^{n,s}_{m,r} &\propto \delta_{n+m,r+s+1} \\ \mathcal{K}^{n,n-1}_{m,m} &= \mathcal{K}^{n,n}_{m,m-1} \\ \mathcal{K}^{n,s}_{m,r} &= \mathcal{K}^{m,r}_{n,s}.\end{aligned} \tag{5.13}$$

Thus Eq. 5.8 can be written as

$$|V^n_m|^2 = (n+1)mB^n_m|\beta_{\eta,\mathbf{q}}\beta_{\eta',\mathbf{q}'}[C_{22}(\mathbf{q}-\mathbf{q}',q_z) - C_{11}(\mathbf{q}-\mathbf{q}',q_z)]|^2 \tag{5.14}$$

where B^n_m is a bosonicity factor depending on the coefficients $\mathcal{K}^{n,s}_{m,r}$. Its expression is cumbersome, but it can be obtained putting together Eqs. (5.8), (5.9) and (5.11). Such a quantity depends on the Hopfield coefficients and on excitation numbers m and n normalized to the total number of electrons N in the ground state. In Fig. 5.2, we report B^0_m versus m/N obtained by a numerical evaluation of recursive relation in Eq. 5.12. For normalized excitation densities $\frac{m+n}{N}$ smaller than 0.1, we find that B^n_m is well approximated by the formula

$$B^n_m \simeq 1 - \zeta\frac{m+n}{N}, \tag{5.15}$$

where ζ depends on the Hopfield coefficients of the polariton modes and varies from 0 for pure photonic excitations (perfect bosons) to 1 for pure matter ones.

5.4 Scattering rate and lasing threshold

Using the Fermi golden rule and calling $A(\mathbf{q}-\mathbf{q}',q_z,\omega)$ the optical phonon's spectral function, we have

$$\Gamma^{m,n}_{sc} = 2\pi\sum_{q_z}\int d\omega|V^n_m|^2 A(\mathbf{q}-\mathbf{q}',q_z,\omega)\delta(\omega_\eta(q) - \omega_{\eta'}(q') + \omega), \tag{5.16}$$

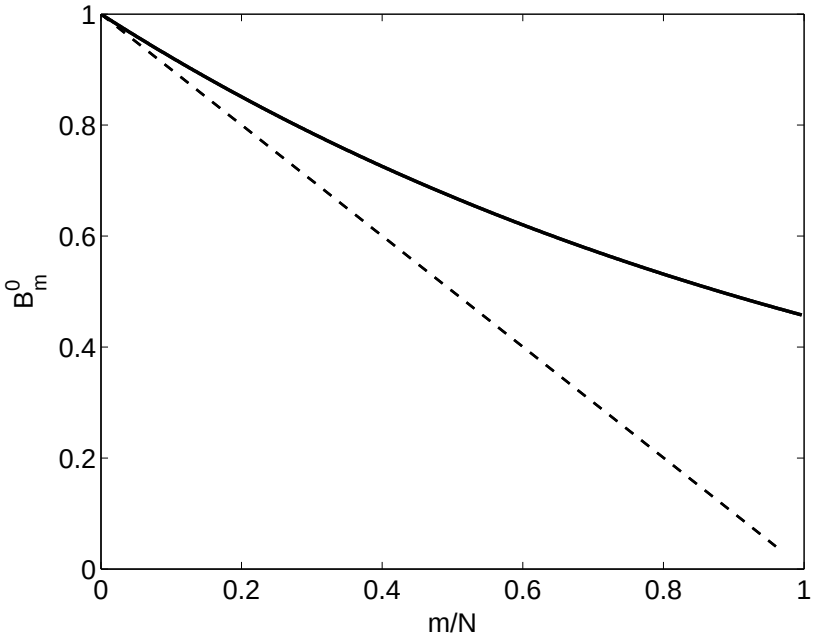

Figure 5.2: The solid line represents the bosonicity factor $B_m^{n=0}$ versus m/N for the pump and signal polariton modes considered in Fig. 5.1. For pure bosons B_m^n is always 1. The dashed line is the same quantity for pure matter excitations. For $m/N \ll 1$, deviations from perfect bosonicity are negligible.

where $\Gamma_{sc}^{m,n}$ is the number of polaritons per unit time scattered from the pump mode (with occupancy m) into the final signal mode (with occupancy n).

Using a Lorentzian shape of width Γ_{LO} for the phonon spectral function and neglecting the LO-phonon dispersion, we thus obtain

$$\Gamma_{sc}^{m,n} = \frac{m}{S}(n+1)B_m^n|\beta_{\eta,\mathbf{q}}|^2|\beta_{\eta',\mathbf{q}'}|^2\frac{\omega_{LO}}{\Gamma_{LO}}\frac{4e^2L_{QW}F_\sigma}{\epsilon\hbar}. \tag{5.17}$$

This expression contains the effect of final-state stimulation through the $(1+n)$ term and the deviations from ideal bosonic behavior through the bosonicity factor B_m^n. The other parameters in the formula are S the sample surface, L_{QW} the QW length and F_σ a form factor (depending on $\sigma = L_{QW}|\mathbf{q}-\mathbf{q}'|$) describing the overlap between the conduction subband and the phonon envelope wavefunctions [85]. For typical QW widths and photonic wavevectors, $\sigma \ll 1$. In the case of a QW with infinite barriers, $F_{\sigma\simeq 0} \simeq 0.1$. For GaAs optical phonons, the ratio $\frac{\omega_{LO}}{\Gamma_{LO}} \approx 100$ [88].

In order to have a sizeable polariton-phonon interaction, both the initial and final polariton modes must have significant electronic components, quantified by $|\beta_{\eta',\mathbf{q}'}|^2$ and $|\beta_{\eta,\mathbf{q}}|^2$ (only the matter part of the polariton *sees* the interaction with phonons). At the same time, in order to have a good coupling to the extracavity electromagnetic field (required for optical pumping and detection) also the photonic components $|\alpha_{\eta',\mathbf{q}'}|^2$ and $|\alpha_{\eta,\mathbf{q}}|^2$ need to be significant. These conditions can be simply met by choosing the pump mode in the upper polaritonic branch and the signal mode in the lower polaritonic one ($\eta = LP$ and $\eta' = UP$, as shown in Fig. 5.1), when the polariton energy splitting $2\Omega_R(q_{res}) = 2\hbar\chi(q_{res})\sqrt{N}$ at the resonant wavector q_{res} (such as $\omega_c(q_{res}) = \omega_{12}$) is a non negligible fraction of the optical phonon energy (36 meV for GaAs). This situation is already realized in recent microcavity samples [67, 49, 39] with mid-infrared intersubband transition frequencies. In Fig. 5.3, we report the calculation of the spontaneous in-scattering rate $\Gamma_{sc}^{m,0}$ (i.e., $n = 0$, unoccupied final state) for the process shown in Fig. 5.1 for a GaAs system with $\hbar\omega_{12} = 150$ meV (mid-infrared), $L_{QW} = 10$ nm, $N/S = 10^{12}$ cm^{-2}. In order to have a build-up of the occupation number of the final state and to enter the regime of stimulated scattering, the spontaneous in-scattering rate $\Gamma_{sc}^{m,0}$ must be compared with the polariton damping rate given by the formula

$$\Gamma_{\eta,q}^{loss} \simeq |\alpha_{\eta,\mathbf{q}}|^2\Gamma_{cav,q}^{loss} + |\beta_{\eta,\mathbf{q}}|^2\Gamma_{12}^{loss}, \tag{5.18}$$

where $\Gamma_{cav,q}^{loss}$ is the damping rate for the cavity mode (due to the finite mirror transmission) and Γ_{12}^{loss} is the intersubband excitation damping rate due to

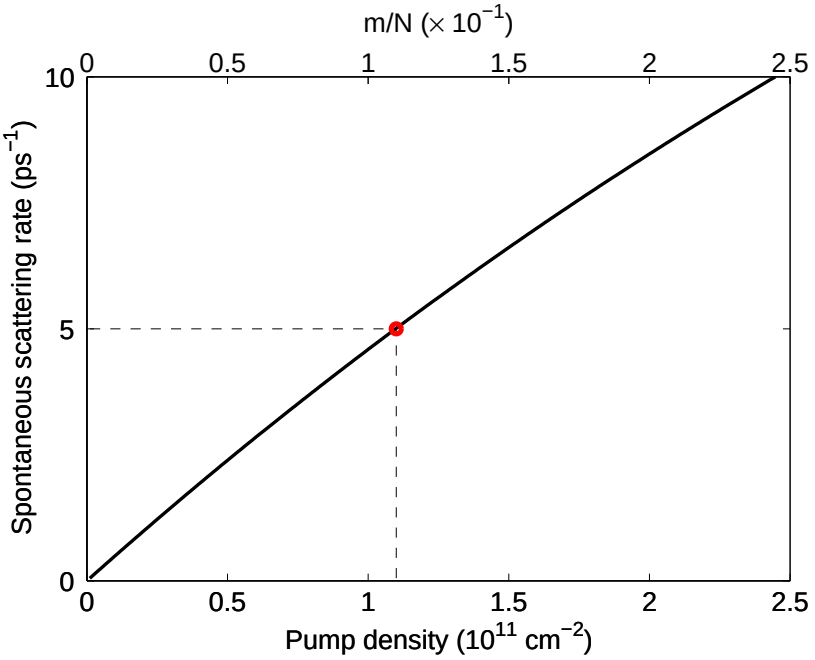

Figure 5.3: Spontaneous scattering rate $\Gamma_{sc}^{m,n=0}$ from the pumped polariton to the signal polariton mode for the process depicted in Fig. 5.1 versus the pump polariton density m/S. The electron density in the ground state is $N/S = 10^{12}$ cm^{-2}. In the considered range of excitation densities, $m/N < 0.25$, i.e., much smaller than the onset of electronic population inversion. Other GaAs parameters are given in the text.

non-radiative processes. In the microcavities samples studied up to now, the radiative and non-radiative contribution are comparable (see for example Ref. [24]), giving a total population damping rate of the order a few ps^{-1}, which is consistent with our calculations.

Neglecting the pump depletion (relevant only above an eventual stimulation threshold), we can write two rate equations for the signal and pump mode occupation numbers, namely

$$\begin{aligned} \frac{dn}{dt} &= \Gamma_{sc}^{m,n} - \Gamma_{signal}^{loss}\, n, \\ \frac{dm}{dt} &= \frac{AI_{pump}S}{\hbar\omega_{UP,q'}} - \Gamma_{pump}^{loss}\, m, \end{aligned} \tag{5.19}$$

where Γ_{signal}^{loss} and Γ_{signal}^{pump} are the loss rates of the signal and pump modes given

by Eq. (5.18), A the polariton absorption coefficient at the pump frequency and I_{pump} the optical pump intensity. From the steady-state solution for n, we can calculate the threshold pump density m_{thr}/S to have a lasing instability. For $n \ll m$, $B_m^n \simeq B_m^0$ and $\Gamma_{sc}^{m,n} \simeq (1+n)\Gamma_{sc}^{m,0}$. The threshold pump polariton density m_{thr}/S is then given by the equation $\Gamma_{sc}^{m_{thr},0} = \Gamma_{signal}^{loss}$. The steady-state solution for m gives the threshold pumping intensity versus the polariton threshold density, namely

$$I_{pump}^{thr} = \frac{\Gamma_{pump}^{loss}\hbar\omega_{UP,q'}}{A} m_{thr}/S. \tag{5.20}$$

For a realistic value $\Gamma_{signal}^{loss} = \Gamma_{pump}^{loss} = 5$ ps^{-1}, we obtain a threshold density for the pump mode of 1.1×10^{11} cm^{-2}, i.e. $m/N = 0.11$ (and a total number of electrons in the excited subband of the order of $0.11N|\beta_{\eta',\mathbf{q}'}|^2$), as indicated in Fig. 5.3. With a polariton absorption coefficient $A = 0.4$ [39], this gives a threshold pump intensity of 3.5×10^4 W/cm^2. This is approximately 2 orders of magnitude smaller of what required to achieve electron population inversion in the two subbands [89].

Note that the mechanism described here is different from the standard phonon-assisted lasing based on stimulated Raman photon scattering[90, 91]: in such traditional case, the stimulation concerns the photon field. In our case, it is the *polariton* field to be stimulated and the the pump creates real polariton excitations. Our stimulated polariton scattering process based on a two-subband system is also different from intersubband electronic Raman effects [92] in three-subband systems.

5.5 Conclusions and perspectives

In conclusion, we have derived a theory for the stimulated scattering of intersubband cavity polariton excitations of a dense two-dimensional electron gas. The intersubband cavity polariton excitations are composite bosons arising from the strong light-matter coupling and are not associated to any bound electronic states. We have shown exactly how the bosonicity of these excitations is controlled by density of the two-dimensional electron gas in the ground state. The present theory could pave the way to the experimental demonstration of fundamental quantum degeneracy phenomena and unconventional lasing devices without population inversion based on composite bosons with controllable properties and interactions. A question still open is if it is possible to exploit the theory of polariton scattering developed in this Chapter, to

obtain an electrically pumped polaritonic laser. Apart from its fundamental interest to the field of coherent phenomena in condensed matter systems, such laser could also be of great technological interest, both for its extremely low treshold and for its potential capability to operate at room-temperature.

General conclusions

Intersubband polaritons are recently discovered [24] low energy excitations in microcavity embedded quantum wells. While some aspects of their physics are reminiscent of the better known exciton polaritons, they present various properties that make them particularly interesting both for fundamental and applied research. On the fundamental side, their unprecedented light-matter coupling [25] permits to investigate new regimes of cavity quantum electrodynamics. On the applied side, they are promising systems for the realization of efficient, room-temperature [49] light emitting devices in the mid-infrared and Terahertz.

This thesis introduced various aspects of the physics of intersubband polaritons. I presented a quantum theory that predicts the emission of quantum vacuum radiation when the ultra-strong light-matter interaction is non-adiabatically modulated [34]. While various other proposals had been advanced in order to measure such effect [62, 63], we believe that the present one is particularly promising due to the large value of predicted quantum vacuum radiation. I also participated in two preliminary experimental works toward the observation of such effect [32, 37], that proved how a non-adiabatic modulation of the ultra-strong light-matter coupling can be achieved in intersubband polariton systems. Now that both the theoretical predictions and the preliminary experiments are in place, experimentalists will have the opportunity to work toward the measure of the quantuum vacuum radiation itself, completing, we hope, a quest that started almost forty years ago [93]. These works could have an impact also in other fields, such as circuit quantum electrodynamics, where similar experiments are being performed [94, 95] and in general in all domains where it is possible to obtain a non-adiabatic change in the light-matter coupling.

On a more applied level, I studied how the strong coupling regime impacts on electron transport and electroluminescence in microcavity embedded quan-

tum wells. I developed an efficient numerical method [38] capable to model electroluminescence under incoherent electron injection. Apart for its usefulness in modelling real word devices, it shows that, by increasing the light-matter coupling in such structures, it si possible to increase their quantum efficiency, giving evidence of a strong coupling extension of the Purcell effect [2]. Realization of samples with even larger vacuum Rabi couplings [32] may soon permit an experimental verification of such effects and thus to increase the efficiency of ligh emitting devices in the mid-infrared and Terahertz.

In the strong coupling regime, when the light-matter coupling is bigger than all the other spurious couplings, electrons are *dressed* by the quantum vacuum fluctuations of the electromagnetic field [96], leading to an electron spectral function qualitatively different from the unperturbed one. This modification in the spectral function can be exploited to selectively excite superradiant states by resonant electron injection. This kind of effect can be observed if the electrons are injected in the structure with an energy resolution comparable to the vacuum Rabi energy. Given the Rabi energy of actual samples, we hope that it will be soon possible to observe such injection effect, thus dramatically improving quantum efficiency of intersubband light emitting devices.

I also studied the possibility for intersubband polaritons to undergo stimulated scattering. The results presented here prove that, despite of saturation effects at higher densities, it is possible to reach the stimulated scattering regime, obtaining a low-threshold, inversionless optical pumped laser [40]. Realization of such laser, apart from its applied interest, will give physicist working in the field of condensed matter coherent phenomena the possibility to study a new kind of room-temperature degenerate quantum gas.

In conclusion, this thesis work may stimulate many interesting experimental and theoretical studies in the growing fields of cavity quantum electrodynamics, quantum opto-electronics, intersubband polaritonics and light-matter interaction in general.

Appendix A

Second quantized Hamiltonian

In this Appendix we will derive the second quantized Hamiltonian introduced in Chapter 1. We invite the reader to refer to that Chapter for a detailed description of the physical system under consideration.

We have a two-dimensional electron gas in a microcavity. We will call N the number of electrons, $S = L_x \times L_y$ the surface of the sample, L_{QW} the thickness of the quantum well and L_{cav} the cavity length. For a clearer derivation we will consider here perfect metallic boundary conditions for the electromagnetic field. Introducing the photonic creation and annihilation operators $a^\dagger_{\sigma,\mathbf{q}}$ and $a_{\sigma,\mathbf{q}}$, whose commutation relations are $[a_{\sigma,\mathbf{q}} a^\dagger_{\sigma',\mathbf{q}'}] = \delta(\mathbf{q}-\mathbf{q}')\delta_{\sigma,\sigma'}$, we can write the quantized vector potential of the free electromagnetic field, fulfilling the boundary conditions, as (see Ref. [97] for details)

$$A(\mathbf{r}) = \sum_{\sigma,\mathbf{q}} \sqrt{\frac{\hbar}{2\epsilon_0 \omega_{cav}(q)}} (a_{\sigma,\mathbf{q}} \mathbf{u}_{\mathbf{q},\sigma} + a^\dagger_{\sigma,\mathbf{q}} \mathbf{u}^*_{\mathbf{q},\sigma}). \tag{A.1}$$

In Eq. A.1 $\sigma = TM, TE$ are the two polarizations of the field, $\mathbf{q} = (\frac{2\pi l_x}{L_x}, \frac{2\pi l_y}{L_y}, \frac{\pi l_z}{L_{cav}})$ is the three-dimensional wavevector of the electromagnetic wave, $l_1, l_2 \in \mathbb{Z}, l_3 \in \mathbb{N}$ and the two spatial modes are given by

$$\begin{aligned} \mathbf{u}_{\mathbf{q},TM} &= \sqrt{\frac{2}{SL_{cav}}} e^{iq_x x + iq_y y} (i \sin(q_z z)\cos(\theta)\mathbf{e_1} + \cos(q_z z)\sin(\theta)\mathbf{e_z}), \\ \mathbf{u}_{\mathbf{q},TE} &= \sqrt{\frac{2}{SL_{cav}}} e^{iq_x x + iq_y y} i \sin(q_z z)\mathbf{e_2}, \end{aligned} \tag{A.2}$$

where $\mathbf{e_1}$ and $\mathbf{e_2}$ are orthogonal vectors in the plane (x, y) with $\mathbf{e_2} \cdot \mathbf{q} = 0$, θ is the angle $\mathbf{q}$ makes with the z axis and $z \in [0, L_{cav}]$.

Anyway, being $L_{QW} \ll L_{cav}$, we have $q_z z \ll 1$, that is the electrons see an electromagnetic field constant along the z-axis. Placing the quantum well containing the electron gas at $z = 0$, only the TM mode is coupled to the electrons and it has the form

$$\mathbf{u}_{\mathbf{q},TM} = \sqrt{\frac{2}{SL_{cav}}} e^{iq_x x + iq_y y} \sin(\theta) \mathbf{e_z}. \tag{A.3}$$

Being only the TM mode coupled with the electron gas, we will drop the polarization index from photonic operators.

Due to translational invariance in the $x - y$ plane, the uncoupled electron eigenstates can be put in the form

$$\psi_{\mathbf{k},j}(\mathbf{r}, z) = e^{i\mathbf{k}\cdot\mathbf{r}} \phi_j(z), \tag{A.4}$$

where $j = 1, 2$ is the conduction subband index and $\phi_j(z)$ is a function localized inside the quantum well, whose exact form depends upon the well potential shape. We introduce the fermionic creation and annihilation operators $c^\dagger_{j,\mathbf{k}}$ and $c_{j,\sigma,\mathbf{k}}$ for electrons in the state $\psi_{\mathbf{k},j}(\mathbf{r}, z)$ with spin σ, such that $\{c_{j,\sigma,\mathbf{k}}, c^\dagger_{j',\sigma',\mathbf{k}'}\} = \delta(\mathbf{k} - \mathbf{k}')\delta_{j,j'}\delta_{\sigma,\sigma'}$.

The Hamiltonian describing the coupled light-matter system is given by minimally coupling the electrons to the electromagnetic field

$$H = \sum_{j=1}^{N} \frac{(\mathbf{p} - eA(\mathbf{r}))^2}{2m^\star}. \tag{A.5}$$

Developing Eq. A.5 we can isolate three terms: a free term, a term linear in the vector potential and a term quadratic in the vector potential. We will now quantize these three terms. The free part of the Hamiltonian is automatically diagonalized because we chose its eigenstates (in Eq. A.4) as second quantization basis. It thus read

$$H_F = \sum_{\mathbf{k},\sigma,j=1,2} \hbar\omega_{c,j}(k) c^\dagger_{j,\sigma,\mathbf{k}} c_{j,\sigma,\mathbf{k}}. \tag{A.6}$$

The part linear in the vector potential can be evaluated from Eqs. A.1, A.3 and A.5, introducing the matrix element of the momentum operator between two electronic eigenstates $p_{12} = \int \phi_1(z) p_z \phi_2(z) dz$. Notice that being p_z an odd operator only electronic states between different subbands are coupled by this term. We have thus

$$\begin{aligned} H_L = & \sum_{\mathbf{q}} \hbar\omega_{cav}(q) a^\dagger_{\mathbf{q}} a_{\mathbf{q}} + \sum_{\sigma,\mathbf{k},\mathbf{q}} \sqrt{\frac{\hbar e^2}{m^{\star\,2}\epsilon_0 \omega_{cav}(q) SL_{cav}}} \cos(k_z z) \sin(\theta) p_{12} \\ & [(a_{\mathbf{q}} + a^\dagger_{-\mathbf{q}}) c^\dagger_{2,\sigma,\mathbf{k}+\mathbf{q}} c_{1,\sigma,\mathbf{k}} + (a_{-\mathbf{q}} + a^\dagger_{\mathbf{q}}) c^\dagger_{1,\sigma,\mathbf{k}} c_{2,\sigma,\mathbf{k}+\mathbf{q}}]. \end{aligned} \tag{A.7}$$

For a deep rectangular well almost all the oscillator strength is concentrated in the lowest transition, with the effects of higher energy transitions accounting only for minor corrections. This approximation becomes exact in the case of a parabolic confinement, for which $p_{12} = \sqrt{\hbar m^\star \omega_{12}/2}$. In the following we will thus consider the case of a parabolic quantum well in order to simplify the resulting expressions.

The part quadratic in the vector potential can be obtained in the same way, but this time the Hamiltonian depends neither on z nor on p_z and thus only electronic states in the same subband are coupled. The resulting Hamiltonian reads

$$H_Q = \sum_{\sigma,\mathbf{k},\mathbf{q}} \frac{\hbar e^2 \sin(\theta)^2}{2\epsilon_0 \omega_{cav}(q) m^\star S L_{cav}} (c^\dagger_{1,\sigma,\mathbf{k}} c_{1,\sigma,\mathbf{k}} + c^\dagger_{2,\sigma,\mathbf{k}} c_{2,\sigma,\mathbf{k}})(a_{\mathbf{q}} + a^\dagger_{-\mathbf{q}})(a_{-\mathbf{q}} + a^\dagger_{\mathbf{q}}). \tag{A.8}$$

Eq. A.8 can be greatly simplified by noticing that

$$\sum_{\sigma,\mathbf{k}} (c^\dagger_{1,\sigma,\mathbf{k}} c_{1,\sigma,\mathbf{k}} + c^\dagger_{2,\sigma,\mathbf{k}} c_{2,\sigma,\mathbf{k}}) \quad = \quad N \tag{A.9}$$

is the total number of electrons in the quantum well, and it is thus equal to N times the identity if the number of electrons is fixed to N. We can thus rewrite Eq. A.8 as

$$H_Q = \sum_{\mathbf{q}} \frac{\hbar e^2 \sin(\theta)^2 N}{2\epsilon_0 \omega_{cav}(q) m^\star S L_{cav}} (a_{\mathbf{q}} + a^\dagger_{-\mathbf{q}})(a_{-\mathbf{q}} + a^\dagger_{\mathbf{q}}). \tag{A.10}$$

In order to obtain Eq. A.8 we neglected the terms of the form $c^\dagger_{j,\sigma,\mathbf{k}} c_{j,\sigma,\mathbf{k}+\mathbf{q}-\mathbf{q}'} a^\dagger_{\mathbf{q}} a_{\mathbf{q}'}$. This approximation, necessary to put the Hamiltonian in the quadratic form of Eq. A.10 is justified by the fact that the photonic wavevectors $\mathbf{q}$ and $\mathbf{q}'$ are much smaller than the electronic ones. In fact terms like $c^\dagger_{j,\sigma,\mathbf{k}} c_{j,\sigma,\mathbf{k}+\mathbf{q}-\mathbf{q}'} a^\dagger_{\mathbf{q}} a_{\mathbf{q}'}$, describe processes in which a photon is scattered by an electron. This kind of process is possible only if the initial electronic state is filled and the final one is empty and thus only if $\mathbf{k}+\mathbf{q}-\mathbf{q}'$ is inside the Fermi sea and $\mathbf{k}$ is outside. To neglect these terms is thus equivalent to neglect the tiny fraction of electrons just on the border of the Fermi surface (at a distance of the order of the resonant photonic wavevector).

Defining

$$\chi(q)^2 = \frac{e^2 \sin(\theta)^2}{2\epsilon_0 \omega_{cav}(q) m^\star S L_{cav}} \tag{A.11}$$

and

$$D(q) = \frac{\chi(q)^2}{\omega_{12}} \tag{A.12}$$

we can thus write Hamiltonian in Eq. A.5 in the form

$$\begin{aligned} H &= \sum_{\mathbf{k}} \hbar\omega_{c,1}(k) c^\dagger_{1,\sigma,\mathbf{k}} c_{1,\sigma,\mathbf{k}} + \hbar\omega_{c,2}(k) c^\dagger_{2,\sigma,\mathbf{k}} c_{2,\sigma,\mathbf{k}} \\ &+ \sum_{\mathbf{q}} \hbar\omega_{cav}(q) a^\dagger_{\mathbf{q}} a_{\mathbf{q}} + \hbar D(q)(a_{1,-\mathbf{q}} + a^\dagger_{1,\mathbf{q}})(a_{1,\mathbf{q}} + a^\dagger_{1,-\mathbf{q}}) \\ &+ \sum_{\mathbf{k},\mathbf{q}} \hbar\chi(q)(a_{\mathbf{q}} + a^\dagger_{-\mathbf{q}}) c^\dagger_{2,\sigma,\mathbf{k}+\mathbf{q}} c_{1,\sigma,\mathbf{k}} + \hbar\chi(q)(a_{-\mathbf{q}} + a^\dagger_{\mathbf{q}}) c^\dagger_{1,\sigma,\mathbf{k}} c_{2,\sigma,\mathbf{k}+\mathbf{q}}. \end{aligned} \tag{A.13}$$

Appendix B

Input-output formalism

In this Appendix we will introduce the input-output formalism that will allow us to theoretically describe the coupling of the system with the environment. The environment will be modeled by two baths of harmonic excitations, one coupled to the cavity electromagnetic field, the other to the electronic polarization. The first bath models the external electromagnetic field coupled to the microcavity photons by the finite reflectivity of the mirrors, the second models all the spurious degrees of freedom (for example phonons and thermal electronic excitations) coupled to the electrons.

We will consider the following model Hamiltonian:

$$H = H_{bos} + H_{phot}^{bath} + H_{el}^{bath}, \tag{B.1}$$

where H_{bos} is the Hamiltonian is the Hamiltonian of Section 1.11 describing the microcavity embedded quantum wells, while H_{ph}^{bath} and H_{el}^{bath} describe the terms due to the photonic and electronic reservoir respectively.

The presence of extra-cavity electromagnetic modes can be modeled by the Hamiltonian:

$$\begin{aligned} H_{ph}^{bath} &= \int dq_z \sum_{\mathbf{q}} \hbar\omega_{ph}(\mathbf{q}, q_z)\alpha^{\dagger}_{\mathbf{q},q_z}\alpha_{\mathbf{q},q_z} \\ &+ i\hbar \int dq_z \sum_{\mathbf{q}} (\kappa_{ph}(\mathbf{q}, q_z)\alpha_{\mathbf{q},q_z}a^{\dagger}_{\mathbf{q}} - \kappa^{*}_{ph}(\mathbf{q}, q_z)\alpha^{\dagger}_{\mathbf{q},q_z}a_{\mathbf{q}}). \end{aligned} \tag{B.2}$$

Here, $\omega_{ph}(\mathbf{q}, q_z)$ is the frequency of an extra-cavity photon with wavevector $(\mathbf{q}, q_z)$ and $\alpha^{\dagger}_{\mathbf{q},q_z}$ is the corresponding creation operator (extra-cavity photon modes are three dimensional). The coupling between the cavity and the extra-cavity radiation fields is quantified by the matrix element $\kappa_{ph}(\mathbf{q}, q_z)$, whose

value depends on the specific mirror structure and can be calculated through a solution of the Maxwell equations for the cavity system. The coupling part of this Hamiltonian has been obtained using the Rotating Wave Approximation (see Section 1.2.4), for a thoughtful justification of this see Ref. [33]. In the same way the coupling to the electronic bath can be modeled by the Hamiltonian:

$$\begin{aligned} H_{el}^{bath} &= \int dq_z \sum_{\mathbf{q}} \hbar\omega_{el}(\mathbf{q}, q_z)\beta^{\dagger}_{\mathbf{q},q_z}\beta_{\mathbf{q},q_z} \\ &+ i\hbar \int dq_z \sum_{\mathbf{q}} (\kappa_{el}(\mathbf{q}, q_z)\beta_{\mathbf{q},q_z} b^{\dagger}_{\mathbf{q}} - \kappa^{*}_{el}(\mathbf{q}, q_z)\beta^{\dagger}_{\mathbf{q},q_z} b_{\mathbf{q}}), \end{aligned} \tag{B.3}$$

where we kept the same notation of Eq. B.2 even if now q_z does not need to be a wavevector component but it is a general index over the states of the bath. From Eqs. B.1 and B.2 we can calculate the equation of motion for the extra-cavity photon operator in Heisemberg representation

$$\frac{d\alpha_{\mathbf{q},q_z}(t)}{dt} = -\frac{i}{\hbar}[\alpha_{\mathbf{q},q_z}(t), H] = -i\omega_{ph}(\mathbf{q}, q_z)\alpha_{\mathbf{q},q_z}(t) - \kappa^{*}_{ph}(\mathbf{q}, q_z)a_{\mathbf{q}}(t), \tag{B.4}$$

and its solution can be formally written as

$$\alpha_{\mathbf{q},q_z}(t) = e^{-i\omega_{ph}(\mathbf{q},q_z)(t-t_0)}\alpha_{\mathbf{q},q_z}(t_0) - \kappa^{*}_{ph}(\mathbf{q}, q_z)\int_{t_0}^{t} dt' e^{-i\omega_{ph}(\mathbf{q},q_z)(t-t')}a_{\mathbf{q}}(t'), \tag{B.5}$$

t_0 being the initial time. These formulas con be inserted into the evolution equation for the cavity photon amplitude:

$$\begin{aligned} \frac{da_{\mathbf{q}}(t)}{dt} &= -\frac{i}{\hbar}[a_{\mathbf{q}}(t), H_{bos}] + \int dq_z \kappa_{ph}(\mathbf{q}, q_z)\alpha_{\mathbf{q},q_z}(t) \qquad \text{(B.6)} \\ &= -\frac{i}{\hbar}[a_{\mathbf{q}}, H_{bos}] + \int dq_z \kappa_{ph}(\mathbf{q}, q_z)\alpha_{\mathbf{q},q_z}(t_0)e^{-i\omega_{ph}(\mathbf{q},q_z)(t-t_0)} \\ &\quad - \int dq_z |\kappa_{ph}(\mathbf{q}, q_z)| \int_{t_0}^{t} dt' e^{-i\omega_{ph}(\mathbf{q},q_z)(t-t')}a_{\mathbf{q}}(t'). \end{aligned}$$

Using the standard definition

$$\begin{aligned} \alpha^{in}_{\mathbf{q},q_z} &\equiv \lim_{t_0\to-\infty} \alpha_{\mathbf{q},q_z}(t_0)e^{-i\omega_{ph}(\mathbf{q},q_z)t_0}, \qquad \text{(B.7)} \\ \alpha^{out}_{\mathbf{q},q_z} &\equiv \lim_{t\to\infty} \alpha_{\mathbf{q},q_z}(t)e^{-i\omega_{ph}(\mathbf{q},q_z)t}, \end{aligned}$$

for the input and output fields one can cast Eq. B.6 in the form of a quantum Langevin equation

$$\frac{da_{\mathbf{q}}(t)}{dt} = -\frac{i}{\hbar}[a_{\mathbf{q}}, H_{bos}] - \int dt' \Gamma_{cav,q}(t-t')a_{\mathbf{q}}(t') + F_{cav,\mathbf{q}}(t), \tag{B.8}$$

where the (causal) damping memory kernel is given by

$$\Gamma_{cav,q}(t) = \Theta(t) \int dq_z |\kappa_{ph}(\mathbf{q}, q_z)|^2 e^{-i\omega_{ph}(\mathbf{q},q_z)t}, \tag{B.9}$$

and the fluctuating Langevin force is represented by the operator

$$F_{cav,\mathbf{q}}(t) = \int dq_z \kappa_{ph}(\mathbf{q}, q_z) e^{-i\omega_{ph}(q,\mathbf{q})t} \alpha^{in}_{q,\mathbf{q}}. \tag{B.10}$$

Applying the same procedure for the bath coupled with the electrons we thus obtain a set of quantum Langevin equations describing, by means of a non-Markovian dynamics and of fluctuating forces, the system coupled with its environment

$$\begin{aligned} \frac{da_{\mathbf{q}}}{dt} &= -\frac{i}{\hbar}[a_{\mathbf{q}}, H_{bos}] - \int dt' \Gamma_{cav,q}(t-t') a_{\mathbf{q}}(t') + F_{cav,\mathbf{q}}(t) \qquad \text{(B.11)} \\ \frac{db_{\mathbf{q}}}{dt} &= -\frac{i}{\hbar}[b_{\mathbf{q}}, H_{bos}] - \int dt' \Gamma_{12,q}(t-t') b_{\mathbf{q}}(t') + F_{12,\mathbf{q}}(t). \end{aligned}$$

Once the intra-cavity fields have been determined by solving Eq. B.11, the extra-cavity emitted field can be found by inserting Eq. B.7 into Eq. B.5 and taking $t_0 \to -\infty$ and $t \to \infty$. We obtain

$$\alpha^{out}_{\mathbf{q},q_z} = \alpha^{in}_{\mathbf{q},q_z} + \kappa^*_{ph}(\mathbf{q}, q_z) \tilde{a}_{\mathbf{q}}(\omega_{ph}(\mathbf{q}, q_z)). \tag{B.12}$$

From Eq. B.12 we can get an expression for the number operator for the extra cavity photons

$$\begin{aligned} \alpha^{out\,\dagger}_{\mathbf{q},q_z} \alpha^{out}_{\mathbf{q},q_z} &= \alpha^{in\,\dagger}_{\mathbf{q},q_z} \alpha^{in}_{\mathbf{q},q_z} + \kappa^*_{ph}(\mathbf{q}, q_z) \alpha^{in\,\dagger}_{\mathbf{q},q_z} \tilde{a}_{\mathbf{q}}(\omega_{ph}(\mathbf{q}, q_z)) \qquad \text{(B.13)} \\ &+ \kappa_{ph}(\mathbf{q}, q_z) \tilde{a}^\dagger_{\mathbf{q}}(\omega_{ph}(\mathbf{q}, q_z)) \alpha^{in}_{\mathbf{q},q_z} + |\kappa_{ph}(\mathbf{q}, q_z)|^2 \tilde{a}^\dagger_{\mathbf{q}}(\omega_{ph}(\mathbf{q}, q_z)) \tilde{a}_{\mathbf{q}}(\omega_{ph}(\mathbf{q}, q_z)). \end{aligned}$$

Multiplying both sides of the equation for the extra-cavity photonic density of states $\rho^{ph}_{\mathbf{q}}(\omega_{ph}(\mathbf{q}, q_z))$, considering the extra-cavity field initially in its vacuum state and introducing the spectrum of emitted radiation

$$S_q(\omega(\mathbf{q}, q_z)) = \rho^{ph}_{\mathbf{q}}(\omega_{ph}(\mathbf{q}, q_z)) \langle \alpha^{out\,\dagger}_{\mathbf{q},q_z} \alpha^{out}_{\mathbf{q},q_z} \rangle, \tag{B.14}$$

we thus obtain

$$S_q(\omega) = \frac{1}{\pi} \Re(\tilde{\Gamma}_{cav,q}(\omega)) \langle \tilde{a}^\dagger_{\mathbf{q}}(\omega) \tilde{a}_{\mathbf{q}}(\omega) \rangle. \tag{B.15}$$

We end this Appendix with the explicit calculation of the expectation values of quadratic forms of the Langevin forces:

$$\begin{aligned}
< \tilde{F}^{\dagger 3}_{\mathbf{q}}(\omega)\tilde{F}^{3}_{\mathbf{q}}(\omega') > &= < \tilde{F}_{cav,-\mathbf{q}}(-\omega)\tilde{F}^{\dagger}_{cav,-\mathbf{q}}(-\omega') > \\
&= \sum_{q_z,q'_z} \kappa^{ph}_{q_z,-\mathbf{q}}\kappa^{ph*}_{q'_z,-\mathbf{q}} 4\pi^2\delta(-\omega-\omega_{q_z,-\mathbf{q}})\delta(-\omega'-\omega_{q'_z,-\mathbf{q}}) \\
&\quad < \alpha^{in}_{q_z,-\mathbf{q}}\alpha^{\dagger in}_{q'_z,-\mathbf{q}} > \\
&= \sum_{q_z} |\kappa^{ph}_{q_z,-\mathbf{q}}|^2 4\pi^2\delta(-\omega-\omega_{\mathbf{q},q_z})\delta(\omega-\omega') \\
&= 4\pi\delta(\omega-\omega')\Re(\tilde{\Gamma}_{cav,-q}(-\omega)), \\
< \tilde{F}^{\dagger 4}_{\mathbf{q}}(\omega)\tilde{F}^{4}_{\mathbf{q}}(\omega') > &= < \tilde{F}_{12,-\mathbf{q}}(-\omega)\tilde{F}^{\dagger}_{12,-\mathbf{q}}(-\omega') > \\
&= \sum_{q_z,q'_z} \kappa^{el}_{q_z,-\mathbf{q}}\kappa^{el*}_{q'_z,-\mathbf{q}} 4\pi^2\delta(-\omega-\omega^{bath}_{q_z,-\mathbf{q}})\delta(-\omega'-\omega^{bath}_{q'_z,-\mathbf{q}}) \\
&\quad < \beta^{in}_{q_z,-\mathbf{q}}\beta^{\dagger in}_{q'_z,-\mathbf{q}} > \\
&= \sum_{q_z} |\kappa^{el}_{q_z,-\mathbf{q}}|^2 4\pi^2\delta(-\omega-\omega^{bath}_{q_z,-\mathbf{q}})\delta(\omega-\omega') \\
&= 4\pi\delta(\omega-\omega')\Re(\tilde{\Gamma}_{12,-q}(-\omega)). \qquad \text{(B.16)}
\end{aligned}$$

All the other possible combinations are zero because, being the input state the vacuum, it is annihilated by both $\alpha^{in}_{\mathbf{q},q_z}$ and $\beta^{in}_{\mathbf{q},q_z}$ operators.

Appendix C

Factorization scheme

As explained in Chapter 3, we used a cluster expansion and truncation scheme to obtain a closed set of algebraic equations describing the electronic and photonic populations. Here we briefly review the principles of this method following [76, 77, 78] and apply it to the actual case.

If we consider each bosonic operator or each pair of fermionic operators as an excitation operator and we write the expectation value of an N excitation operator as $< N >$, then the Heisenberg equation of motion takes the form

$$i\frac{\partial}{\partial t} < N >= T[< N >] + V[< N+1 >], \tag{C.1}$$

where the N-excitation expectation value is coupled to higher order quantities via the functional V. An N-excitation truncation scheme is obtained if we factorize all the expectation values of more than N excitations in all the possible ways and considering the sign exchange for the fermionic operators in order to obtain a factorized expression that respects the commutation and anticommutation properties of the original one.

We are interested in incoherent emission only, so the only nonzero one-excitation operators we consider are $< c^{\dagger}_{1,\sigma,\mathbf{k}} c_{1,\sigma,\mathbf{k}} >$ and $< c^{\dagger}_{2,\sigma,\mathbf{k}} c_{2,\sigma,\mathbf{k}} >$. We choose $N = 2$, that is we factorize all the 3 or more excitation operators. The

3 excitations operators have been factorized in the following way

$$\begin{aligned}
< a_{\mathbf{q}} c_{1,\sigma,\mathbf{k}} c^{\dagger}_{2,\sigma,\mathbf{k}'} c^{\dagger}_{2,\sigma',\mathbf{k}''} c_{2,\sigma',\mathbf{k}'''} > &= - < a_{\mathbf{q}} c^{\dagger}_{2,\sigma,\mathbf{k}'} c_{1,\sigma,\mathbf{k}} >< c^{\dagger}_{2,\sigma',\mathbf{k}''} c_{2,\sigma',\mathbf{k}'''} > \\
&\quad + < a_{\mathbf{q}} c^{\dagger}_{2,\sigma',\mathbf{k}''} c_{1,\sigma,\mathbf{k}} >< c^{\dagger}_{2,\sigma,\mathbf{k}'} c_{2,\sigma',\mathbf{k}'''} > \\
&= - < a_{\mathbf{q}} c^{\dagger}_{2,\sigma,\mathbf{k}'} c_{1,\sigma,\mathbf{k}} > \delta_{\mathbf{k}'',\mathbf{k}'''} n_{2,\mathbf{k}''} \\
&\quad + < a_{\mathbf{q}} c^{\dagger}_{2,\sigma,\mathbf{k}''} c_{1,\sigma,\mathbf{k}} > \delta_{\mathbf{k}',\mathbf{k}'''} \delta_{\sigma,\sigma'} n_{2,\mathbf{k}'}, \qquad \text{(C.2)} \\
< a_{\mathbf{q}} c^{\dagger}_{2,\sigma,\mathbf{k}} c_{1,\sigma,\mathbf{k}'} c_{1,\sigma',\mathbf{k}''} c^{\dagger}_{1,\sigma',\mathbf{k}'''} > &= - < a_{\mathbf{q}} c^{\dagger}_{2,\sigma,\mathbf{k}} c_{1,\sigma',\mathbf{k}''} >< c_{1,\sigma,\mathbf{k}'} c^{\dagger}_{1,\sigma',\mathbf{k}'''} > \\
&\quad + < a_{\mathbf{q}} c^{\dagger}_{2,\sigma,\mathbf{k}} c_{1,\sigma,\mathbf{k}'} >< c_{1,\sigma',\mathbf{k}''} c^{\dagger}_{1,\sigma',\mathbf{k}'''} > \\
&= - < a_{\mathbf{q}} c^{\dagger}_{2,\sigma,\mathbf{k}} c_{1,\sigma,\mathbf{k}''} > \delta_{\mathbf{k}',\mathbf{k}'''} \delta_{\sigma,\sigma'} (1 - n_{1,\mathbf{k}'}) \\
&\quad + < a_{\mathbf{q}} c^{\dagger}_{2,\sigma,\mathbf{k}} c_{1,\sigma,\mathbf{k}'} > \delta_{\mathbf{k}'',\mathbf{k}'''} (1 - n_{1,\mathbf{k}''}).
\end{aligned}$$

For the two-time quantities in the calculation of luminescence spectrum, we proceed analogously and obtain:

$$\begin{aligned}
< a^{\dagger}_{\mathbf{q}}(0) a_{\mathbf{q}'} c^{\dagger}_{2,\sigma,\mathbf{k}+\mathbf{q}} c_{2,\sigma,\mathbf{k}+\mathbf{q}'} > &= < a^{\dagger}_{\mathbf{q}}(0) a_{\mathbf{q}'} >< c^{\dagger}_{2,\sigma,\mathbf{k}+\mathbf{q}} c_{2,\sigma,\mathbf{k}+\mathbf{q}'} > \delta_{\mathbf{q},\mathbf{q}'}, \\
< a^{\dagger}_{\mathbf{q}}(0) a_{\mathbf{q}'} c^{\dagger}_{1,\sigma,\mathbf{k}} c_{1,\sigma,\mathbf{k}+\mathbf{q}-\mathbf{q}'} > &= < a^{\dagger}_{\mathbf{q}}(0) a_{\mathbf{q}'} >< c^{\dagger}_{1,\sigma,\mathbf{k}} c_{1,\sigma,\mathbf{k}+\mathbf{q}-\mathbf{q}'} > \delta_{\mathbf{q},\mathbf{q}'}.
\end{aligned} \qquad \text{(C.3)}$$

By means of this factorization scheme we arrived in Chapter 3 to the system of coupled nonlinear differential equations described in Eq. 3.7. In the steady-state regime, neglecting the photonic wavevector into sums over electronic wavevectors, it can be cast in the form of a system of algebraic equations, well suited for numerical calculations

$$\begin{aligned}
0 &= \frac{B_{\mathbf{q}}}{D} \sum_{\mathbf{k}} (1 - D_{\mathbf{k}}) \left(\frac{n_{1,\mathbf{k}} - n^0_{1,\mathbf{k}}}{\tau_{\mathbf{k}}} + \Gamma^{out}_{1,\mathbf{k}} n_{1,\mathbf{k}} - \Gamma^{in}_{1,\mathbf{k}} (1 - n_{1,\mathbf{k}}) \right) - \frac{2 B_{\mathbf{q}} F \Gamma_X}{D} \\
&\quad + \left(B_{\mathbf{q}} (\gamma + \Gamma_X) + \left(\frac{\delta^2_{\mathbf{q}}}{\Gamma_Y} + \frac{G_{\mathbf{q}} \Gamma_X}{2 D \chi(q)^2} \right) \gamma \right) n_{a,\mathbf{q}}, \qquad \text{(C.4)}
\end{aligned}$$

$$\begin{aligned}
0 &= \left(\sum_{\mathbf{q}} \frac{B_{\mathbf{q}} \chi(q)^2}{G_{\mathbf{q}} \Gamma_X} (1 - D_{\mathbf{k}}) + \frac{1}{2} \right) \left(\frac{n_{1,\mathbf{k}} - n^0_{1,\mathbf{k}}}{\tau_{\mathbf{k}}} + \Gamma^{out}_{1,\mathbf{k}} n_{1,\mathbf{k}} - \Gamma^{in}_{1,\mathbf{k}} (1 - n_{1,\mathbf{k}}) \right) \\
&\quad + \frac{D_{\mathbf{k}}}{\Gamma_X \Gamma_Y} \sum_{\mathbf{q}} \frac{\chi(q)^2 n_{a,\mathbf{q}}}{G_{\mathbf{q}}} (\Gamma_Y B_{\mathbf{q}} (\gamma + \Gamma_X) + \delta^2_{\mathbf{q}} \gamma) - 2 F_{\mathbf{k}} \sum_{\mathbf{q}} \frac{B_{\mathbf{q}} \chi(q)^2}{G_{\mathbf{q}}},
\end{aligned}$$

$$0 = - \frac{n_{2,\mathbf{k}} - n^0_{2,\mathbf{k}}}{\tau_{\mathbf{k}}} - \Gamma^{out}_{2,\mathbf{k}} n_{2,\mathbf{k}} + \Gamma^{in}_{2,\mathbf{k}} (1 - n_{2,\mathbf{k}}) - \frac{n_{1,\mathbf{k}} - n^0_{1,\mathbf{k}}}{\tau_{\mathbf{k}}} - \Gamma^{out}_{1,\mathbf{k}} n_{1,\mathbf{k}} + \Gamma^{in}_{1,\mathbf{k}} (1 - n_{1,\mathbf{k}}),$$

where

$$\begin{aligned} D_{\mathbf{k}} &= n_{1,\mathbf{k}} - n_{2,\mathbf{k}} \\ F_{\mathbf{k}} &= n_{2,\mathbf{k}}(1 - n_{1,\mathbf{k}}) \\ D &= \sum_{\mathbf{k}} D_{\mathbf{k}} \\ F &= \sum_{\mathbf{k}} F_{\mathbf{k}} \\ B_{\mathbf{q}} &= \Gamma_Y + \frac{2\chi(q)^2}{\Gamma_X} D \\ \delta_{\mathbf{q}} &= \omega_c(\mathbf{q}) - \omega_{12} \\ G_{\mathbf{q}} &= (\omega_c(\mathbf{q}) - \omega_{12})^2 + (\Gamma_Y + \frac{2\chi(q)^2 D}{\Gamma_X})^2. \end{aligned} \tag{C.5}$$

The equilibrium populations $n^0_{1,\mathbf{k}}$ and $n^0_{2,\mathbf{k}}$ are given by

$$\begin{aligned} n^0_{1,\mathbf{k}} &= \frac{1}{\exp \beta(\omega_1(\mathbf{k}) - \epsilon_F) + 1}, \\ n^0_{2,\mathbf{k}} &= \frac{1}{\exp \beta(\omega_2(\mathbf{k}) - \epsilon_F) + 1}, \end{aligned} \tag{C.6}$$

where ϵ_F is calculated by inverting the relation

$$\sum_{\mathbf{k}} n_{1,\mathbf{k}} + n_{2,\mathbf{k}} = \frac{m^*}{2\pi\hbar^2} \int_0^\infty d\epsilon \frac{1}{\exp \beta(\epsilon - \epsilon_F) + 1} + \frac{1}{\exp \beta(\epsilon + E_{12} - \epsilon_F) + 1}. \tag{C.7}$$

Discretizing the electronic and photonic wavevectors on a grid of respectively $N_{\mathbf{k}}$ and $N_{\mathbf{q}}$ points, we obtain a system of $2N_{\mathbf{k}} + N_{\mathbf{q}}$ equations that can be numerically solved, e.g., with a Newton algorithm.

Appendix D

Diagonalization procedure

In Chapter 4 we showed how it is possible, in order to study the electron injection, to restrict ourselves to the one-excitation subspace $\hat{Q} = 1$. Moreover we showed how only a tiny (but still infinite-dimensional) subspace of this subspace is relevant for our results. Namely we claimed that the dynamics of the system can be accurately described restraining to the subspace $\{|C\rangle, |A, \mathbf{q}\rangle, |B, \mathbf{q}, \mathbf{k}'\rangle, |B, \mathbf{q}, \mathbf{k}''\rangle, \dots, |A, \mathbf{q}'\rangle, |B, \mathbf{q}', \mathbf{k}'\rangle, |B, \mathbf{q}', \mathbf{k}''\rangle, \dots\}$, where the definition of the aforementioned kets can be found in Section 4.2. In such subspace the Hamiltonian in Eq. 4.2 reads

$$\mathcal{H}_{N+1,\mathbf{k},1} = \hbar \begin{pmatrix} \omega_{c,2}(k) & v(q) & v(q') & v(q'') & \cdots \\ v(q)^T & M(\mathbf{q}) & 0 & 0 & \cdots \\ v(q')^T & 0 & M(\mathbf{q}') & 0 & \cdots \\ v(q'')^T & 0 & 0 & M(\mathbf{q}'') & \ddots \\ \vdots & \vdots & \vdots & \ddots & \ddots \end{pmatrix} \tag{D.1}$$

and $M(\mathbf{q})$ is the Hamiltonian matrix block in the subspace spanned by $\{|A, \mathbf{q}\rangle, |B, \mathbf{q}, \mathbf{k}'\rangle, |B, \mathbf{q}, \mathbf{k}''\rangle, \dots\}$. It effectively describes the system in pres-

ence of one photon with a well defined wavevector $\mathbf{q}$

$$M(\mathbf{q}) = \begin{pmatrix} \omega_{cav}(q)+\omega_{c,1}(|\mathbf{k}-\mathbf{q}|)) & \chi(q) & \chi(q) & \cdots \\ \chi(q) & \omega_{c,2}(|\mathbf{k}'+\mathbf{q}|)-\omega_{c,1}(k')+\omega_{c,1}(|\mathbf{k}-\mathbf{q}|) & 0 & \cdots \\ \chi(q) & 0 & \omega_{c,2}(|\mathbf{k}''+\mathbf{q}|)-\omega_{c,1}(k'')+\omega_{c,1}(|\mathbf{k}-\mathbf{q}|) & \ddots \\ \vdots & \vdots & \ddots & \ddots \end{pmatrix}, \tag{D.2}$$

where $v(q) = [\chi(q), 0, 0, \ldots]$. Since the typical wavevector q of the resonantly coupled cavity photon mode is much smaller than k_F, we can perform the standard approximation $\omega_{c,2}(|\mathbf{k}+\mathbf{q}|) - \omega_{c,1}(k) \simeq \omega_{c,2}(k) - \omega_{c,1}(k) = \omega_{12}$. This way, we can exactly diagonalize each of the $M(\mathbf{q})$ blocks. As expected from the theory of optically excited polaritons [25], by diagonalizing the matrix $M(\mathbf{q})$ we find two bright electronic states (i.e., with a photonic mixing component)

$$|\pm, \mathbf{q}\rangle = \frac{(\omega_{\pm}(q)-\omega_{12})|A,\mathbf{q}\rangle + \chi(q)\sum_{\mathbf{k}}|B,\mathbf{q},\mathbf{k}\rangle}{\sqrt{(\omega_{\pm}(q)-\omega_{12})^2 + |\chi(q)|^2 N}}, \tag{D.3}$$

with energies $\hbar\omega_{c,1}(k) + \hbar\omega_{\pm}(q)$, where

$$\omega_{\pm}(q) = \frac{\omega_{cav}(q)+\omega_{12}}{2} \pm \sqrt{\left(\frac{\omega_{cav}(q)-\omega_{12}}{2}\right)^2 + N|\chi(q)|^2}. \tag{D.4}$$

Note that $\hbar\omega_{\pm}(q)$ are the energies of the two branches of intersubband cavity polaritons [25]. The other orthogonal states are dark (no photonic component), with eigenvalues $\omega_{c,2}(k) = \omega_{c,1}(k) + \omega_{12}$ and eigenvectors

$$|l,\mathbf{q}\rangle = \frac{\sum_{\mathbf{k}}\beta_l(\mathbf{q},\mathbf{k})|B,\mathbf{q},\mathbf{k}\rangle}{\sqrt{N}} \tag{D.5}$$

where the $\beta_l(\mathbf{q},\mathbf{k})$ are such that

$$\begin{aligned} \sum_{\mathbf{k}}\beta_l(\mathbf{q},\mathbf{k}) &= 0, \\ \sum_{\mathbf{k}}\beta_l(\mathbf{q},\mathbf{k})\beta^*_{l'}(\mathbf{q},\mathbf{k}) &= \delta_{l,l'}. \end{aligned} \tag{D.6}$$

Since $\langle l, \mathbf{q}| H\ c^\dagger_{2,\mathbf{k}}|F_N\rangle = 0$, the dark states $|l, \mathbf{q}\rangle$ are also eigenstates of the matrix $\mathcal{H}_{N+1,\mathbf{k},1}$ and do not contribute to the electron spectral function, because they have zero overlap with the state $|C\rangle = c^\dagger_{2,\mathbf{k}}|F_N\rangle = 0$. In contrast, this is not the case for the bright eigenstates of each block $M(\mathbf{q})$, as we find

$$\langle \pm, \mathbf{q}| H\ c^\dagger_{2,\mathbf{k}}|F_N\rangle = \frac{\chi(q)(\omega_\pm(q) - \omega_{12})}{\sqrt{(\omega_\pm(q) - \omega_{12})^2 + |\chi(q)|^2 N}} = J_\pm(q)\ . \tag{D.7}$$

Therefore, the representation of H in the subspace $\{|C\rangle, |+, \mathbf{q}\rangle, |-, \mathbf{q}\rangle, |+, \mathbf{q}'\rangle, |-, \mathbf{q}'\rangle, \dots\}$ reads

$$\mathcal{H'}_{N+1,\mathbf{k},1} = \hbar \begin{pmatrix} \omega_{c,1}(k) + \omega_{12} & J_+(q) & J_-(q) & J_+(q') & J_-(q') & \cdots \\ J_+(q) & \omega_{c,1}(k) + \omega_+(q) & 0 & 0 & 0 & \cdots \\ J_-(q) & 0 & \omega_{c,1}(k) + \omega_-(q) & 0 & 0 & \cdots \\ J_+(q') & 0 & 0 & \omega_{c,1}(k) + \omega_+(q') & 0 & \cdots \\ J_-(q') & 0 & 0 & 0 & \omega_{c,1}(k) + \omega_-(q') & \ddots \\ \vdots & \vdots & \vdots & \vdots & \ddots & \ddots \end{pmatrix}.$$

Hence, here we have demonstrated that the bare electron state $c^\dagger_{2,\mathbf{k}}|F_N\rangle$ is coupled to the continuum of the polariton modes with all the different wavevectors $\mathbf{q}$. Since the polariton frequencies $\omega_\pm$ and the coupling $J_\pm$ depend only on the modulus of $\mathbf{q}$, we can further simplify the diagonalization problem by introducing the 'annular' bright states

$$|\pm, q\rangle = \frac{1}{\sqrt{Lq}} \sum_{|\mathbf{q}|=q} |\pm, \mathbf{q}\rangle\ , \tag{D.8}$$

where $L = \sqrt{S}$ and $2\pi/L$ is the linear density of modes in reciprocal space. All annular states are coupled to $|C\rangle$. Instead, all the orthogonal linear combinations of $|\pm, \mathbf{q}\rangle$ (with $|\mathbf{q}| = q$) are uncoupled and therefore do not contribute to the electron spectral function. The matrix representation of H in the subspace $\{|C\rangle, |+, q\rangle, |-, q\rangle, |+, q'\rangle, |-, q'\rangle, \dots\}$ reads

$$\mathcal{H''}_{N+1,\mathbf{k},1} = \hbar \begin{pmatrix} \omega_{c,1}(k) + \omega_{12} & J_+(q)\sqrt{Lq} & J_-(q)\sqrt{Lq} & J_+(q')\sqrt{Lq'} & J_-(q')\sqrt{Lq'} & \cdots \\ J_+(q)\sqrt{Lq} & \omega_{c,1}(k) + \omega_+(q) & 0 & 0 & 0 & \cdots \\ J_-(q)\sqrt{Lq} & 0 & \omega_{c,1}(k) + \omega_-(q) & 0 & 0 & \cdots \\ J_+(q')\sqrt{Lq'} & 0 & 0 & \omega_{c,1}(k) + \omega_+(q') & 0 & \cdots \\ J_-(q')\sqrt{Lq'} & 0 & 0 & 0 & \hbar\omega_{c,1}(k) + \omega_-(q') & \ddots \\ \vdots & \vdots & \vdots & \vdots & \ddots & \ddots \end{pmatrix}.$$

Hence, in the subspace $(N+1, \mathbf{k}, 1)$, we have found that eigenstates of H with a finite overlap with the bare electron have the form

$$|N+1, \mathbf{k}, 1, \zeta\rangle = \mu_\zeta\ c^\dagger_{2\,\mathbf{k}}|F_N\rangle + \sum_{q,\sigma=\pm} \lambda_{\zeta,\sigma,q}|\sigma, q\rangle\ . \tag{D.9}$$

The coefficients μ_ζ and $\lambda_{\zeta,\sigma,q}$ as well as the corresponding energy eigenvalues $\hbar\omega_\zeta$ can be calculated though a numerical diagonalization of the matrix ${\mathcal{H}''}_{N+1,\mathbf{k},1}$.

Appendix E

Matrix elements recursive relation

In this Appendix we will write down the algebra leading to results of Chapter 5. The first step is to work out the commutator algebra for the intersubband excitation operators, originally defined in Section 1.4.3. The creation and annihilation operators for intersubband excitations with in-plane wavevector $\mathbf{q}$ can be written as

$$\begin{aligned} b^{\dagger}_{\mathbf{q}} &= \frac{1}{\sqrt{N}} \sum_{\mathbf{k}} c^{\dagger}_{2,\mathbf{k}+\mathbf{q}} c_{1,\mathbf{k}}, \\ b_{\mathbf{q}} &= \frac{1}{\sqrt{N}} \sum_{\mathbf{k}} c^{\dagger}_{1,\mathbf{k}} c_{2,\mathbf{k}+\mathbf{q}}. \end{aligned} \tag{E.1}$$

Using the fermionic anticommutator relations

$$\begin{aligned} \{c_{i,\mathbf{k}}, c^{\dagger}_{j,\mathbf{k}'}\} &= \delta(\mathbf{k}-\mathbf{k}')\delta_{i,j}, \\ \{c_{i,\mathbf{k}}, c_{j,\mathbf{k}'}\} &= 0, \end{aligned} \tag{E.2}$$

we obtain

$$\begin{aligned} [b_{\mathbf{q}}, b^{\dagger}_{\mathbf{q}'}] &= \frac{1}{N} \sum_{\mathbf{k},\mathbf{k}'} [c^{\dagger}_{1,\mathbf{k}} c_{2,\mathbf{k}+\mathbf{q}}, c^{\dagger}_{2,\mathbf{k}'+\mathbf{q}'} c_{1,\mathbf{k}'}] \\ &= \frac{1}{N} \sum_{\mathbf{k}} c^{\dagger}_{1,\mathbf{k}} c_{1,\mathbf{k}+\mathbf{q}-\mathbf{q}'} - c^{\dagger}_{2,\mathbf{k}+\mathbf{q}'} c_{2,\mathbf{k}+\mathbf{q}} = \delta(\mathbf{q}-\mathbf{q}') - D_{\mathbf{q},\mathbf{q}'}, \end{aligned} \tag{E.3}$$

where the deviation from Boson operator $D_{\mathbf{q},\mathbf{q}'}$ has been defined as

$$D_{\mathbf{q},\mathbf{q}'} = \delta(\mathbf{q}-\mathbf{q}') - \frac{1}{N} \sum_{\mathbf{k}} c^{\dagger}_{1,\mathbf{k}} c_{1,\mathbf{k}+\mathbf{q}-\mathbf{q}'} - c^{\dagger}_{2,\mathbf{k}+\mathbf{q}'} c_{2,\mathbf{k}+\mathbf{q}}. \tag{E.4}$$

Commuting it with the intersubband operators and rescaling the indexes we thus obtain

$$\begin{aligned} [D_{\mathbf{q},\mathbf{q}'}, b^\dagger_{\mathbf{q}''}] &= \frac{2}{N} b^\dagger_{\mathbf{q}''+\mathbf{q}'-\mathbf{q}}, \\ [b_{\mathbf{q}''}, D_{\mathbf{q},\mathbf{q}'}] &= \frac{2}{N} b_{\mathbf{q}''+\mathbf{q}-\mathbf{q}'}. \end{aligned} \tag{E.5}$$

By iteration

$$\begin{aligned} [D_{\mathbf{q},\mathbf{q}'}, b^{\dagger\, m}_{\mathbf{q}''}] &= \frac{2m}{N} b^\dagger_{\mathbf{q}''+\mathbf{q}'-\mathbf{q}} b^{\dagger\, m-1}_{\mathbf{q}''}, \\ [b^m_{\mathbf{q}''}, D_{\mathbf{q},\mathbf{q}'}] &= \frac{2m}{N} b^{m-1}_{\mathbf{q}''} b_{\mathbf{q}''+\mathbf{q}-\mathbf{q}'}, \\ [b_{\mathbf{q}}, b^{\dagger\, m}_{\mathbf{q}'}] &= m b^{\dagger\, m-1}_{\mathbf{q}'} [\delta(\mathbf{q}-\mathbf{q}') - D_{\mathbf{q},\mathbf{q}'}] - \frac{m(m-1)}{N} b^\dagger_{\mathbf{2q}'-\mathbf{q}} b^{\dagger\, m-2}_{\mathbf{q}'}, \\ [b^m_{\mathbf{q}}, b^\dagger_{\mathbf{q}'}] &= m[\delta(\mathbf{q}-\mathbf{q}') - D_{\mathbf{q},\mathbf{q}'}] b^{m-1}_{\mathbf{q}} - \frac{m(m-1)}{N} b_{\mathbf{2q}-\mathbf{q}'} b^{m-2}_{\mathbf{q}}. \end{aligned} \tag{E.6}$$

From Eq. E.4 we have that the action of $D_{\mathbf{q},\mathbf{q}'}$ on the N-electrons ground state $|F\rangle = \prod_{k<k_F} c^\dagger_{1,\mathbf{k}}|0\rangle$ gives

$$D_{\mathbf{q},\mathbf{q}'}|F\rangle = \delta(\mathbf{q}-\mathbf{q}')|F\rangle - \frac{1}{N} \prod_{\substack{k>k_F \\ |\mathbf{k}+\mathbf{q}-\mathbf{q}'|<k_F}} c^\dagger_{1,\mathbf{k}}|0\rangle. \tag{E.7}$$

The second term of Eq. E.7 is gives a contribution of the order of $\frac{q_{res}}{k_F}$ and will be thus neglected. We will now introduce the four-indexes $\mathcal{K}$ coefficients, that will play a prominent role in our recursive calculation procedure. Let us define the $\mathcal{K}$ coefficients as

$$\begin{aligned} n!m!\mathcal{K}^{n,s}_{m,r} &= \langle F| b^n_{\mathbf{q}} b^m_{\mathbf{q}'} b^{\dagger\, s}_{\mathbf{q}} b^{\dagger\, r}_{\mathbf{q}'} b^\dagger_{\mathbf{Q}} |F\rangle, \\ \mathbf{Q} &= \mathbf{q}(n-s) + \mathbf{q}'(m-r). \end{aligned} \tag{E.8}$$

It is obvious from the definition that $\mathcal{K}^{n,s}_{m,r} \propto \delta(n+m-r-s-1)$ and that $\mathcal{K}^{n,s}_{m,r} = \mathcal{K}^{m,r}_{n,s}$. With the chosen normalization the $\mathcal{K}$ coefficients, for small m and n, are of the order $1/N$ if $n \neq s$ and $m \neq r$ and of order 1 otherwise (for real bosons $\langle F| b^n_{\mathbf{q}} b^m_{\mathbf{q}'} b^{\dagger\, m}_{\mathbf{q}'} b^{\dagger\, n}_{\mathbf{q}} |F\rangle = n!m!$). Let us notice that in the case $n = s$ or $m = r$ the definition of the indexes is not unique, in fact

$$\begin{aligned} \langle F| b^n_{\mathbf{q}} b^m_{\mathbf{q}'} b^{\dagger\, m}_{\mathbf{q}'} b^{\dagger\, n}_{\mathbf{q}} |F\rangle &= \langle F| b^n_{\mathbf{q}} b^m_{\mathbf{q}'} b^{\dagger\, m}_{\mathbf{q}'} b^{\dagger\, n-1}_{\mathbf{q}} b^\dagger_{\mathbf{q}} |F\rangle = n!m!\mathcal{K}^{n,n-1}_{m,m} \\ &= \langle F| b^n_{\mathbf{q}} b^m_{\mathbf{q}'} b^{\dagger\, m-1}_{\mathbf{q}'} b^\dagger_{\mathbf{q}'} b^{\dagger\, n}_{\mathbf{q}} |F\rangle = n!m!\mathcal{K}^{n,n}_{m,m-1}, \end{aligned} \tag{E.9}$$

but this does not cause any ambiguity, simply certain symmetries of the resulting expressions will be hidden (e.g. the $m \leftrightarrow n$ symmetry). Now by commuting one of the creation operators in the definition of $\mathcal{K}$ coefficients in Eq. E.8 all the way to the left, until it annihilates on the ground state, we find a recursive relations for the $\mathcal{K}$ coefficients

$$\begin{aligned}
\langle F|b_{\mathbf{q}}^{n}b_{\mathbf{q}'}^{m}b_{\mathbf{q}}^{\dagger\, s}b_{\mathbf{q}'}^{\dagger\, r}b_{\mathbf{Q}}^{\dagger}|F\rangle &= \langle F|b_{\mathbf{q}}^{n}b_{\mathbf{Q}}^{\dagger}b_{\mathbf{q}'}^{m}b_{\mathbf{q}}^{\dagger\, s}b_{\mathbf{q}'}^{\dagger\, r}|F\rangle \\
&\quad +m\delta(\mathbf{q}'-\mathbf{Q})\langle F|b_{\mathbf{q}}^{n}b_{\mathbf{q}'}^{m-1}b_{\mathbf{q}}^{\dagger\, s}b_{\mathbf{q}'}^{\dagger\, r}|F\rangle \\
&\quad -m\langle F|b_{\mathbf{q}}^{n}D_{\mathbf{q}',\mathbf{Q}}b_{\mathbf{q}'}^{m-1}b_{\mathbf{q}}^{\dagger\, s}b_{\mathbf{q}'}^{\dagger\, r}|F\rangle \\
&\quad -\frac{m(m-1)}{N}\langle F|b_{\mathbf{q}}^{n}b_{\mathbf{2q}'-\mathbf{Q}}b_{\mathbf{q}'}^{m-2}b_{\mathbf{q}}^{\dagger\, s}b_{\mathbf{q}'}^{\dagger\, r}|F\rangle \\
&= n\delta(\mathbf{q}-\mathbf{Q})\langle F|b_{\mathbf{q}}^{n-1}b_{\mathbf{q}'}^{m}b_{\mathbf{q}}^{\dagger\, s}b_{\mathbf{q}'}^{\dagger\, r}|F\rangle \\
&\quad -\frac{n(n-1)}{N}\langle F|b_{\mathbf{2q}-\mathbf{Q}}b_{\mathbf{q}}^{n-2}b_{\mathbf{q}'}^{m}b_{\mathbf{q}}^{\dagger\, s}b_{\mathbf{q}'}^{\dagger\, r}|F\rangle \\
&\quad +m\delta(\mathbf{q}'-\mathbf{Q})\langle F|b_{\mathbf{q}}^{n}b_{\mathbf{q}'}^{m-1}b_{\mathbf{q}}^{\dagger\, s}b_{\mathbf{q}'}^{\dagger\, r}|F\rangle \\
&\quad -\frac{2mn}{N}\langle F|b_{\mathbf{q}}^{n-1}b_{\mathbf{q}+\mathbf{q}'-\mathbf{Q}}b_{\mathbf{q}'}^{m-1}b_{\mathbf{q}}^{\dagger\, s}b_{\mathbf{q}'}^{\dagger\, r}|F\rangle \\
&\quad -\frac{m(m-1)}{N}\langle F|b_{\mathbf{q}}^{n}b_{\mathbf{2q}'-\mathbf{Q}}b_{\mathbf{q}'}^{m-2}b_{\mathbf{q}}^{\dagger\, s}b_{\mathbf{q}'}^{\dagger\, r}|F\rangle,
\end{aligned} \tag{E.10}$$

and so

$$\begin{aligned}
\mathcal{K}_{m,r}^{n,s} &= \delta(m-r)\delta(n-s-1)\mathcal{K}_{m,m-1}^{n-1,n-1}+\delta(m-r-1)\delta(n-s)\mathcal{K}_{m-1,m-1}^{n,n-1} \\
&\quad -\frac{s!r!}{n!m!N}[n(n-1)\mathcal{K}_{r,m}^{s,n-2}+m(m-1)\mathcal{K}_{r,m-2}^{s,n}+2nm\mathcal{K}_{r,m-1}^{s,n-1}].
\end{aligned} \tag{E.11}$$

This recursion relation permits us to numerically calculate the $\mathcal{K}$ coefficients for realistic parameters in a reasonable computing time. Having calculated the $\mathcal{K}$ coefficients we can pass to calculate the Hamiltonian matrix elements between states with multiple intersubband excitations. In order to simplify the algebra, in the Hamiltonian in Eq. 5.1, we will neglect the C_{12} and C_{21} terms. These terms describe an intersubband phonon emission, that is an electron falls from the second to the first conduction subband emitting a LO-phonon. The process involved thus destroys an intersubband excitation and can not give a stimulated scattering to the first order. It could give a stimulated scattering effect to higher orders, for example in a process in which two polaritons scatter, one of them is annihilated and the other is scattered in the final state. These processes are anyway much weaker then the first order processes given by

intrasubband C_{11} and C_{22} scattering terms. We thus obtain

$$[H, b^\dagger_{\mathbf{q}}] = \omega_{12} b^\dagger_{\mathbf{q}} + \sum_{\mathbf{q}', q_z} [C_{22}(\mathbf{q}', q_z) - C_{11}(\mathbf{q}', q_z)](d^\dagger_{-\mathbf{q}', q_z} + d_{\mathbf{q}', q_z}) b^\dagger_{\mathbf{q}+\mathbf{q}'}. \tag{E.12}$$

Using iteratively Eq. E.12 we can calculate the (unnormalized) scattering matrix element as

$$\begin{aligned}
&\langle F | b^{n+1}_{\mathbf{q}} b^{m-1}_{\mathbf{q}'} d_{\mathbf{q}'-\mathbf{q}, q_z} H_{phon} b^{\dagger\, m}_{\mathbf{q}'} b^{\dagger\, n}_{\mathbf{q}} | F \rangle = \sum_{\mathbf{q}''} [C_{22}(\mathbf{q}'', q_z) - C_{11}(\mathbf{q}'', q_z)] \\
&(n \langle F | b^{n+1}_{\mathbf{q}} b^{m-1}_{\mathbf{q}'} b^{\dagger\, m}_{\mathbf{q}'} b^\dagger_{\mathbf{q}+\mathbf{q}''} b^{\dagger\, n-1}_{\mathbf{q}} | F \rangle + m \langle F | b^{n+1}_{\mathbf{q}} b^{m-1}_{\mathbf{q}'} b^\dagger_{\mathbf{q}'+\mathbf{q}''} b^{\dagger\, m-1}_{\mathbf{q}'} b^{\dagger\, n}_{\mathbf{q}} | F \rangle) \\
&= [C_{22}(\mathbf{q}-\mathbf{q}', q_z) - C_{11}(\mathbf{q}-\mathbf{q}', q_z)] \\
&(n \langle F | b^{n+1}_{\mathbf{q}} b^{m-1}_{\mathbf{q}'} b^{\dagger\, m}_{\mathbf{q}'} b^\dagger_{\mathbf{2q}-\mathbf{q}'} b^{\dagger\, n-1}_{\mathbf{q}} | F \rangle + m \langle F | b^{n+1}_{\mathbf{q}} b^{m-1}_{\mathbf{q}'} b^{\dagger\, m-1}_{\mathbf{q}'} b^{\dagger\, n+1}_{\mathbf{q}} | F \rangle) \\
&= (n+1)! m! [C_{22}(\mathbf{q}-\mathbf{q}', q_z) - C_{11}(\mathbf{q}-\mathbf{q}', q_z)] (\frac{n}{m} \mathcal{K}^{m-1,m}_{n+1,n-1} + \mathcal{K}^{m-1,m-1}_{n+1,n})
\end{aligned} \tag{E.13}$$

and so the normalized squared matrix element

$$\frac{|\langle F | b^{n+1}_{\mathbf{q}} b^{m-1}_{\mathbf{q}'} d_{\mathbf{q}'-\mathbf{q}, q_z} H_{phon} b^{\dagger\, m}_{\mathbf{q}'} b^{\dagger\, n}_{\mathbf{q}} | F \rangle|^2}{\langle F | b^{n+1}_{\mathbf{q}} b^{m-1}_{\mathbf{q}'} b^{\dagger\, m-1}_{\mathbf{q}'} b^{\dagger\, n+1}_{\mathbf{q}} | F \rangle \langle F | b^{n}_{\mathbf{q}} b^{m}_{\mathbf{q}'} b^{\dagger\, m}_{\mathbf{q}'} b^{\dagger\, n}_{\mathbf{q}} | F \rangle} \tag{E.14}$$

is equal to

$$\frac{(n+1) m [C_{22}(\mathbf{q}-\mathbf{q}', q_z) - C_{11}(\mathbf{q}-\mathbf{q}', q_z)]^2 (\frac{n}{m} \mathcal{K}^{m-1,m}_{n+1,n-1} + \mathcal{K}^{m-1,m-1}_{n+1,n})^2}{\mathcal{K}^{m,m}_{n,n-1} \mathcal{K}^{m-1,m-1}_{n+1,n}} \tag{E.15}$$

that as expected scales as $m(n+1)$ for small occupation numbers.

We thus know how to calculate scattering matrix elements of intersubband excitations. From these results it is straightforward to calculate scattering matrix elements involving microcavity intersubband polariton states. Considering the polariton creation and annihilation operators (see Eq. 5.2)

$$\begin{aligned}
p^\dagger_{\eta, \mathbf{q}} &= \bar{\alpha}_{\eta, \mathbf{q}} a^\dagger_{\mathbf{q}} + \bar{\beta}_{\eta, \mathbf{q}} b_{\mathbf{q}}, \\
p_{\eta, \mathbf{q}} &= \alpha_{\eta, \mathbf{q}} a_{\mathbf{q}} + \beta_{\eta, \mathbf{q}} b^\dagger_{\mathbf{q}},
\end{aligned} \tag{E.16}$$

we can write multi-polariton matrix elements as binomial expansions involving light or matter terms. Given that a_η and b_η operators commute and that photon operators commute with H_{phon}, we will obtain all the intersubband polaritons matrix elements as expressions containing only $\mathcal{K}$ coefficients and Hopfield coefficients.

The multi-polariton normalization is given by

$$\begin{aligned}
\langle F|p^n_{\eta,\mathbf{q}}p^m_{\eta',\mathbf{q}'}p^{\dagger\,m}_{\eta',\mathbf{q}'}p^{\dagger\,n}_{\eta,\mathbf{q}}|F\rangle &= \langle F|\sum_j \binom{n}{j}\alpha^j_{\eta,\mathbf{q}}a^j_{\mathbf{q}}\beta^{n-j}_{\eta,\mathbf{q}}b^{n-j}_{\mathbf{q}}\sum_y \binom{m}{y}\alpha^y_{\eta,\mathbf{q}'}a^y_{\mathbf{q}'}\beta^{m-y}_{\eta',\mathbf{q}'}b^{m-y}_{\mathbf{q}'} \\
&\quad \sum_h \binom{m}{h}\bar{\alpha}^h_{\eta',\mathbf{q}'}a^{\dagger\,h}_{\mathbf{q}'}\bar{\beta}^{m-h}_{\eta',\mathbf{q}'}b^{\dagger\,m-h}_{\mathbf{q}'}\sum_l \binom{n}{l}\bar{\alpha}^l_{\eta,\mathbf{q}}a^{\dagger\,l}_{\mathbf{q}}\bar{\beta}^{n-l}_{\eta,\mathbf{q}}b^{\dagger\,n-l}_{\mathbf{q}}|F\rangle \\
&= \sum_{l,h}\binom{n}{l}^2\binom{m}{h}^2|\alpha_{\eta,\mathbf{q}}|^{2l}|\beta_{\eta,\mathbf{q}}|^{2(n-l)}|\alpha_{\eta',\mathbf{q}'}|^{2h}|\beta_{\eta',\mathbf{q}'}|^{2(m-h)} \\
&\quad h!l!\langle F|b^{n-l}_{\mathbf{q}}b^{m-h}_{\mathbf{q}'}b^{\dagger\,m-h}_{\mathbf{q}'}b^{\dagger\,n-l}_{\mathbf{q}}|F\rangle \\
&= n!m!\sum_{l,h}\binom{n}{l}\binom{m}{h}|\alpha_{\eta,\mathbf{q}}|^{2l}|\beta_{\eta,\mathbf{q}}|^{2(n-l)}|\alpha_{\eta',\mathbf{q}'}|^{2h} \\
&\quad |\beta_{\eta',\mathbf{q}'}|^{2(m-h)}\mathcal{K}^{n-l,n-l}_{m-h,m-h-1} \qquad \text{(E.17)}
\end{aligned}$$

and the unnormalized matrix element by

$$\begin{aligned}
&\langle F|p^{n+1}_{\eta,\mathbf{q}}p^{m-1}_{\eta',\mathbf{q}'}d_{\mathbf{q}'-\mathbf{q},q_z}H_{phon}p^{\dagger\,m}_{\eta',\mathbf{q}'}p^{\dagger\,n}_{\eta,\mathbf{q}}|F\rangle = \langle F|\sum_j\binom{n+1}{j}\alpha^j_{\eta,\mathbf{q}}a^j_{\mathbf{q}}\beta^{n+1-j}_{\eta,\mathbf{q}}b^{n+1-j}_{\mathbf{q}} \\
&\sum_y\binom{m-1}{y}\alpha^y_{\eta',\mathbf{q}'}a^y_{\mathbf{q}'}\beta^{m-1-y}_{\eta',\mathbf{q}'}b^{m-1-y}_{\mathbf{q}'}d_{\mathbf{q}'-\mathbf{q},q_z}H_{phon}\sum_h\binom{m}{h}\bar{\alpha}^h_{\eta',\mathbf{q}'}a^{\dagger\,h}_{\mathbf{q}'}\bar{\beta}^{m-h}_{\eta',\mathbf{q}'}b^{\dagger\,m-h}_{\mathbf{q}'} \\
&\sum_l\binom{n}{l}\bar{\alpha}^l_{\eta,\mathbf{q}}a^{\dagger\,l}_{\mathbf{q}}\bar{\beta}^{n-l}_{\eta,\mathbf{q}}b^{\dagger\,n-l}_{\mathbf{q}}|F\rangle = \beta_{\eta,\mathbf{q}}\bar{\beta}_{\eta',\mathbf{q}'}\sum_{j,y}\binom{n+1}{j}\binom{n}{j}|\alpha_{\eta,\mathbf{q}}|^{2j}|\beta_{\eta,\mathbf{q}}|^{2(n-j)} \\
&\binom{m-1}{y}\binom{m}{y}|\alpha_{\eta',\mathbf{q}'}|^{2y}|\beta_{\eta',\mathbf{q}'}|^{2(m-1-y)}y!j!\langle F|b^{m-y-1}_{\mathbf{q}'}b^{n+1-j}_{\mathbf{q}}d_{\mathbf{q}'-\mathbf{q},q_z}H_{phon}b^{\dagger\,m-y}_{\mathbf{q}'}b^{\dagger\,n-j}_{\mathbf{q}}|F\rangle \\
&= \beta_{\eta,\mathbf{q}}\bar{\beta}_{\eta',\mathbf{q}'}(n+1)!m![C_{22}(\mathbf{q}-\mathbf{q}',q_z)-C_{11}(\mathbf{q}-\mathbf{q}',q_z)]\sum_{j,y}\binom{n}{j}\binom{m-1}{y} \\
&|\alpha_{\eta,\mathbf{q}}|^{2j}|\beta_{\eta,\mathbf{q}}|^{2(n-j)}|\alpha_{\eta',\mathbf{q}'}|^{2y}|\beta_{\eta',\mathbf{q}'}|^{2(m-1-y)}(\frac{n-j}{m-y}\mathcal{K}^{m-y-1,m-y}_{n-j+1,n-j-1}+\mathcal{K}^{m-y-1,m-y-1}_{n-j+1,n-j}). \qquad \text{(E.18)}
\end{aligned}$$

The expression for the squared normalized polariton scattering matrix element that we need for the Fermi golden rule

$$\hbar^2|V^n_m|^2 = \frac{|\langle F|p^{n+1}_{\eta,\mathbf{q}}p^{m-1}_{\eta',\mathbf{q}'}d_{\mathbf{q}'-\mathbf{q},q_z}H_{phon}p^{\dagger\,m}_{\eta',\mathbf{q}'}p^{\dagger\,n}_{\eta,\mathbf{q}}|F\rangle|^2}{\langle F|p^n_{\eta,\mathbf{q}}p^m_{\eta',\mathbf{q}'}p^{\dagger\,m}_{\eta',\mathbf{q}'}p^{\dagger\,n}_{\eta,\mathbf{q}}|F\rangle\langle F|p^{n+1}_{\eta,\mathbf{q}}p^{m-1}_{\eta',\mathbf{q}'}p^{\dagger\,m-1}_{\eta',\mathbf{q}'}p^{\dagger\,n+1}_{\eta,\mathbf{q}}|F\rangle} \qquad \text{(E.19)}$$

can thus be obtained by putting together Eqs. E.17 and E.18 and from the resulting expression we can read out the B^n_m coefficient (see Eq.5.14).

In order to obtain the final expression for the scattering rate (Eq. 5.17) only remain to calculate the $C_{11}(\mathbf{q}, q_z)$ and $C_{22}(\mathbf{q}, q_z)$ coefficients. They are given by matrix elements of the Frölich Hamiltonian [85]

$$\sum_{\mathbf{q}} \alpha(\mathbf{q}, q_z) e^{-i(\mathbf{rq}+zq_z)} d^{\dagger}_{\mathbf{q},q_z} + \bar{\alpha}(\mathbf{q}, q_z) e^{i(\mathbf{rq}+zq_z)} d_{\mathbf{q},q_z}, \tag{E.20}$$

between electronic states corresponding respectively to the first and second conduction subband, where

$$|\alpha(\mathbf{q}, q_z)|^2 = 2\pi\hbar\omega_{LO} \frac{e^2}{\epsilon S L_{cav}(q^2 + q_z^2)}. \tag{E.21}$$

For definiteness in order to obtain the formula of Chapter 5, we considered the case of a infinite rectangular potential well.

Bibliography

[1] L. Vaidman, *Quantum mechanics: Evolution stopped in its tracks*, Nature **451**, 137 (2008).

[2] E. M. Purcell, *Spontaneous emission probabilities at radio frequencies*, Physical Review **69**, 681 (1946).

[3] P. Goy, J. M. Raimond, M. Gross & S. Haroche, *Observation of Cavity-Enhanced Single-Atom Spontaneous Emission*, Physical Review Letters **50**, 1903 (1983).

[4] G. Gabrielse & H. Dehmelt, *Observation of inhibited spontaneous emission*, Physical Review Letters **55**, 67 (1985).

[5] R. G. Hulet, E. S. Hilfer & D. Kleppner, *Inhibited Spontaneous Emission by a Rydberg Atom*, Physical Review Letters **55**, 2137 (1985).

[6] W. Jhe, A. Anderson, E. A. Hinds, D. Meschede, L. Moi & S. Haroche, *Suppression of spontaneous decay at optical frequencies: Test of vacuum-field anisotropy in confined space*, Physical Review Letters **58**, 666 (1987).

[7] S. Peil & G. Gabrielse, *Observing the Quantum Limit of an Electron Cyclotron: QND Measurements of Quantum Jumps between Fock States*, Physical Review Letters **83**, 1287 (1999).

[8] D. Meschede, H. Walther & G. Müller, *One-Atom Maser*, Physical Review Letters **54**, 551 (1985).

[9] G. Rempe, H. Walther & N. Klein, *Observation of quantum collapse and revival in a one-atom maser*, Physical Review Letters **58**, 353 (1987).

[10] R. J. Thompson, G. Rempe & H. J. Kimble, *Observation of normal-mode splitting for an atom in an optical cavity*, Physical Review Letters **68**, 1132 (1992).

[11] C. Weisbuch, M. Nishioka, A. Ishikawa & Y. Arakawa, *Observation of the coupled exciton-photon mode splitting in a semiconductor quantum microcavity*, Physical Review Letters **69**, 3314 (1992).

[12] A. Wallraff, D. I. Schuster, A. Blais, L. Frunzio, R. S. Huang, J. Majer, S. Kumar, S. M. Girvin & R. J. Schoelkopf, *Strong coupling of a single photon to a superconducting qubit using circuit quantum electrodynamics*, Nature **431**, 162 (2004).

[13] V. Savona, Z. Hradil, A. Quattropani & P. Schwendimann, *Quantum theory of quantum-well polaritons in semiconductor microcavities*, Physical Review B **49**, 8774 (1994).

[14] D. S. Citrin, *Exciton polaritons in double versus single quantum wells: Mechanism for increased luminescence linewidths in double quantum wells*, Physical Review B **49**, 1943 (1994).

[15] D. S. Citrin, *Material and optical approaches to exciton polaritons in multiple quantum wells: Formal results*, Physical Review B **50**, 5497 (1994).

[16] V. Savona, C. Piermarocchi, A. Quattropani, F. Tassone & P. Schwendimann, *Microscopic Theory of Motional Narrowing of Microcavity Polaritons in a Disordered Potential*, Physical Review Letters **78**, 4470 (1997).

[17] C. Ciuti, P. Schwendimann, B. Deveaud & A. Quattropani, *Theory of the angle-resonant polariton amplifier*, Physical Review B **62**, R4825 (2000).

[18] B. Deveaud, A. Quattropani & P. Schwendimann, éditeurs, *Electron and photon confinement in semiconductor nanostructures*, Proceedings of the International School of Physics "Enrico Fermi" – course 150 (IOS Press (Amsterdam, Washington D.C), 2003).

[19] B. Deveaud, editor, *The physics of semiconductor microcavities: from fundamentals to nanoscale devices* (Wiley-VCH, 2007).

[20] J. Kasprzak, M. Richard, S. Kundermann, A. Baas, P. Jeambrun, J. M. J. Keeling, F. M. Marchetti, M. H. Szymanska, R. Andre, J. L. Staehli, V. Savona, P. B. Littlewood, B. Deveaud & Le Si Dang, *Bose-Einstein condensation of exciton polaritons*, Nature **443**, 409 (2006).

[21] S. I. Tsintzos, N. T. Pelekanos, G. Konstantinidis, Z. Hatzopoulos & P. G. Savvidis, *A GaAs polariton light-emitting diode operating near room temperature*, Nature **453**, 372 (2008/05/15/print).

[22] G. Malpuech, A. Di Carlo, A. V. Kavokin, J. J. Baumberg, M. Zamfirescu & P. Lugli, *Room-temperature polariton lasers based on GaN microcavities*, Applied Physics Letters **81**, 412 (2002).

[23] S. Christopoulos, G. Baldassarri Hoger von Hogersthal, A. J. D. Grundy, P. G. Lagoudakis, A. V. Kavokin, J. J. Baumberg, G. Christmann, R. Butte, E. Feltin, J.-F. Carlin & N. Grandjean, *Room-Temperature Polariton Lasing in Semiconductor Microcavities*, Physical Review Letters **98**, 126405 (2007).

[24] D. Dini, R. Köhler, A. Tredicucci, G. Biasiol & L. Sorba, *Microcavity Polariton Splitting of Intersubband Transitions*, Physical Review Letters **90**, 116401 (2003).

[25] C. Ciuti, G. Bastard & I. Carusotto, *Quantum vacuum properties of the intersubband cavity polariton field*, Physical Review B **72**, 115303 (2005).

[26] M. H. Devoret, S. M. Girvin & R. J. Schoelkopf, *Circuit-QED: How strong can the coupling between a Josephson junction atom and a transmission line resonator be?*, Annalen der Physik **16**, 767 (2007).

[27] R. H. Dicke, *Coherence in Spontaneous Radiation Processes*, Physical Review **93**, 99 (1954).

[28] D. S. Citrin, *Radiative lifetimes of excitons in quantum wells: Localization and phase-coherence effects*, Physical Review B **47**, 3832 (1993).

[29] D. S. Citrin & J. B. Khurgin, *Microcavity effect on the electron-hole relative motion in semiconductor quantum wells*, Physical Review B **68**, 205325 (2003).

[30] G. Oohata, T. Nishioka, D. Kim, H. Ishihara & M. Nakayama, *Giant Rabi splitting in a bulk CuCl microcavity*, Physical Review B **78**, 233304 (2008).

[31] G. Christmann, R. Butte, E. Feltin, A. Mouti, P. A. Stadelmann, A. Castiglia, J. Carlin & N. Grandjean, *Large vacuum Rabi splitting in a multiple*

quantum well GaN-based microcavity in the strong-coupling regime, Physical Review B **77**, 085310 (2008).

[32] A. A. Anappara, S. De Liberato, A. Tredicucci, C. Ciuti, G. Biasiol & L. Sorba, *Signatures of the ultrastrong light-matter coupling regime*, Physical Review B **79**, 201303(R) (2009).

[33] C. Ciuti & I. Carusotto, *Input-output theory of cavities in the ultrastrong coupling regime: The case of time-independent cavity parameters*, Physical Review A **74**, 033811 (2006).

[34] S. De Liberato, C. Ciuti & I. Carusotto, *Quantum Vacuum Radiation Spectra from a Semiconductor Microcavity with a Time-Modulated Vacuum Rabi Frequency*, Physical Review Letters **98**, 103602 (2007).

[35] M. Kardar & R. Golestanian, *The "friction of vacuum", and other fluctuation-induced forces*, Review of Modern Physics **71**, 1233 (1999).

[36] W. G. Unruh, *Second quantization in the Kerr metric*, Physical Review D **10**, 3194 (1974).

[37] G. Günter, A. A. Anappara, J. Hees, A. Sell, G. Biasiol, L. Sorba, S. De Liberato, C. Ciuti, A. Tredicucci, A. Leitenstorfer & R. Huber, *Sub-cycle switch-on of ultrastrong light-matter interaction*, Nature **458**, 178 (2009).

[38] S. De Liberato & C. Ciuti, *Quantum model of microcavity intersubband electroluminescent devices*, Physical Review B **77**, 155321 (2008).

[39] L. Sapienza, A. Vasanelli, R. Colombelli, C. Ciuti, Y. Chassagneux, C. Manquest, U. Gennser & C. Sirtori, *Electrically Injected Cavity Polaritons*, Physical Review Letters **100**, 136806 (2008).

[40] S. De Liberato & C. Ciuti, *Stimulated Scattering and Lasing of Intersubband Cavity Polaritons*, Physical Review Letters **102**, 136403 (2009).

[41] P. L. Knight & P. M. Radmore, *Quantum origin of dephasing and revivals in the coherent-state Jaynes-Cummings model*, Physical Review A **26**, 676 (1982).

[42] J. Gea-Banacloche, *Atom- and field-state evolution in the Jaynes-Cummings model for large initial fields*, Physical Review A **44**, 5913 (1991).

[43] A. Auffeves, P. Maioli, T. Meunier, S. Gleyzes, G. Nogues, M. Brune, J. M. Raimond & S. Haroche, *Entanglement of a Mesoscopic Field with an Atom Induced by Photon Graininess in a Cavity*, Physical Review Letters **91**, 230405 (2003).

[44] R. Bonifacio & G. Preparata, *Coherent Spontaneous Emission*, Physical Review A **2**, 336 (1970).

[45] R. Bonifacio, P. Schwendimann & Fritz Haake, *Quantum Statistical Theory of Superradiance. I*, Physical Review A **4**, 302 (1971).

[46] R. Bonifacio, P. Schwendimann & Fritz Haake, *Quantum Statistical Theory of Superradiance. II*, Physical Review A **4**, 854 (1971).

[47] D. I. Schuster, A. A. Houck, J. A. Schreier, A. Wallraff, J. M. Gambetta, A. Blais, L. Frunzio, J. Majer, B. Johnson, M. H. Devoret, S. M. Girvin & R. J. Schoelkopf, *Resolving photon number states in a superconducting circuit*, Nature **445**, 515 (2007).

[48] J. Johansson, S. Saito, T. Meno, H. Nakano, M. Ueda, K. Semba & H. Takayanagi, *Vacuum Rabi Oscillations in a Macroscopic Superconducting Qubit LC Oscillator System*, Physical Review Letters **96**, 127006 (2006).

[49] A. A. Anappara, A. Tredicucci, F. Beltram, G. Biasiol, L. Sorba, S. De Liberato & C. Ciuti, *Cavity polaritons from excited-subband transitions*, Applied Physics Letters **91**, 231118 (2007).

[50] J. M. Raimond, P. Goy, M. Gross, C. Fabre & S. Haroche, *Statistics of Millimeter-Wave Photons Emitted by a Rydberg-Atom Maser: An Experimental Study of Fluctuations in Single-Mode Superradiance*, Physical Review Letters **49**, 1924 (1982).

[51] A. Blais, J. Gambetta, A. Wallraff, D. I. Schuster, S. M. Girvin, M. H. Devoret & R. J. Schoelkopf, *Quantum-information processing with circuit quantum electrodynamics*, Physical Review A **75**, 032329 (2007).

[52] R. Colombelli, C. Ciuti, Y. Chassagneux & C. Sirtori, *Quantum cascade intersubband polariton light emitters*, Semiconductor Science and Technology **20**, 985 (2005).

[53] L. Sapienza, A. Vasanelli, C. Ciuti, C. Manquest, C. Sirtori, R. Colombelli & U. Gennser, *Photovoltaic probe of cavity polaritons in a quantum cascade structure*, Applied Physics Letters **90**, 201101 (2007).

[54] C. Sirtori, F. Capasso, J. Faist & S. Scandolo, *Nonparabolicity and a sum rule associated with bound-to-bound and bound-to-continuum intersubband transitions in quantum wells*, Physical Review B **50**, 8663 (1994).

[55] J. J. Hopfield, *Theory of the Contribution of Excitons to the Complex Dielectric Constant of Crystals*, Physical Review **112**, 1555 (1958).

[56] F. Tassone & Y. Yamamoto, *Exciton-exciton scattering dynamics in a semiconductor microcavity and stimulated scattering into polaritons*, Physical Review B **59**, 10830 (1999).

[57] J. N. Munday, Federico Capasso & V. Adrian Parsegian, *Measured long-range repulsive Casimir-Lifshitz forces*, Nature **457**, 170 (2009).

[58] S. K. Lamoreaux, *Demonstration of the Casimir Force in the 0.6 to* $6\mu m$ *Range*, Physical Review Letters **78**, 5 (1997).

[59] U. Mohideen & Anushree Roy, *Precision Measurement of the Casimir Force from 0.1 to* $0.9\mu m$, Physical Review Letters **81**, 4549 (1998).

[60] G. Bressi, G. Carugno, R. Onofrio & G. Ruoso, *Measurement of the Casimir Force between Parallel Metallic Surfaces*, Physical Review Letters **88**, 041804 (2002).

[61] S. W. Hawking, *Black hole explosions?*, Nature **248**, 30 (1974).

[62] A. Lambrecht, M. Jaekel & S. Reynaud, *Motion Induced Radiation from a Vibrating Cavity*, Physical Review Letters **77**, 615 (1996).

[63] A. Lambrecht, *Electromagnetic pulses from an oscillating high-finesse cavity: possible signatures for dynamic Casimir effect experiments*, Journal of Optics B: Quantum and Semiclassical Optics **7**, S3 (2005).

[64] V. V. Dodonov, A. B. Klimov & D. E. Nikonov, *Quantum phenomena in nonstationary media*, Physical Review A **47**, 4422 (1993).

[65] C. K. Law, *Effective Hamiltonian for the radiation in a cavity with a moving mirror and a time-varying dielectric medium*, Physical Review A **49**, 433 (1994).

[66] M. Sandberg, C. M. Wilson, F. Persson, T. Bauch, G. Johansson, V. Shumeiko, T. Duty & P. Delsing, *Tuning the field in a microwave resonator faster than the photon lifetime*, Applied Physics Letters **92**, 203501 (2008).

[67] A. A. Anappara, A. Tredicucci, G. Biasiol & L. Sorba, *Electrical control of polariton coupling in intersubband microcavities*, Applied Physics Letters **87**, 051105 (2005).

[68] A. A. Anappara, A. Tredicucci, F. Beltram, G. Biasiol & L. Sorba, *Tunnel-assisted manipulation of intersubband polaritons in asymmetric coupled quantum wells*, Applied Physics Letters **89**, 171109 (2006).

[69] D. F. Walls & G. J. Milburn, *Quantum Optics* (Springer-Verlag Berlin, 1994).

[70] A. Blais, R. Huang, A. Wallraff, S. M. Girvin & R. J. Schoelkopf, *Cavity quantum electrodynamics for superconducting electrical circuits: An architecture for quantum computation*, Physical Review A **69**, 062320 (2004).

[71] R. Grimshaw, *Nonlinear Ordinary Differential equations* (CRC Press, 1993).

[72] H. C. Liu & F. Capasso, éditeurs, *Intersubband Transitions in Quantum Wells: Physics and Device Applications I* (Academic Press, San Diego, 2000).

[73] J. Faist, F. Capasso, D. L. Sivco, C. Sirtori, A. L. Hutchinson & A. Y. Cho, *Quantum Cascade Laser*, Science **264**, 553 (1994).

[74] R. Kohler, A. Tredicucci, F. Beltram, H. E. Beere, E. H. Linfield, A. G. Davies, D. A. Ritchie, R. C. Iotti & F. Rossi, *Terahertz semiconductor-heterostructure laser*, Nature **417**, 156 (2002).

[75] Raffaele Colombelli, Kartik Srinivasan, Mariano Troccoli, Oskar Painter, Claire F. Gmachl, Donald M. Tennant, A. Michael Sergent, Deborah L. Sivco, Alfred Y. Cho & Federico Capasso, *Quantum Cascade Surface-Emitting Photonic Crystal Laser*, Science **302**, 1374 (2003).

[76] J. Fricke, *Transport Equations Including Many-Particle Correlations for an Arbitrary Quantum System: A General Formalism*, Annals of Physics **252**, 479 (1996).

[77] J. Fricke, *Improved Transport Equations Including Correlations for Electron–Phonon Systems: Comparison with Exact Solutions in One Dimension Annals of Physics, Volume 253, Issue 1, 1 January 1997, Pages 177-197*, Annals of Physics **253**, 177 (1997).

[78] M. Kira, W. Hoyer, T. Stroucken & S. W. Koch, *Exciton Formation in Semiconductors and the Influence of a Photonic Environment*, Physical Review Letters **87**, 176401 (2001).

[79] D. E. Nikonov, A. Imamoğlu, L. V. Butov & H. Schmidt, *Collective Intersubband Excitations in Quantum Wells: Coulomb Interaction versus Subband Dispersion*, Physical Review Letters **79**, 4633 (1997).

[80] L. Sapienza, *Dispositif électrique á semiconducteur fonctionnant dans le régime de couplage fort lumière-matière*, Thèse de doctorat, Université Paris Diderot-Paris 7 (2007).

[81] S. Datta, *Quantum Transport: Atom to Transistor* (Cambridge University Press, 2005).

[82] U. Fano, *Effects of Configuration Interaction on Intensities and Phase Shifts*, Physical Review **124**, 1866 (1961).

[83] M. H. Anderson, J. R. Ensher, M. R. Matthews, C. E. Wieman & E. A. Cornell, *Observation of Bose-Einstein Condensation in a Dilute Atomic Vapor*, Science **269**, 198 (1995).

[84] A. J. Leggett, *Quantum Liquids: Bose Condensation and Cooper Pairing in Condensed-Matter Systems* (Oxford University Press, 2006).

[85] R. Ferreira & G. Bastard, *Evaluation of some scattering times for electrons in unbiased and biased single- and multiple-quantum-well structures*, Physical Review B **40**, 1074 (1989).

[86] M. Combescot, O. Betbeder-Matibet & R. Combescot, *Exciton-exciton scattering: Composite boson versus elementary boson*, Physical Review B **75**, 174305 (2007).

[87] M. Combescot, O. Betbeder-Matibet & F. Dubin, *The many-body physics of composite bosons*, Physics Reports **463**, 215 (2008), ISSN 0370-1573.

[88] P. Y. Yu & M. Cardona, *Fundamentals of Semiconductors* (Springer, 2001).

[89] O. Gauthier-Lafaye, P. Boucaud, F. H. Julien, S. Sauvage, S. Cabaret, J.-M. Lourtioz, V. Thierry-Mieg & R. Planel, *Long-wavelength ([approximate] 15.5 mu m) unipolar semiconductor laser in GaAs quantum wells*, Applied Physics Letters **71**, 3619 (1997).

[90] R. W. Hellwarth, *Theory of Stimulated Raman Scattering*, Physical Review **130**, 1850 (1963).

[91] H. C. Liu, Iva W. Cheung, A. J. SpringThorpe, C. Dharma-wardana, Z. R. Wasilewski, D. J. Lockwood & G. C. Aers, *Intersubband Raman Laser*, Applied Physics Letters **78**, 3580 (2001).

[92] J. B. Khurgin & H. C. Liu, *Stimulated polariton scattering in intersubband lasers: Role of motional narrowing*, Physical Review B **74**, 035317 (2006).

[93] Gerald T. Moore, *Quantum Theory of the Electromagnetic Field in a Variable-Length One-Dimensional Cavity*, Journal of Mathematical Physics **11**, 2679 (1970).

[94] A. V. Dodonov, L. C. Celeri, F. Pascoal, M. D. Lukin & S. F. Yelin, *Photon generation from vacuum in non-stationary circuit QED*, arXiv:0806.4035v3.

[95] S. De Liberato, D. Gerace, I. Carusotto & C. Ciuti, *External quantum vacuum radiation from a cavity-embedded qubit*, in preparation.

[96] S. De Liberato & C. Ciuti, *Quantum theory of electron tunneling into intersubband cavity polariton states*, Physical Review B **79**, 075317 (2009).

[97] K. Kakazu & Y. S. Kim, *Quantization of electromagnetic fields in cavities and spontaneous emission*, Physical Review A **50**, 1830 (1994).